

Diss. ETH No. 20549

QCD Corrections and Non-linear Mappings

A dissertation submitted to

ETH Zurich

for the degree of

Doctor of Sciences

presented by

Franz Herzog

MPhys, University of Edinburgh

born May 07th, 1984

citizen of Germany

accepted on the recommendation of

Prof. C. Anastasiou examiner

Prof. E. N. Glover co-examiner

2012

Abstract

Complicated overlapping singularities are faced in higher order perturbative QCD calculations. In this thesis we develop a new technique to factorise singularities of dimensionally regulated singular integrals. The technique will be based on a special non-linear mapping, which allows to rescale parameters of integration with respect to each other. We will demonstrate that this approach can be applied quite systematically on a number of examples. We will then consider some of the most singular one and two-loop integrals and demonstrate how they can be factorised and evaluated numerically.

Furthermore, we will consider infra-red singular phase-space integrals as they occur in next-to and next-to-next-to-leading-order perturbative QCD corrections in both decay and hadronic production processes. In particular we shall develop a method, based on the non-linear mapping, for double real emission corrections to hadronic productions of massive final states.

With the techniques developed we will compute the fully differential decay width of a Higgs boson decaying into a bottom quark anti-quark pair at the next-to-next-to-leading order accuracy. For this purpose we compute and present all the required amplitudes needed for the calculation using conventional Feynman diagrammatic methods. We check that our result is in agreement with existing inclusive results and present a number of differential observables, namely jet rates and the distribution of the maximum energy of the leading jet.

Furthermore, we compute the fully differential next-to-next-to-leading-order Higgs production cross section in bottom quark anti-quark annihilation. We present a number of differential distributions, including the rapidity and transverse momentum distribution as well as jet-rates and pt-veto plots of the 125 GeV Higgs-boson at the LHC. We study the factorisation and renormalisation scale dependence of a number of fully differential observables as well as a number of observables associated with the Higgs boson decay into two photons.

Zusammenfassung

Komplizierte überlappende Singularitäten treten in höheren Korrekturen der perturbativen QCD auf. In dieser Dissertation, wird eine neue Methode zur Faktorisierung solcher Singularitäten in dimensionell regularisierten Integralen entwickelt. Diese Methode basiert auf speziellen nicht-linearen Transformationen welche es erlauben Integrationsparameter miteinander zu reskalieren. Anhand von mehreren Beispielen wird gezeigt wie diese Methode systematisch angewendet werden kann. Die Methode wird dann auf einige maximal singuläre Ein- und Zwei-Schleifenintegrale angewandt.

Des weiteren werden infrarot divergente Phasenraumintegrale, für Zerfalls- und hadronische Produktions-Prozesse, in Betracht gezogen. Hierbei wird eine allgemeine Methode für doppelt reelle Emissionen zur hadronischen Produktion von massiven Endzuständen entwickelt.

Als erste praktische Anwendung der Methoden wird die voll-differentielle Zerfallsbreite des Higgs-Bosons in ein Bottomquark-Antiquark Paar zur dritten Ordnung berechnet. Für die Rechnung werden alle benötigten Amplituden mit modernen Feynman diagrammatischen Methoden berechnet. Es wird gezeigt dass das berechnete Resultat für die inklusive Zerfallsbreite mit existierenden Resultaten übereinstimmt. Ausserdem werden Jetraten und die Energieverteilung des führenden Jets berechnet.

Des weiteren wird der voll-differentielle Wirkungsquerschnitt des Higgs-Bosons in der Bottomquark Annihilierung zur dritten Ordnung berechnet. Es werden einige differentielle Verteilungen präsentiert, unter anderem beinhalten diese die Rapiditäts- und die Transversalimpuls- Verteilung und Jetraten des 125 GeV Higgs-Bosons am LHC. Die Abhängigkeit von Renormierungs- und Faktorisierungs-Skalen einiger Observablen werden analysiert und ein paar Observablen im Photonen-Zerfall des Higgs-Bosons präsentiert.

Acknowledgements

There are many people who have had a great influence on this work and without whom I would have never come as far as I have.

First of all I most warmly thank my supervisor Babis Anastasiou for the exceptional guidance and care which i have received from him throughout my time as a PhD student at ETH. While he has given me enough room at times, such that I could develop my own ways of thinking about problems, he did not in the very least miss an opportunity to push me to finish a project when it was required. It has been very inspiring to have him as my supervisor and I consider myself very lucky to have been part of the very exceptional, communicational and vivid group which he has created at ETH. Indeed it is not an uncommon experience that a professor has to come from the other side of the institute to close our office doors because our (mostly) physics based discussions have once again crossed the critical noise level.

Further I most warmly thank Achilleas Lazopoulos, without whom this thesis would not have been possible and whose advice was always most valuable. His enthusiasm has made working with him a great experience throughout.

Much thanks also goes to Stephan Buehler with whom I had the pleasure of working together on a number of joint projects and whose exceptional talent of making us laugh has always greatly enhanced the spirit of the group.

Special thanks goes to Julian Cancino, Romain Mueller, Bernhard Mistlberger, Falko Dulat, Gabriel Abelof, Mathias Brucherseifer and Florian Goertz for proof reading chapters of this thesis. Due to my exceptional talent for typos, their help was essential to finishing this thesis. Much thanks goes to Romain Müller with whom I share a similarly frantic enthusiasm towards physics and who was certainly influential on the subject of non-linear mappings.

I shall also not forget Stephan Bucherer and Elisabetta Furlan who have helped me much in my first years of my PHD. Especially Stephan Bucherer has been very helpful in the beginning. Further Thanks goes to Andrea Banfi with whom I have

had countless hours of dinner discussions and to whom I owe much of my understanding of QCD and QFT in general.

At last I shall not miss the opportunity to greatly thank Zoltan Kunszt, of whom I have learned so very much in many discussions and who was very influential in my successful career planning.

At the very last I must greatly thank my girlfriend Claire. She has been immensely supportive throughout the final months of this project, and had to put up with me during this time.

Declaration

I declare that I have not previously submitted any material presented in this thesis for any other degree at this or any other university.

The research presented in this thesis has been carried out in collaboration with C. Anastasiou, A. Lazopoulos, S. Buehler and R. Mueller. Aspects of chapters 3 to 8 have been published in the following publications:

- C. Anastasiou, F. Herzog and A. Lazopoulos, *On the factorization of overlapping singularities at NNLO*, *JHEP* **1103** (2011) 038 [arXiv:1011.4867 [hep-ph]].
- C. Anastasiou, F. Herzog and A. Lazopoulos, *The Fully differential decay rate of a Higgs boson to bottom-quarks at NNLO in QCD*, *JHEP* **1203** (2012) 035 [arXiv:1110.2368 [hep-ph]].
- S. Buehler, F. Herzog, A. Lazopoulos and R. Mueller, *The Fully differential hadronic production of a Higgs boson via bottom quark fusion at NNLO*, arXiv:1204.4415 [hep-ph].

Contents

1	Introduction	1
2	Perturbative QCD	6
2.1	The QCD Lagrangian	6
2.2	Feynman rules for QCD	8
2.3	Divergences, renormalisation and dimensional regularisation	8
2.3.1	Renormalisation	10
2.3.2	Infrared Divergences	12
2.4	The d -dimensional phase space measure	13
2.5	Cross sections and decay rates	13
3	Divergent integrals and non-linear mappings	15
3.1	Factorised singularities	15
3.2	Overlapping singularities	17
3.3	Methods for overlapping singularities	20
3.3.1	The subtraction method for overlapping singularities	21
3.3.2	Sector Decomposition	22
3.3.3	Non-linear mappings	22
3.3.4	A more complicated example with non-linear mappings	27
3.3.5	A two-variable non-linear mapping	29
3.3.6	A more complicated example with non-linear mappings II	30
3.3.7	A more complicated example with non-linear mappings III	30
3.4	Line singularities	31
3.5	Conclusion	32
4	Factorising singular loop integrals with non-linear mappings	33
4.1	The massless one-loop box with sector decomposition	33

4.2	The massless one-loop box with non-linear mappings	35
4.3	The one-loop box with two external masses	37
4.4	The non-planar massless two-loop triangle	39
4.5	Conclusion	41
5	Real corrections to the hadronic production of massive states	42
5.1	Notational setup for the NNLO partonic cross section	44
5.2	Single real emission for massive final states	46
5.3	Double real emissions for massive final states	49
5.3.1	Factorisation of the double emission phase space	52
5.3.2	Energies and angles parametrisation	53
5.3.3	A more general κ parameterisation	57
5.3.4	Hierarchical parameterization	58
5.3.5	Numerical evaluation of double-real radiation phase-space in- tegrals	61
5.4	On the dimensionality of the massive LO n -particle phase space in higher order calculations	67
5.5	Conclusions	69
6	Real corrections to $1 \rightarrow 2$ massless decays	70
6.1	Notational setup for $1 \rightarrow 2$ decays at NNLO	70
6.2	A $1 \rightarrow 2$ phase space parametrisation	72
6.3	A $1 \rightarrow 3$ phase space parametrisation	72
6.4	A $1 \rightarrow 4$ phase space parametrisation	73
6.5	Integration of most singular double-real integrals	74
6.6	Conclusion	77
7	The $H \rightarrow b\bar{b}$ decay width	78
7.1	Notation and set-up	79
7.2	Squared amplitudes	80
7.2.1	Decay to two partons	80
7.2.2	Decay to three partons	82
7.2.3	Decay to four partons	84
7.3	Integration over phase-space	85
7.4	Integration of the real-virtual	86
7.5	Numerical results	87
7.6	Conclusions	88

8	Hadronic $b\bar{b} \rightarrow H$ production	90
8.1	Notation and set-up	92
8.1.1	The hadronic cross section	92
8.1.2	The partonic cross section	93
8.2	Squared amplitudes	94
8.3	Details on the calculation	95
8.3.1	Analytic continuations for the real-virtual	96
8.3.2	Separation of Soft and Hard	97
8.4	Collinear Factorisation	101
8.5	Numerical Results	104
8.6	Conclusion	113
9	The $H \rightarrow gggg$ amplitude and ϵ–helicities	115
9.1	The helicity approach with ϵ polarisations	116
9.2	Discussion	120
10	Conclusions	122
A	$H \rightarrow b\bar{b}$ double real amplitudes	126
B	The pdf convolution	135
B.1	Parametrisation 1	135
B.2	Parametrisation 2	136
B.3	Parametrisation 3	136
B.4	Numerical performance	137
C	The one-loop box with one external mass	139
D	Scale dependence and separation	141

List of Figures

2.1	Gluon self interactions	9
2.2	Gluon,fermion and ghost interactions	9
2.3	Gluon,fermion and ghost propagators	10
4.1	The massless non-planar two-loop triangle with one massive external leg	39
5.1	Singular Feynman diagrams for single real emissions	46
5.2	Phase space factorisation: q_i are massless particles while p_i are massive.	47
5.3	The most singular topologies: C_1, C_2, C_3, C_4	49
5.4	Double real phase space factorisation	52
6.1	Most singular Feynman diagrams in real emissions to $1 \rightarrow 2$ massless decays	72
6.2	Most singular Feynman Diagrams in $1 \rightarrow 2$ massless Decays	74
7.1	The energy spectrum of the leading jet in the decay $H \rightarrow b\bar{b}$ in the rest frame of the Higgs boson through NNLO. The jet clustering is performed with the JADE algorithm with $y_{cut} = 0.1$	89
8.1	The Higgs rapidity distribution for $m_H = 125$ GeV at the 8 TeV LHC. The bands describe the uncertainty due to factorisation scale	105
8.2	The Higgs transverse momentum distribution for $m_H = 125$ GeV at the 8 TeV LHC.	105
8.3	Differential distribution in rapidity and transverse momentum of the Higgs boson for $m_H = 125$ GeV at the 8 TeV LHC.	107
8.4	The cumulative distribution of the Higgs p_T for $m_H = 125$ GeV at the 8 TeV LHC.	107

8.5	The cross section in the presence of a jet veto (the 0-jet rate) for $m_H = 125$ GeV at the 8 TeV LHC.	108
8.6	The average p_T (left) and rapidity (right) of the Higgs as a function of μ_F for $m_H = 125$ GeV at the 8 TeV LHC.	109
8.7	The 0-, 1- and 2-jet rate as a function of the p_T used in the jet definition for $m_H = 125$ GeV at the 8 TeV LHC.	109
8.8	The distribution of the Higgs p_T per initial state channel for $m_H = 125$ GeV at the 8 TeV LHC	110
8.9	The distribution of the Higgs absolute rapidity, $ y $ per initial state channel for $m_H = 125$ GeV at the 8 TeV LHC	111
8.10	The average p_T of the two photons and the Y^* distribution for $b\bar{b} \rightarrow H + X \rightarrow \gamma\gamma + X$ for $m_H = 125$ GeV at the 8 TeV LHC, in the presence of cuts described in the text.	112

List of Tables

5.1	The most singular integrals to double real emission of massive final states	51
B.1	Using MSTW NLO central set and $\mu_f = 100$, $\tau = 0.1$, 10^6 points with Cuba Vegas	137
B.2	Using MSTW NLO central set and $\mu_f = 100$, $\tau = 0.0001$, 10^6 points with Cuba Vegas	138

Abbreviations

BSM Beyond the Standard Model

IR infra-red

LHC Large Hadron Collider

LO leading-order

NLO next-to-leading-order

NNLO next-to-next-to-leading-order

PDF Parton Distribution Function

QCD Quantum Chromo Dynamics

QED Quantum Electro Dynamics

SM The Standard Model

UV Ultraviolet

Chapter 1

Introduction

The interactions of all the visible matter of the universe are believed to be governed by four fundamental forces of nature. These are the electromagnetic force, the weak and strong nuclear forces, and the force of gravity. At the quantum level the Standard Model (SM) of particle physics successfully describes all of these but gravity. Gravity, however, is not expected to play a role at current collider energies, where the dominant interactions are governed by the strong and electro-weak forces.

Having survived numerous experimental tests, many aspects of the SM have been validated at a very high level of precision. Furthermore, the SM has made a number of predictions. The most important may be the discovery of the massive gauge bosons W^+ , W^- and Z at the UA1 experiment, and the discovery of the top quark at Tevatron. These discoveries already constitute a huge success of the theory.

Only the Higgs sector of the SM has not been fully confirmed by the experiments yet, although the LHC has already shown strong hints towards the existence of a 125 GeV SM Higgs. Without the Higgs sector the SM is known to lose its predictive power at energies well within the scope of the Large Hadron Collider (LHC). It is therefore certain that something new must be found at the LHC. This is either at least one Higgs boson, or some new strongly coupled force usually termed Technicolor.

The SM realisation of the Higgs sector is a minimal one, where only one scalar particle can be observed experimentally. Extensions beyond the Standard Model (BSM) are plentiful and large classes of models predict more involved Higgs sectors, where five or more fundamental scalars could be observed. Many models, such as those based on supersymmetry or extra-dimensions, also predict a wealth of new heavy particles which should be observed experimentally. Such BSM models may

also explain other puzzles of fundamental physics such as the unification of forces, the existence of dark matter, the hierarchy problem or the size of the matter-antimatter asymmetry.

New discoveries at Collider experiments, such as the LHC, may only be made through an excellent understanding of the already known physics of the SM. This is primarily because it is generally not possible to observe the new particles directly. Rather heavy states are mostly very short-lived and immediately decay into lighter SM particles. The situation may be different for very stable particles such as dark matter candidates. These particles will still leave traces of missing energy, and it is then essential to know the Standard Model background of missing Energy which consists of neutrinos. Moreover, new physics events will only constitute a very tiny fraction of the SM events, or background events, produced in the collisions. Isolating these events therefore requires not only very precise experimental measurements, but also very precise knowledge of the scattering rates and their kinematical distributions.

To a large extent the dynamics of particles at modern Collider experiments, now most importantly the LHC, are governed by QCD. In order for new physics to be found at the LHC, may it be the existence of the Higgs boson, dark matter, supersymmetry or extra-dimensions, it is therefore necessary to have full control over QCD driven effects. At high enough energies QCD becomes asymptotically free, allowing the use of perturbation theory. However, higher order effects in perturbative QCD are generally still large, even at typical LHC energies, and must be included to a sufficient degree for comparisons of theory and experiments to be meaningful.

Historically it was indeed the impact of radiative corrections which marked the first successes of QCD. In the deep inelastic scattering experiments it was small violations of Bjorken scaling which were correctly predicted by the radiative corrections computed by G. Altarelli and O. Parisi in 1977 [1]. Around the same time also the Drell Yan cross section could be accounted for with the inclusion of next-to-leading-order (NLO) corrections, via the famous calculations by G. Altarelli, K. Ellis and G. Martinelli in 1977 [2], later confirmed in [3]. These results finally gave physicists confidence that QCD was indeed the correct theory to describe the strong interaction instead of the string models whose popularity then was still comparable.

With NLO corrections generally large, the convergence of the perturbative series was still highly questionable and demanded the computations of yet higher orders.

The first fully inclusive NNLO corrections were pioneered in the late 80s and early 90s with the heroic computations of the process $e^+e^- \rightarrow \text{hadrons}$ by S. G. Gorishny, A. L. Kataev and S. A. Larin in 1988 [4] and the computation of the Drell-Yan cross-section by R. Hamberg, W.L. van Neerven and T. Matsuura in 1990 [5]. Both computations showed that the corrections were larger than may have been expected. Nevertheless, theoretical uncertainties were reduced and were found to greatly improve the theoretical definition of QCD observables. Having knowledge of the NNLO correction also allowed for a more precise extraction of the strong coupling constant from the $e^+e^- \rightarrow \text{hadrons}$ measurements.

NLO corrections to the production of a Higgs boson in gluon fusion, computed in the heavy quark effective theory in 1990 [6] and independently in [7], were particularly large. It took more than a decade for the inclusive NNLO calculation to appear by R. Harlander and W. Kilgore in 2002 [8] and independently in [9]. This calculation showed, even though the NNLO correction were found to be much larger than for the Drell-Yann process, a considerable reduction of the scale uncertainties. It was clear that in order to discover the Higgs boson the full kinematic information was required. This and the large NNLO corrections found in the $gg \rightarrow H$ process strongly motivated the computation of differential observables at NNLO. The first fully differential NNLO calculation for a hadronic cross-section was eventually computed by C. Anastasiou, K. Melnikov and F. Petriello in 2004 [10] with the method of sector decomposition [11, 12, 13].

The last decade has seen tremendous progress in the development of fully differential methods for LO, NLO and NNLO computations. Tree-level amplitudes are meanwhile computed with powerful recursion relations. The fastest available method remains, at least for more than 8 external gluons, the Berends-Giele recursion relation developed in 1987 by W. T. Giele and F. A. Berends [14]. More recent work, inspired by twistor string theory, lead to the BCFW recursion relation by R. Britto, F. Cachazo, B. Feng in 2004 [15].

Developments on the NLO frontier have been at least as dramatic, especially in the last few years. NLO corrections are naturally split into a real emission correction and a one-loop correction. Since both contributions are separately divergent, methods had to be developed to handle this complication. The divergences are regulated by computing in $d = 4 - 2\epsilon$ dimensions, which allows to isolate the divergent

contributions as poles in ϵ . In the earlier NLO calculations, for example in [2], the divergences were dealt with via simple subtractions which allow expansions in terms of distributions. To handle the complexity of more complicated final states including jets, more elaborate methods were needed for the real emission corrections.

A number of general methods, designed to handle these complexities, were developed. The first general approach was put forward by W.T Giele and E.W.N. Glover in 1991 [16, 17] and was based on the idea of phase space slicing. Two, now commonly used methods, are based on the idea of subtraction. The first of these was derived by S. Frixione, Z. Kunszt and A. Signer in 1995 [18, 19, 20] and is known as FKS subtraction. The second was developed by S. Catani and M.H. Seymour in 1996 and is known as the dipole subtraction method [21, 22].

The bottleneck of NLO was for long the virtual correction but there has been tremendous progress since the methods of 'tHooft and Veltman [23] and Passarino and Veltman [24] in 1978. There now exist a number of completely automated tools. Many of these methods rely on the use of unitarity in order to find the coefficients of scalar integrals numerically. It was long known that all scalar one-loop n -point integrals could be spanned by a basis containing only 4-, 3- and 2-point integrals [25, 26]. The original idea of using unitarity for one-loop computations was developed by Z. Bern, L.J. Dixon, D. C. Dunbar and D. A. Kosower in 1994 [27]. These ideas obtained a major boost with the development of generalised unitarity by R. Britto, F. Cachazo, B. Feng [28] in 2004 which generalised the former idea of unitarity for complex valued momenta. The development of such novel techniques lead to the computation of even $2 \rightarrow 5$ processes [29] at NLO.

Also at NNLO progress has been impressive over the last years. Further collider processes for which differential calculations have been completed, apart from the $gg \rightarrow H$, are the Drell-Yan process, $e^+e^- \rightarrow 3 \text{ jets}$, $pp \rightarrow WH$, $pp \rightarrow \gamma\gamma$ and $b\bar{b} \rightarrow H$ [30, 31, 32, 33, 34]. Only in the last year have the first complete NNLO corrections for $2 \rightarrow 2$ scattering processes been computed. Still many processes exist for which NNLO calculations are in particular demand, such as $pp \rightarrow jj, jW, jZ, jH, WW, ZZ, ZH, t\bar{t}$ to list just the most important. Large efforts are ongoing and still required to complete these calculations.

Computing observables beyond NLO remains an extremely challenging task and constantly requires the developments of more powerful methods to tackle the growing mathematical complexity. Due to the appearance of overlapping singularities, the cancellation of infra-red divergences becomes highly non-trivial at higher orders. A number of different approaches have been developed to deal with this problem.

While first successful fully differential NNLO calculations were accomplished using Sector Decomposition [35, 36, 37, 38, 39, 40], many other methods have been put forward. Earlier developments proved that the phase space slicing method was also capable of dealing with the kinds of singularities met at NNLO [41]. Later methods were mostly based on the subtraction idea. These methods are the Antenna-subtraction method [42, 43, 44, 45], kt subtraction [46] and general subtraction [47, 48, 49, 50, 51]. Further propositions were presented in [52, 53, 54]. None of these approaches can yet claim a similar level of automation as the NLO methods. A further problem at NNLO is the appearance of highly singular multi scale two-loop integrals. While powerful integration techniques have been developed, like the differential equations methods [55, 26, 56] or the Mellin Barnes representation method [57, 58, 59, 60], many problems are still faced at this frontier.

In this thesis we shall develop a technique for the factorization of overlapping singularities, based on non-linear mappings. With the non-linear mapping we will show that singularities can be factorised in a more economical way, then with the previous sector decomposition approach which easily leads to a proliferation of integrals. We will demonstrate how the non-linear mapping can be applied systematically to loop and phase-space integrals. We shall use the method to obtain a number of phenomenologically important results.

The thesis is organised as follows. A more technical introduction to some of the key concepts underlying perturbative QCD, which are needed at later stages, will be given in chapter 2. Chapter 3 discusses typical forms of factorised and non-factorised singularities. Further more, we will here develop the method of non-linear mappings. In chapter 4 we apply non-linear mappings to factorise singular loop integrals. In chapter 5 we will introduce a method to factorise and evaluate phase-space integrals of single and double real radiation for the hadronic production of massive systems. In chapter 6 we will introduce a method to factorise and evaluate phase-space integrals of single and double real radiation for decay processes of massive particles into two massless particles. An application of the methods developed in chapter 6 to the fully differential calculation of the decay width of a Higgs boson into a bottom quark anti-quark pair is given in chapter 7. An application of the methods developed in chapter 5 to the fully differential calculation of the hadronic production of a Higgs boson in bottom quark fusion is given in chapter 8. In chapter 9 we present d-dimensional helicity amplitudes for the process $H \rightarrow gggg$.

Chapter 2

Perturbative QCD

2.1 The QCD Lagrangian

In this section we will briefly review some of the key concepts underlying QCD. This is intended mainly to establish the notation, which will be used throughout this work. For derivations and more complete discussions of the quantum field theory involved, the references [61, 62, 63, 64, 65, 66, 67, 68] should be consulted, though this list is by no means complete.

The theory of QCD is formulated as a non-abelian gauge theory of gauge group $SU(3)$. However since considerable interest exists in the more general case of $SU(N)$, we shall keep the number of color charges N a free parameter throughout.

At the heart of QCD lies its classical Lagrangian,

$$\mathcal{L}_{\text{classical}} = -\frac{1}{4}F_{\mu\nu}^a F_a^{\mu\nu} + \sum_{i=1}^{n_f} \bar{q}_i (i\not{D} - m_i) q_i, \quad (2.1)$$

where the field strength F is defined as

$$F_{\mu\nu}^a = \partial_\mu A_\nu^a - \partial_\nu A_\mu^a - gf^{abc} A_\mu^b A_\nu^c \quad (2.2)$$

and the covariant derivative is defined via

$$\not{D} = D_\mu \gamma^\mu = (\partial_\mu - ig A_\mu^a T^a) \gamma^\mu. \quad (2.3)$$

Here we used the standard Feynman slash notation, $\not{p} = p_\mu \gamma^\mu$. The γ -matrices

satisfy the anti-commutation relation

$$\{\gamma^\mu, \gamma^\nu\} = 2g^{\mu\nu}. \quad (2.4)$$

The Lagrangian describes interactions of non-abelian spin 1 gauge fields A^μ with spin $\frac{1}{2}$ fields q_i of flavor i and mass m_i , which live in the fundamental representation of $SU(N)$. n_f shall denote the number of different quark flavors. The gauge group $SU(N)$ is generated by the generators T^a where $a = 1, \dots, N^2 - 1$, which satisfy the commutation relation

$$[T^a, T^b] = if^{abc}T^c. \quad (2.5)$$

The antisymmetric structure constants f^{abc} are directly related to the generators of the adjoint representation by the relation $(T_A)^a_{bc} = -if^{abc}$. We will use the fairly common normalisation

$$\text{Tr}(T^a T^b) = T_F \delta^{ab}, \quad T_F = \frac{1}{2}; \quad (2.6)$$

such that

$$\text{Tr}(T_A^a T_A^b) = C_A \delta^{ab}, \quad C_A = N \quad (2.7)$$

and

$$\sum_b (T_A^b T_A^b)_{ac} = C_F \delta_{ac}, \quad C_F = \frac{N^2 - 1}{2N}. \quad (2.8)$$

The Lagrangian is invariant under local gauge transformations of the gauge and quark fields:

$$\begin{aligned} A_\mu^a T^a &\rightarrow U \left(A_\mu^a T^a + \frac{i}{g} \partial_\mu \right) U^\dagger \\ q &\rightarrow U q \\ \bar{q} &\rightarrow \bar{q} U^\dagger, \end{aligned} \quad (2.9)$$

where

$$U = \exp(i\theta^a(x)T^a). \quad (2.10)$$

The parameter $\theta^a(x)$ can be an arbitrary function of space-time and parametrises the gauge freedom. For non-physical polarisation states of the gauge field not to affect physical quantities, we must further include a ghost term $\mathcal{L}_{\text{ghost}}$, as well as a

gauge fixing term $\mathcal{L}_{\text{gauge-fixing}}$. The complete QCD Lagrangian is therefore

$$\mathcal{L}_{\text{QCD}} = \mathcal{L}_{\text{classical}} + \mathcal{L}_{\text{ghost}} + \mathcal{L}_{\text{gauge-fixing}}, \quad (2.11)$$

where

$$\mathcal{L}_{\text{gauge-fixing}} = -\frac{1}{2\xi} (\partial^\mu A_\mu^a)^2, \quad (2.12)$$

with ξ a free parameter through which a certain gauge may be selected, and

$$\mathcal{L}_{\text{ghost}} = \partial_\mu c^{a\dagger} D_{ab}^\mu c^b, \quad (2.13)$$

where the ghost field c is an anti-commuting scalar field.

2.2 Feynman rules for QCD

The Feynman rules for QCD can be derived in the Path Integral formalism. This subject is covered very well in many standard texts, e.g. [61, 62, 63, 64]. For our convenience we present the Feynman rules here. Gluon self interactions are presented in Figure 2.1, gluon-fermion and ghost interactions are presented in Figure 2.2 and gluon, fermion and ghost propagators are presented in Figure 2.3. We shall adopt the convention that all momenta, denoted by p_i^μ and k^μ , are outgoing. ε is a small real positive parameter. The gluon self interactions are expressed in terms of the Lorentz generators,

$$\mathcal{J}^{\mu\nu;\alpha\beta} = i (g^{\mu\alpha} g^{\nu\beta} - g^{\nu\alpha} g^{\mu\beta}), \quad (2.14)$$

of the vector representation. Further we use the notation $\mathcal{J}^{p\nu;\alpha\beta} \equiv p_\mu \mathcal{J}^{\mu\nu;\alpha\beta}$.

2.3 Divergences, renormalisation and dimensional regularisation

Beyond tree-level, most quantum field theories suffer from divergences and are thus not defined without a prescription which allows to regularise these divergences. A number of regularisation schemes exist, the most commonly used ones are dimensional regularisation, Pauli-Villars regularisation and cut-off regularisation. In this work we will only be concerned with dimensional regularisation, which is generally regarded to as the scheme of choice, since it preserves both Lorentz and gauge symmetry. Dimensional regularisation amounts to an analytic continuation of the theory

$$\begin{aligned}
&= -g^2 \left[\begin{aligned} &+ f^{a_1 a_2 a} f^{a a_3 a_4} \mathcal{J}^{\mu_1 \mu_2; \mu_3 \mu_4} \\ &+ f^{a_1 a_3 a} f^{a a_2 a_4} \mathcal{J}^{\mu_1 \mu_3; \mu_2 \mu_4} \\ &+ f^{a_1 a_4 a} f^{a a_3 a_2} \mathcal{J}^{\mu_1 \mu_4; \mu_3 \mu_2} \end{aligned} \right] \\
&= -ig f^{a_1 a_2 a_3} \left[\mathcal{J}^{p_1 \mu_1; \mu_2 \mu_3} + \mathcal{J}^{p_2 \mu_2; \mu_3 \mu_1} + \mathcal{J}^{p_3 \mu_3; \mu_1 \mu_2} \right]
\end{aligned}$$

Figure 2.1: Gluon self interactions

$$\begin{aligned}
&= ig T_{ji}^a \gamma^\mu \\
&= gf^{abc} p^\mu
\end{aligned}$$

Figure 2.2: Gluon, fermion and ghost interactions

to $d = 4 - 2\epsilon$ dimensions. The origin of the divergences can be traced back to particular kinematic configurations of real or virtual particles. One type of divergence occurs when a virtual particle, circulating in a loop, gains infinite momentum. Such divergences are termed UV divergences. Another class of divergences occur when massless particles have either zero energy or become collinear to each other. We

[illegible]

$$i \quad \longrightarrow \quad j \quad = \quad \frac{i\delta_{ij}(k+m)}{k^2 - m^2 + i\varepsilon}$$

$$a \quad \text{---} \rightarrow \text{---} \quad b = \frac{i\delta_{ab}}{k^2 + i\varepsilon}$$

Figure 2.3: Gluon, fermion and ghost propagators

shall denote these singularities as IR divergences.

2.3.1 Renormalisation

In renormalisable Quantum Field Theories, these include abelian and non-abelian gauge theories, UV divergences are finite for $d < 4$. Working in $d = 4 - 2\epsilon$ therefore allows to treat these divergences as poles in ϵ . UV divergences can be dealt with by absorbing these poles into physical parameters and external wave-functions. This procedure is known as *renormalisation*. For QCD, renormalisation results in the following replacements:

$$\begin{aligned} q &\rightarrow Z_q^{1/2}q, & \bar{q} &\rightarrow Z_q^{1/2}\bar{q}, \\ A^\alpha &\rightarrow Z_A^{1/2}A^\alpha, & c &\rightarrow Z_c^{1/2}c, \\ m &\rightarrow Z_m m\mu^\epsilon, & g &\rightarrow Z_g g\mu^\epsilon, & \xi &\rightarrow Z_\xi \xi. \end{aligned} \quad (2.15)$$

In the above we also introduced the regularisation scale μ in the renormalisation of the gauge coupling g and quark mass m_i . This is to keep the action,

$$S = \int d^d x \mathcal{L}_{\text{QCD}}, \quad (2.16)$$

dimensionless in d dimensions, without having to alter the dimension of the fields. In this work we will only need the renormalisation of the gauge coupling strength

$\alpha_s = g^2/(4\pi)$ and the mass parameter m_i . In the $\overline{\text{MS}}$ scheme these read:

$$m_i \rightarrow m_i S_\epsilon^{-1/2} \left\{ 1 - \frac{\alpha_s}{4\pi} \frac{3C_F}{\epsilon} + \left(\frac{\alpha_s}{4\pi} \right)^2 \left[-\frac{1}{\epsilon^2} \left(2T_F n_f - \frac{9}{2}C_F - \frac{11}{2}C_A \right) + \frac{1}{\epsilon} \left(\frac{5T_F}{3} n_f - \frac{3C_F}{4} - \frac{97}{12}C_A \right) \right] C_F + \mathcal{O}(\alpha_s^3) \right\} \quad (2.17)$$

$$\alpha_s \rightarrow \alpha_s S_\epsilon^{-1} \left\{ 1 - \frac{\alpha_s}{4\pi} \frac{1}{\epsilon} \left[\frac{11C_A}{3} - \frac{4T_F n_f}{3} \right] + \mathcal{O}(\alpha_s^2) \right\}, \quad (2.18)$$

where

$$S_\epsilon = \left(\frac{4\pi}{\mu^2 e^{\gamma_E}} \right)^\epsilon = 1 + \epsilon(\log 4\pi - \log \mu^2 - \gamma_E) + \mathcal{O}(\epsilon^2) \quad (2.19)$$

and $\gamma_E \simeq 0.577215665$ is the Euler-Mascheroni constant. The renormalized strong coupling and quark mass parameter depend on the regularisation scale μ ,

$$\alpha_s \equiv \alpha_s(\mu) \quad m_i \equiv m_i(\mu), \quad (2.20)$$

and satisfy the following evolution equations

$$\begin{aligned} \frac{\partial \alpha_s(\mu)}{\partial \log \mu^2} &= \beta(\mu) \alpha_s(\mu), \\ \frac{\partial m_i(\mu)}{\partial \log \mu^2} &= \gamma^{(i)}(\mu) m_i(\mu). \end{aligned} \quad (2.21)$$

The beta function $\beta(\mu)$ as well as the anomalous dimension of the quark mass $\gamma(\mu)$ may themselves be expanded perturbatively

$$\begin{aligned} \beta(\mu) &= - \sum_{n=0}^{\infty} \beta_n \left(\frac{\alpha_s(\mu)}{\pi} \right)^{n+1} \\ \gamma(\mu) &= - \sum_{n=0}^{\infty} \gamma_n \left(\frac{\alpha_s(\mu)}{\pi} \right)^{n+1}. \end{aligned} \quad (2.22)$$

The coefficients of $\beta(\mu)$ and $\gamma(\mu)$ are directly connected to the Z s we introduced in eq.(2.15). This can be seen by noting that before renormalisation the bare coupling constant were, of course, independent of the scale μ . Hence also after renormalisation the products $Z_\alpha \alpha \mu^{2\epsilon}$ and $Z_{m_i} m_i \mu$ must be independent of μ , leading to the conclusion that the coefficients β_i and γ_i can be matched to the coefficients of the perturbative expansions of Z_α and Z_{m_i} order by order in perturbation theory. In

our convention this leads to the following relations:

$$\begin{aligned}\gamma_0 &= \frac{3}{4}C_F, & \gamma_1 &= \frac{97}{96}C_FC_A + \frac{3}{32}C_F^2 - \frac{5}{24}T_Fn_f, \\ \beta_0 &= \frac{11}{12}C_A - \frac{1}{3}T_Fn_f, & \beta_1 &= \frac{17}{24}C_A^2 - \frac{1}{4}(C_F + 10C_A)T_Fn_f.\end{aligned}\quad (2.23)$$

The fact that the coupling in QCD decreases with increasing scale, as can be readily confirmed from the above coefficients, is known as property of *asymptotic freedom* and lead to the Nobel Prize in Physics 2004, awarded jointly to David J. Gross, H. David Politzer and Frank Wilczek. QCD therefore becomes more weakly coupled at higher energies, making the perturbative series a more reliable tool. It further means that, unlike QED, QCD is well defined at higher energies. In Appendix D we discuss in some detail the implications of renormalisation group invariance on the scale dependence of cross-sections. Further discussions on the topic of renormalisation are left to the literature, e.g. [61, 62, 63, 64, 65, 66, 67, 69].

2.3.2 Infrared Divergences

Unlike UV divergences, IR divergences cancel for infra-red safe observables like cross-sections or decay widths. Nevertheless since the divergences are there at intermediate states in higher order calculations, they require regularisation.

Fortunately dimensional regularisation can be used also here. Since IR divergences are of logarithmic nature, IR divergent amplitudes are finite for $d > 4$ and are thus well defined for $\epsilon < 0$. This is in contrast to UV divergences, which formally require $\epsilon > 0$. A possible strategy would be to separate the UV divergences for $\epsilon > 0$ and from the IR divergences defined at $\epsilon < 0$ and evaluate the integrals separately. This can in fact always be achieved, see for example [69], but is rather impractical in calculations. Instead what is done is to treat IR and UV divergences on the same footing, i.e. by using an identical ϵ for both types. This even leads to cancellations of the latter. Since the final result for a given infra-red safe observable should be free of poles, whether UV or IR, and is therefore finite in the limit $\epsilon \rightarrow 0$, it is only an academic exercise to keep track of the precise way in which the poles are cancelled and we are therefore free to treat them on the same footing when performing calculations of scattering rates.

2.4 The d -dimensional phase space measure

The Lorentz invariant phase space measure is of key importance to all computations of cross-section and decay-rates in particle physics. In order to regularise infra-red divergences which manifest themselves in certain regions of phase-space it is essential to keep the measure d -dimensional. We define the expression for the phase-space measure here, since we shall often make use of it later.

$$d\Phi_n(\sqrt{s}; m_1, \dots, m_n) = \left(\prod_{i=1}^n \frac{d^d p_i}{(2\pi)^d} \delta^+(p_i^2 - m_i^2) (2\pi) \right) \delta^{(d)} \left(q_1 + q_2 - \sum_{i=1}^n p_i \right) (2\pi)^d. \quad (2.24)$$

Here we use the notation $\delta^+(p_i^2 - m_i^2) = \delta(p_i^2 - m_i^2) \theta(p^0)$, to indicate that only positive energy solutions are allowed. The phase-space volume satisfies the following useful factorization property

$$\Phi_n(\sqrt{s}; m_1, \dots, m_n) = \int \frac{ds_{k..n}}{(2\pi)} \Phi_k(\sqrt{s}; m_1, \dots, m_{k-1}, \sqrt{s_{k..n}}) \Phi_{n-k+1}(\sqrt{s_{k..n}}; m_k, \dots, m_n), \quad (2.25)$$

where $1 < k < n$ and we defined

$$s_{k..n} = (p_k + \dots + p_n)^2. \quad (2.26)$$

This factorization property can be proven straight forwardly by inserting

$$\begin{aligned} 1 &= \int \frac{ds_{k..n}}{(2\pi)} \delta^+(s_{k..n} - (p_k + \dots + p_n)^2) (2\pi) \\ &\times \int \prod_{i=1}^n \frac{d^d p_{k..n}}{(2\pi)^d} \delta^{(d)} \left(p_{k..n} - \sum_{i=k}^n p_i \right) (2\pi)^d \end{aligned} \quad (2.27)$$

into eq.(2.24).

2.5 Cross sections and decay rates

The formula for computing a cross-section, $\sigma_{2 \rightarrow n}(s; \{m_i\})$, corresponding to the scattering of 2 massless particles of center of mass energy \sqrt{s} into n massive particles of masses m_i is given by

$$\sigma_{2 \rightarrow n}(\sqrt{s}; \{m_i\}) = \frac{1}{2s} \int d\Phi_n(\sqrt{s}; m_1, \dots, m_n) |\mathcal{A}_{2 \rightarrow n}(\{p\})|^2, \quad (2.28)$$

where $d\Phi_n(\sqrt{s}; m_1, \dots, m_n)$ is the differential, Lorentz invariant, phase space element defined in eq.(2.24). With $|\mathcal{A}_{2 \rightarrow n}(\{p\})|^2$ we shall denote the spin summed and averaged squared amplitude for the $2 \rightarrow n$ scattering process, which is in general a function of the set of Lorentz invariant scalar products of the set of all momenta involved in the process. The amplitudes for all QCD processes can, at least in principle, be computed to a given order with the Feynman rules we presented in section 2.2. The formula corresponding to the decay rate of a particle of mass m into n massive particles of masses m_i is, in the same notation, given by

$$\Gamma_{1 \rightarrow n}(m; \{m_i\}) = \frac{1}{2m} \int d\Phi_n(m; m_1, \dots, m_n) |\mathcal{A}_{1 \rightarrow n}(\{p\})|^2. \quad (2.29)$$

Chapter 3

Divergent integrals and non-linear mappings

Loop and phase-space integrals which arise in perturbative Quantum Field Theory often suffer from infra-red and ultra-violet divergences in four space-time dimensions. Analytic continuation of the dimension to $d = 4 - 2\epsilon$, allows to isolate the divergent pieces as poles in ϵ .

It is always possible to represent loop and phase-space integrals as multi-dimensional integrals on the unit-hypercube. In this chapter we will discuss typical forms which singularities take in such integrals. Further we will review existing methods to achieve Laurent expansions for arbitrary numerator functions, focusing in particular on numerical approaches. The technique for the factorisation of overlapping singularities via non-linear mappings will be introduced and developed.

3.1 Factorised singularities

The simplest divergent structure one may encounter contains a single factorised logarithmic singularity at $x = 0$:

$$I = \int_0^1 dx x^{-1+\alpha\epsilon} f(x), \tag{3.1}$$

where $f(x)$ is an integrable function which is finite but non-zero at the point of the singularity. It is easy to see that a singularity at $x = 0$ is equivalent to a singularity

at $x = 1$ via the mapping $x \mapsto \bar{x}$, where we introduced

$$\boxed{\bar{x} \equiv 1 - x.} \quad (3.2)$$

One also often encounters both singularities at the same time, i.e. integrals of the form

$$I = \int_0^1 dx x^{-1+\alpha\epsilon} \bar{x}^{-1+\beta\epsilon} f(x). \quad (3.3)$$

Using the partial fractioning identity

$$x^{-1+\alpha\epsilon} \bar{x}^{-1+\beta\epsilon} = x^{\alpha\epsilon} \bar{x}^{-1+\beta\epsilon} + x^{-1+\alpha\epsilon} \bar{x}^{\beta\epsilon} \quad (3.4)$$

we can always write eq.(3.3) as a sum of two integrals of type eq.(3.1). Alternatively such divergences may be separated by splitting the integral into two sectors, such that $x \in [0, 1/2]$ in the first and $x \in [1/2, 1]$ in the second sector. We may therefore continue our discussion by focusing only on integrals of type eq.(3.1).

Taylor expanding the numerator of eq.(3.1), $f(x)$, around $x = 0$ we obtain

$$I = \sum_{n=0}^{\infty} \frac{f^{(n)}(0)}{n!} \int_0^1 dx x^{-1+n+\alpha\epsilon}, \quad f^{(n)}(x) = \frac{\partial^n f(x)}{\partial x^n}. \quad (3.5)$$

It is then clear that the logarithmic singularity is only present in the first term of the Taylor series, and that its residue is $f(0)$. The singular piece of eq.(3.1) can thus easily be subtracted out, allowing us to obtain the full Laurent expansion in ϵ as

$$\begin{aligned} I &= f(0) \int_0^1 dx x^{-1+\alpha\epsilon} + \int_0^1 dx x^{\alpha\epsilon} \left(\frac{f(x) - f(0)}{x} \right) \\ &= \frac{f(0)}{\alpha\epsilon} + \sum_{n=0}^{\infty} \frac{(\alpha\epsilon)^n}{n!} \int_0^1 dx \log^n(x) \left(\frac{f(x) - f(0)}{x} \right). \end{aligned} \quad (3.6)$$

It is worth remarking that it was not necessary to perform any non-trivial integrals in order to obtain this Laurent expansion. Furthermore the coefficients of ϵ^n are now well defined convergent integrals which may even be computed numerically, if an analytic evaluation should appear to be infeasible. This option may become particularly attractive when the boundaries of the integral are wanted to be kept arbitrary or only a subspace of the integration range would be of interest according to, for example, the wishes of the experimentalists. Since our major motivation is phenomenological, this point will be of crucial importance in the chapters to come.

Indeed eq.(3.6) can be summarized neatly in the following identity:

$$x^{-1+\alpha\epsilon} = \frac{\delta(x)}{\alpha\epsilon} + \sum_{n=0}^{\infty} \frac{(\alpha\epsilon)^n}{n!} \mathcal{D}_n(x), \quad (3.7)$$

where $\mathcal{D}_n(x) = \left[\frac{\ln^n(x)}{x} \right]_+$ and the plus-distribution is defined through

$$\int_0^1 dx f(x) \left[\frac{g(x)}{x} \right]_+ = \int_0^1 dx g(x) \left(\frac{f(x) - f(0)}{x} \right). \quad (3.8)$$

Laurent expansions for integrals of the type

$$I = \int_0^1 \left(\prod_{i=1}^n dx_i x_i^{-1+\alpha_i\epsilon} \bar{x}_i^{-1+\beta_i\epsilon} \right) f(x_1, \dots, x_n) \quad (3.9)$$

can then be obtained via eq.(3.4) and eq.(3.7).

While divergences in gauge theories are only believed to be of logarithmic degree, it may occur that one encounters divergences in partial results, which appear to have a worse behaviour. Let us for example consider the integral

$$I = \int_0^1 dx x^{-2+\alpha\epsilon} f(x), \quad (3.10)$$

which carries a quadratic divergence. Taylor expanding $f(x)$ around $x = 0$ we see that the first term in the expansion, $f(0)$, leads to a pole in $(\alpha\epsilon - 1)$, and that the second term gives the pole in ϵ . In order to obtain a Laurent expansion we must therefore subtract the first two coefficients of the expansion, i.e. rewrite eq.(3.10) as

$$\begin{aligned} I &= f(0) \int_0^1 dx x^{-2+\alpha\epsilon} + f^{(1)}(0) \int_0^1 dx x^{-1+\alpha\epsilon} + \int_0^1 dx x^{\alpha\epsilon} \left(\frac{f(x) - f(0) - x f^{(1)}(0)}{x^2} \right) \\ &= \frac{f(0)}{\alpha\epsilon - 1} + \frac{f^{(1)}(0)}{\alpha\epsilon} + \sum_{n=0}^{\infty} \frac{(\alpha\epsilon)^n}{n!} \int_0^1 dx \log^n(x) \left(\frac{f(x) - f(0) - x f^{(1)}(0)}{x^2} \right). \end{aligned} \quad (3.11)$$

In the same manner yet more divergent integrals may also be subtracted.

3.2 Overlapping singularities

An overlapping singularity arises when two or more variables of integration must simultaneously tend towards a fixed value to create the singularity.

Here we will restrict ourselves to the situation where the overlapping singularity will occur only at the boundary of the region of integration.

For factorised singularities it was rather straight forward to determine the degree of divergence. Indeed the degree of divergence of the integral

$$I = \int_0^1 dx \frac{f(x)}{x^n} \quad (3.12)$$

could be considered to be n . For overlapping singularities the situation is a little more complicated. Let us consider the integral

$$I = \int_0^1 dx_1 dx_2 \frac{f(x_1, x_2)}{h(x_1, x_2)}, \quad (3.13)$$

where $h(x_1, x_2)$ shall denote a function responsible for an overlapping logarithmic singularity at the point $x_1 = 0 = x_2$. Let us focus only on the most divergent part of this integral. In this limit we may consider $f(x_1, x_2) \sim f(0, 0)$. Furthermore we are free to change the upper boundaries of integration since this can also not affect the singular part. Hence we can change the upper boundary of the unit square into a quarter unit disk. This allows us to change variables to polar coordinates,

$$(x_1, x_2) = (r \cos \theta, r \sin \theta), \quad (3.14)$$

such that the overlapping singularity at the point $x_1 = 0 = x_2$ becomes factorised at $r = 0$. The most singular part of the integral is thus also captured by

$$I = f(0, 0) \int_0^{\frac{\pi}{2}} d\theta \int_0^1 dr \frac{r}{h(r \cos \theta, r \sin \theta)}. \quad (3.15)$$

It follows that for a logarithmic singularity to be present we must have $h \propto r^2 + \mathcal{O}(r^3)$. And so the condition for $h(x_1, x_2)$ to contain a singularity of degree k at $x_1 = 0 = x_2$ is that

$$h(x, x) \propto x^{k+1} + \mathcal{O}(x^{k+2}). \quad (3.16)$$

We can generalise the above argument to the n -variable case. The condition for the integral

$$I = \int_0^1 dx_1 dx_2 \dots dx_n \frac{f(x_1, x_2, \dots, x_n)}{h(x_1, x_2, \dots, x_n)} \quad (3.17)$$

to carry an overlapping singularity at the point $x_1 = x_2 = \dots = x_n = 0$, of degree of

divergence k , is thus

$$h(x, x, \dots, x) \propto x^{k+n-1} + \mathcal{O}(x^{k+n}) . \quad (3.18)$$

The latter statement can be proven identically, using polar coordinates in n dimensions. This condition may be faked by, for example, $h(x_1, x_2, \dots, x_n) = x_1^{k+n-1}$, but this singularity would be present in the entire hyperplane defined by $x_1 = 0$, and would therefore give rise to a much higher degree of divergence away from the point $x_1 = x_2 = \dots = x_n = 0$. Let us focus again on the two-dimensional case. If we assume the function h of eq.(3.13) to be a polynomial it must be a quadratic form, if it is to give rise to a logarithmic divergence. A general Ansatz would yield

$$h(x_1, x_2) = a_{11}x_1^2 + 2a_{12}x_1x_2 + a_{22}x_2^2 , \quad (3.19)$$

where the a_{ij} may even be functions of x_1 and x_2 themselves, as long as they do not spoil the overall quadratic behaviour in the singular limit and do not allow for further singularities inside the unit square. However non-polynomial realisations are plentiful, for example

$$h(x_1, x_2) = \frac{(x_1 + x_2)^4}{(ax_1 + x_2)^2} . \quad (3.20)$$

would also scale with r^2 . We shall therefore not be concerned with writing down the most general structure which is possible. Nevertheless eq.(3.19) already captures a number of interesting features. Let us regularize the integral as follows

$$I = \int_0^1 dx_1 dx_2 x_1^{\alpha\epsilon} x_2^{\beta\epsilon} \frac{f(x_1, x_2)}{[h(x_1, x_2)]^{1-\gamma\epsilon}} . \quad (3.21)$$

While this is not the most general choice, it captures typical examples which we encounter in loop and phase space integrals. The case $a_{11} = a_{12} = a_{22} = 1, \alpha = \beta = 0, \gamma = 1$,

$$I_1 = \int_0^1 dx_1 dx_2 \frac{f(x_1, x_2)}{(x_1 + x_2)^{2-2\epsilon}} , \quad (3.22)$$

is an instructive example. In some sense it is a minimal overlapping singularity, since its denominator polynomial is linear while the power by which it is raised is maximal. Similarly the minimal overlapping logarithmic singularity containing n

variables could be defined as

$$I_n = \int_0^1 \left(\prod_{i=1}^n dx_i \right) \frac{f(\{x_i\})}{[\sum_{i=1}^n x_i]^{n-\epsilon}}. \quad (3.23)$$

Another example is the case $a_{11} = a_{12} = 1, a_{22} = 0, \alpha = 1, \beta = 0 = \gamma$:

$$I_2 = \int_0^1 dx_1 dx_2 x_1^\epsilon \frac{f(x_1, x_2)}{x_1(x_1 + x_2)}. \quad (3.24)$$

We will often encounter similar structures in phase-space integrals. Besides the overlapping singularity at $x_1 = 0 = x_2$ the denominator of this integral contains a factorised logarithmic singularity at $x_1 = 0$. We shall highlight this feature by regarding the engagement of x_1 in the overlapping singularity as *active* and the one of x_2 as *passive*. Using the Feynman parameter identity

$$\frac{1}{A_1 A_2} = \int_0^1 dy \frac{1}{[y A_1 + \bar{y} A_2]^2} \quad (3.25)$$

we can combine a product of denominators into a single denominator. Applying this identity with $A_2 = x_1$ and $A_1 = x_1 + x_2$ yields

$$I_2 = \int_0^1 dx_1 dx_2 dy x_1^\epsilon \frac{f(x_1, x_2)}{(x_1 + x_2 y)^2}. \quad (3.26)$$

This integral contains two entangled overlapping singularities, one at $x_1 = 0 = x_2$ and another one at $x_1 = 0 = y$. Of course the engagement of x_1, x_2 and y in the overlapping singularity is now completely *passive*. In turn, Feynman parameters allow us to transform integrals containing active singularities into higher dimensional integrals which contain only passive, but entangled, singularities.

3.3 Methods for overlapping singularities

There are two, commonly used, ways to deal with overlapping singularities in the presence of an arbitrary numerator function:

1. A subtraction which generalises eq.(3.6) to overlapping singularities.
2. A method of factorisation, making it possible to use the simple subtraction identity of eq.(3.7) also for overlapping singularity.

We will describe both approaches in the next sections.

3.3.1 The subtraction method for overlapping singularities

The subtraction method generalises eq.(3.6) to overlapping singularities. As an example let us consider the integral of eq.(3.22). We can expand the function $f(x_1, x_2)$ around the origin as

$$f(x_1, x_2) = f(0, 0) + x_1 \frac{\partial f(0, 0)}{\partial x_1} + x_2 \frac{\partial f(0, 0)}{\partial x_2} + \dots \quad (3.27)$$

As was the case for the factorised singularity, we can use power counting to infer that the logarithmic divergence is only present in the first term of the series. Hence the piece containing the pole can be subtracted as follows

$$I_1 = f(0, 0) \int_0^1 \frac{dx_1 dx_2}{(x_1 + x_2)^{2-2\epsilon}} + \int_0^1 dx_1 dx_2 (x_1 + x_2)^{-2\epsilon} \left[\frac{f(x_1, x_2) - f(0, 0)}{(x_1 + x_2)^2} \right] \quad (3.28)$$

In our simple example the first integral can easily be done analytically,

$$\begin{aligned} \int_0^1 \frac{dx_1 dx_2}{(x_1 + x_2)^{2-2\epsilon}} &= \frac{1}{\epsilon} \frac{2^{2\epsilon-1} - 1}{(2\epsilon - 1)} \\ &= \frac{1}{2\epsilon} + (1 - 2 \log(2)) + \epsilon (2 - 2 \log(2) + 2 \log^2(2)) + \mathcal{O}(\epsilon^2). \end{aligned} \quad (3.29)$$

Hence no longer only the pole but also finite contributions are subtracted through all orders in ϵ . When dealing with more complicated overlapping singularities, especially when more external scales are involved, analytic integration will become more difficult. In such cases powerful methods are needed to tackle the problem. Methods which have been applied in this context are the differential equations methods [55, 26, 56] and the Mellin Barnes representation method [57, 58, 59, 60].

The subtraction method can then be generalised to overlapping singularities but comes at a high cost. While it may appear difficult, if possible, to automatize it generally it has found much application in real radiation problems in QCD. Here subtraction limits can usually be inferred from QCD factorization theorems. We will discuss the different approaches in some more detail in chapter 5.

3.3.2 Sector Decomposition

The first fully automated method to factorise overlapping singularities is sector decomposition [11, 12, 13]. We illustrate the method on our simple example integral eq.(3.22). To factorise the overlapping singularity at $x_1 = 0 = x_2$, we sector decompose by inserting

$$1 = \theta(x_1 - x_2) + \theta(x_2 - x_1) \quad (3.30)$$

where $\theta(x)$ is the Heaviside step function. In each of the two sectors which are created through this decomposition we rescale the integration variable back on the unit hypercube, using $x_2 \mapsto x_1 x_2$ in the first and $x_1 \mapsto x_1 x_2$ in the second sector. This factorizes the integrand since both variables contributing to the overlapping singularity now scale with either x_1 or x_2 in both sectors. We obtain

$$I_1 = \int_0^1 dx_1 dx_2 x_1^{-1+2\epsilon} \frac{f(x_1, x_1 x_2)}{(1+x_2)^{2-2\epsilon}} + \int_0^1 dx_1 dx_2 x_2^{-1+2\epsilon} \frac{f(x_1 x_2, x_2)}{(1+x_1)^{2-2\epsilon}} \quad (3.31)$$

A Laurent expansion can now be achieved by invoking eq.(3.7). The same procedure also works on our second example, we obtain

$$I_2 = \int_0^1 dx_1 dx_2 x_1^{-1+\epsilon} \frac{f(x_1, x_1 x_2)}{1+x_1} + \int_0^1 dx_1 dx_2 (x_1 x_2)^{-1+\epsilon} \frac{f(x_1 x_2, x_2)}{1+x_2}. \quad (3.32)$$

In fact the only information needed for sector decomposition is the location of the singularity in the integrand, here the point $(0, 0)$. A factorisation is then imminent, making the algorithm easy to automate. However when more complicated singularities are encountered, the algorithm will unavoidably lead to a proliferation of integrals. This feature makes it desirable to have a more economical alternative.

3.3.3 Non-linear mappings

In the previous examples of sector decomposition, singularities were factorised by a rescaling of the integration parameters, e.g. $x_1 \mapsto x_1 x_2$ resulted in $x_1(x_1 + x_2) \mapsto x_1 x_2^2(1 + x_1)$. A linear rescaling is not possible on the unit interval without altering the boundaries. However, a rescaling is always possible when the integration boundaries are from zero to infinity. Let us therefore extend our upper boundary to infinity. This may be realised for example with the non-linear mapping

$$x_1 \mapsto \frac{x_1}{1+x_1}. \quad (3.33)$$

There is actually no particular reason here to choose x_1 over x_2 . But due to the $x_1 \leftrightarrow x_2$ symmetry of our example integral, it surely does not matter which one we choose. Our sample integral eq.(3.22) then transforms to

$$I_1 = \int_0^\infty dx_1 \int_0^1 dx_2 \frac{(1+x_1)^{-2\epsilon} f\left(\frac{x_1}{1+x_1}, x_2\right)}{(x_1+x_2(1+x_1))^{2-2\epsilon}}. \quad (3.34)$$

Indeed the rescaling did not alter the position of the singularity, which is still located at the origin. Now we are in a position to apply $x_1 \mapsto x_1 x_2$ without altering the boundaries. We obtain

$$I_1 = \int_0^\infty dx_1 \int_0^1 dx_2 x_2^{-1+2\epsilon} \frac{(1+x_1 x_2)^{-2\epsilon} f\left(\frac{x_1 x_2}{1+x_1 x_2}, x_2\right)}{(x_1 + (1+x_1 x_2))^{2-2\epsilon}}. \quad (3.35)$$

The singularity is now nicely factorised in x_2 and we are free to map the x_1 integral back to $[0, 1]$. The minimal choice is to apply the inverse of eq.(3.33)

$$x_1 \mapsto \frac{x_1}{1-x_1}, \quad (3.36)$$

this yields the final result

$$I_1 = \int_0^1 dx_1 dx_2 x_2^{-1+2\epsilon} (1-x_1+x_1 x_2)^{-2\epsilon} \frac{f\left(\frac{x_1 x_2}{1-x_1+x_1 x_2}, x_2\right)}{(1+x_1 x_2)^{2-2\epsilon}}. \quad (3.37)$$

The overall mapping of x_1 which we performed to factorise the singularity is therefore

$$x_1 \mapsto \frac{x_1 x_2}{1-x_1+x_1 x_2}. \quad (3.38)$$

It is worth pointing out what we have just accomplished. As was the case with Sector Decomposition we have managed to factorise the singularity in a single variable, yet it was not necessary to split the integration range. We have therefore circumvented the problem of proliferation of integrals. Letting $x_1 = x$ and $x_2 = A/B$, for reasons which will become apparent, we can write the general form of eq.(3.38) as:

$$x \mapsto \alpha(x, A, B) \equiv \frac{x A}{x A + \bar{x} B}, \quad \Re(A) > 0, \Re(B) > 0$$

(3.39)

The mapping fulfils a number of useful properties. One of these is that it treats x and \bar{x} on the same footing since

$$\bar{x} \mapsto 1 - \alpha(x, A, B) = \alpha(\bar{x}, B, A). \quad (3.40)$$

It contains the identity mapping,

$$\alpha(x, 1, 1) = x, \quad (3.41)$$

a composition rule,

$$\alpha(\alpha(x, A_1, B_1), A_2, B_2) = \alpha(x, A_1 A_2, B_1 B_2), \quad (3.42)$$

as well as the property

$$\alpha(x, A, B) = \alpha(x, 1/B, 1/A). \quad (3.43)$$

It then also follows that the inverse transformation must be

$$\alpha^{-1}(x, A, B) = \alpha(x, B, A) = \alpha(x, 1/A, 1/B). \quad (3.44)$$

The α -mapping then satisfies the group axioms by containing a composition rule, the identity mapping and the inverse mapping. Another interesting feature is that the α -mapping is intimately linked to Feynman parameters. Reconsider the basic Feynman parameter integral of eq.(3.25), applying $x \mapsto \alpha(x, A_1, A_2)$ results in

$$\int_0^1 dx \frac{1}{[xA_2 + \bar{x}A_1]^2} \mapsto \frac{1}{A_1 A_2} \int_0^1 dx = \frac{1}{A_1 A_2}. \quad (3.45)$$

In other words the α -mapping trivializes the Feynman parameter integral. While we could have obtained the above from the Feynman parameter identity, the α -mapping actually allows us to derive a more general result, valid for arbitrary x -dependent numerator functions

$$\int_0^1 dx \frac{f(x)}{[xA_1 + \bar{x}A_2]^n} \mapsto \int_0^1 dx \frac{[xA_2 + \bar{x}A_1]^{n-2}}{A_1^{n-1} A_2^{n-1}} f(\alpha(x, A_2, A_1)). \quad (3.46)$$

Substituting $A_1 = A_1 + A_2$ in the above yields yet another useful result

$$\int_0^1 dx \frac{f(x)}{[xA_1 + A_2]^n} \mapsto \int_0^1 dx \frac{[A_2 + \bar{x}A_1]^{n-2}}{(A_1 + A_2)^{n-1}A_2^{n-1}} f(\alpha(x, A_2, A_1 + A_2)). \quad (3.47)$$

Since we shall use this mapping frequently we shall denote it by

$$\boxed{\beta(x, A/B) \equiv \alpha(x, A, A + B) = \frac{x A}{A + \bar{x} B}} \quad (3.48)$$

While the use of non-linear mappings goes far beyond eqs.(3.46) and (3.47), one lesson to be learned is that terms which are of the form $xA_1 + \bar{x}A_2$ are naturally factorised with the α -mapping, while terms which are of the form $xA_1 + A_2$ are naturally factorised with the β mapping. As an example we can use eq.(3.47) recursively to factorise the minimal overlapping singularity involving n variables in eq.(3.23). Applying

$$x_1 \mapsto \beta \left(x_1, \sum_{i=2}^n x_i \right) \quad (3.49)$$

yields

$$I = \int_0^1 dx_1 \dots dx_n \frac{\tilde{f}(\{x_i\})}{[\sum_{i=2}^n x_i]^{(n-1)-\epsilon}}, \quad (3.50)$$

where

$$\tilde{f}(\{x_i\}) = \left(\bar{x}_1 + \sum_{i=2}^n x_i \right)^{n-\epsilon-2} \left(1 + \sum_{i=2}^n x_i \right)^{1-n+\epsilon} f(\{x_i\}). \quad (3.51)$$

The latter contains a minimal overlapping singularity involving only $n-1$ variables. Repeating the procedure $n-2$ times, i.e. mapping subsequently

$$\begin{aligned} x_2 &\mapsto \beta \left(x_2, \sum_{i=3}^n x_i \right) \\ x_3 &\mapsto \beta \left(x_3, \sum_{i=4}^n x_i \right) \\ &\vdots \\ x_{n-1} &\mapsto \beta(x_{n-1}, x_n) \end{aligned} \quad (3.52)$$

will thus lead to a single factorised logarithmic singularity.

Let us now explore the effect of non-linear mappings on our second test integral,

eq.(3.24). Since the sector decomposition algorithm essentially realizes all different scalings of the singular integration variables with respect to each other, we can learn much from the example eq.(3.32). There we saw that only the scaling present in the second sector $x_1 \mapsto x_1 x_2$ factorised the passive singularity in x_2 , meaning that it was the active singularity which had to be rescaled.

We therefore suspect ¹ that $x_1 \mapsto \beta(x_1, x_2)$ is the right mapping to use here. Applying it we obtain

$$I_2 = \int_0^1 dx_1 dx_2 (x_1 x_2)^{-1+\epsilon} (1 - x_1 + x_2)^{-\epsilon} f(\beta(x_1, x_2), x_2), \quad (3.53)$$

which indeed contains a factorised singularity structure. On the other hand when we apply $x_2 \mapsto \beta(x_2, x_1)$ we obtain

$$I_2 = \int_0^1 dx_1 dx_2 x_1^\epsilon \frac{f(x_1, x_2)}{x_1(x_1 + \bar{x}_2)}. \quad (3.54)$$

We see that mapping the passive singularity leaves (up to a mapping $x_2 \mapsto \bar{x}_2$) the integral untouched and certainly does not factorise the singularity. We can understand this to some degree by considering the Jacobian of the α -mapping,

$$\frac{\partial \alpha(x, A, B)}{\partial x} = \frac{AB}{[Ax + B\bar{x}]^2}. \quad (3.55)$$

The α (and therefore also β) -mapping therefore creates a quadratic denominator, which introduces a new singularity into the integral. Therefore, unless the variable which is being mapped is at least quadratic in the denominator, the Jacobian will be left at least partially un-cancelled and will introduce a new singularity into the integral. Having understood this concept we can establish the following rule of thumb: *When factorising overlapping singularities with the α -mapping in the presence of active and passive singularities, it is the active singularities which should be remapped.*

Another interesting connection is between non-linear mappings and hypergeometric argument transformations. Let us reconsider our example integral I_2 for the case of

¹ $x_1 \mapsto \alpha(x_1, x_2, 1)$ would have also factorised the singularity.

$f(x_1, x_2) = 1$. Using the integral representation,

$$B(b, c - b) {}_2F_1(a, b; c; z) = \int_0^1 dx x^{b-1} (1-x)^{c-b-1} (1-zx)^{-a} \quad (3.56)$$

we can rewrite I_2 as a one dimensional integral over a ${}_2F_1$ as follows

$$I_2 = \frac{1}{\epsilon} \int_0^1 dx_2 \frac{{}_2F_1(1, \epsilon; 1 + \epsilon; (x_2)^{-1})}{x_2}. \quad (3.57)$$

The overlapping singularity is now hiding at the singular point of the hypergeometric function, and the above integral is therefore not well defined as $\epsilon \rightarrow 0$. Pfaff's transformation can be used to factor out the singular behaviour and yields

$${}_2F_1(1, \epsilon; 1 + \epsilon; -(x_2)^{-1}) = (1 + x_2)^{-\epsilon} x_2^\epsilon {}_2F_1\left(\epsilon, \epsilon; 1 + \epsilon; \frac{1}{1 + x_2}\right). \quad (3.58)$$

Substituting this into eq.(3.57) and then translating it back to the integral representation with eq.(3.56) indeed recovers eq.(3.53) with $f(x) = 1$. While Pfaff's transformation may be seen as an analytic continuation identity, extending a function's range of validity to a different regime, we see that this can also be realised with a non-linear mapping in the integral representation. Non-linear mappings can therefore become an important analysis tool when studying yet unclassified functions. This of course is often the situation with Feynman integrals. Feynman integrals may generally be expressible in terms of hypergeometric functions or their generalisation, but making those connections may be rather non-trivial, if possible at all, for multi-scale multi-loop integrals.

3.3.4 A more complicated example with non-linear mappings

So far we have only discussed the α -mapping in the context of single variable transformations. Let us now consider a more complicated example. The integral

$$I_3 = \int dx_1 \dots dx_4 \frac{f(x_1, \dots, x_4)}{[x_1 x_2 + x_3 x_4]^{2-2\epsilon}} \quad (3.59)$$

illustrates well the kind of problems which we encounter when tackling more difficult integrals. A singularity analysis yields that there are four entangled overlapping singularities located at $x_1 = 0 = x_3$, $x_1 = 0 = x_4$, $x_2 = 0 = x_3$ and $x_2 = 0 = x_4$.

As a guideline we should always consider one variable at the time, rather than immediately try to guess the mapping which factorizes all singularities at once. In our example there is an absolute symmetry between the integration variables and we may just pick x_4 to start with. We then notice that the denominator is of the form $(Ax_4 + B)^n$ and so the identity of eq.(3.47) suggests that we apply

$$x_4 \mapsto \beta \left(x_4, \frac{x_1 x_2}{x_3} \right). \quad (3.60)$$

This results in

$$I_3 = \int dx_1 \dots dx_4 (x_1 x_2)^{-1+2\epsilon} (x_1 x_2 + x_3 \bar{x}_4)^{-2\epsilon} \frac{f(x_1, \dots, x_4)}{[x_1 x_2 + x_3]^{1-2\epsilon}}. \quad (3.61)$$

The mapping activated x_1 and x_2 , but left x_3 passive. We should therefore proceed by mapping either x_1 or x_2 , to scale either of the remaining singularities. We proceed by mapping $x_1 \mapsto \alpha(x_1, x_2, 1)$ to scale out the overlapping singularity in $x_2 = 0 = x_3$. This yields

$$I_3 = \int dx_1 \dots dx_4 (x_1 x_2 x_3)^{-1+2\epsilon} \frac{f(x_1, \dots, x_4)}{[\bar{x}_1 + x_1(x_2 + x_3)]^{1-2\epsilon}} \times (\bar{x}_1 + x_1 x_3)^{-2\epsilon} (x_1 x_2 + \bar{x}_1 \bar{x}_4 + x_1 x_3 \bar{x}_4)^{-2\epsilon}. \quad (3.62)$$

The last remaining overlapping singularity is located at $\bar{x}_1 = 0 = x_2 = 0 = x_3$. Here we must accomplish that all three variables have the same scaling. Since both x_2 and x_3 are active we may rescale them both at the same time with \bar{x}_1 . Applying $(x_2, x_3) \mapsto (\alpha(x_2, \bar{x}_1), \alpha(x_3, \bar{x}_1))$ we obtain

$$I_3 = \int dx_1 \dots dx_4 (x_1 \bar{x}_1 x_2 x_3)^{-1+2\epsilon} \frac{f(x_1, \dots, x_4)}{[1 - x_1^2 x_2 x_3]^{1-2\epsilon}} \times (1 - x_1 x_2)^{-2\epsilon} (\bar{x}_4 + x_1 x_2 x_4 - x_1^2 x_2 x_3)^{-2\epsilon} \quad (3.63)$$

The remaining overlapping singularity at $x_1 = x_2 = x_3 = 1$ is integrable and we are able to obtain its Laurent expansion. For the case $f(x_1, \dots, x_4) = 1$ we numerically obtain

$$I_3 = -\frac{0.25}{\epsilon^3} + \frac{0.49999(5)}{\epsilon^2} - \frac{0.1775(1)}{\epsilon} + 0.0546(5) + \mathcal{O}(\epsilon). \quad (3.64)$$

3.3.5 A two-variable non-linear mapping

The overall three-variable mapping which we effectively created with the last three mappings is:

$$(x_1, x_2, x_3) \mapsto \left(x_1 x_3, \frac{x_2 \bar{x}_3}{1 - x_2 x_3}, \frac{x_1 \bar{x}_3}{1 - x_1 x_3} \right). \quad (3.65)$$

Its apparent simplicity can be traced back to the following identity:

$$\alpha(x_1, \alpha(x_3, 1 - x_1, 1), 1) = x_1 x_3. \quad (3.66)$$

In other words the sequence $x \mapsto \alpha(x, y, 1)$, $y \mapsto \alpha(y, \bar{x}, 1)$ corresponds to the following two-variable mapping:

$$\boxed{(x, y) \mapsto \vec{\gamma}(x, y) \equiv \left(xy, \frac{x\bar{y}}{1 - xy} \right)} \quad (3.67)$$

This mapping has a few interesting properties. One property is that since γ maps x to the product xy , then γ^{-1} maps the product of two variables xy to a single variable x . Another interesting property is that $(x, y) \mapsto \gamma(x, y)$ is completely equivalent to $(\bar{x}, \bar{y}) \mapsto \gamma^{-1}(\bar{x}, \bar{y})$.

In practice the two-variable mapping eq.(3.67) is very useful. One idea is that we can always make two variables scale with a common variable, thereby factoring out the corresponding overlapping singularity. We will illustrate this method in the next section. However if there are more than two variables involved it may be useful to have more variables scale with a common variable. Such a mapping can always be created by recursively applying the γ -mapping. We find that

$$(x_1, x_2, x_3, \dots, x_n) \mapsto \left(x_1 x_2 x_3 \dots x_n, \frac{x_1 \bar{x}_2}{1 - x_1 x_2}, \frac{x_1 x_2 \bar{x}_3}{1 - x_1 x_2 x_3}, \dots, \frac{x_1 x_2 \dots x_{n-1} \bar{x}_n}{1 - x_1 x_2 x_3 \dots x_n} \right) \quad (3.68)$$

with Jacobian

$$J = \frac{x_1^{n-1} x_2^{n-2} x_3^{n-3} \dots x_{n-1}}{(1 - x_1 x_2)(1 - x_1 x_2 x_3) \dots (1 - x_1 x_2 x_3 \dots x_n)} \quad (3.69)$$

indeed qualifies as a valid n -dimensional generalization of the two-variable γ -mapping. As a possible application, this mapping can also be used to completely factorise the minimal n -dimensional logarithmic singularity which we introduced in eq.(3.23).

3.3.6 A more complicated example with non-linear mappings II

Let us now illustrate how the γ -mapping may be used to systematically remove singularities from a denominator. Applying $(x_1, x_3) \mapsto \vec{\gamma}(x_1, x_3)$ to eq.(3.59) yields

$$I_3 = \int dx_1 \dots dx_4 x_1^{-1+2\epsilon} \frac{(1 - x_1 x_3)^{1-2\epsilon} f(x_1, \dots, x_4)}{[x_2 x_3 (1 - x_1 x_3) + (1 - x_3) x_4]^{2-2\epsilon}}. \quad (3.70)$$

The term $(1 - x_1 x_3)$ can not contribute to the overlapping singularity since it is tamed by the corresponding factor in the numerator. We can therefore continue the *Spiel* by removing the overlapping singularity at $x_2 = 0 = x_4$ with $(x_2, x_4) \mapsto \vec{\gamma}(x_2, x_4)$,

$$I_3 = \int dx_1 \dots dx_4 (x_1 x_2)^{-1+2\epsilon} \frac{((1 - x_1 x_3)(1 - x_2 x_4))^{1-2\epsilon} f(x_1, \dots, x_4)}{[x_3 x_4 (1 - x_1 x_3)(1 - x_2 x_4) + \bar{x}_3 \bar{x}_4]^{2-2\epsilon}}. \quad (3.71)$$

Ignoring the factors $(1 - x_3 x_1)(1 - x_2 x_4)$ the remaining singularity looks much like the one of eq.(3.46) and we can factorise it with the final mapping $x_3 \mapsto \alpha(x_3, \bar{x}_4, x_4)$. The numerical convergence we find using this strategy is very similar to our former approach to this integral.

3.3.7 A more complicated example with non-linear mappings III

One may have wondered why we did not make use of eq.(3.47) in eq.(3.61) since the singular denominator was of the form $x_1 x_2 + x_3$. We will now explore this path here. Mapping x_3 will, since it is passive, not factorise the singularity, but mapping

$$x_1 \mapsto \beta \left(x_1, \frac{x_3}{x_2} \right) \quad (3.72)$$

(mapping x_2 would have worked equally well) results in

$$I_3 = \int dx_1 \dots dx_4 (x_1 x_2 x_3)^{-1+2\epsilon} f(x_1, \dots, x_4) \times (x_2(\bar{x}_4 + x_1 x_4) + x_3 \bar{x}_4)^{-2\epsilon} (x_2 \bar{x}_1 + x_3)^{-2\epsilon} (x_2 + x_3)^{2\epsilon}. \quad (3.73)$$

At first sight it appears that all singularities have been factorised into the factor $(x_1 x_2 x_3)^{-1+2\epsilon}$. However the three other factors are all zero valued at the point $x_2 = 0 = x_3$ and thus do not allow for a subtraction at this particular point.

The mapping $(x_2, x_3) \mapsto \gamma(x_2, x_3)$ may be used to factorise the un-subtractable numerators at the expense of a further factorised singularity at $\bar{x}_2 = 0$, we obtain

$$I_3 = \int dx_1 \dots dx_4 (x_1 x_2 \bar{x}_2 x_3)^{-1+2\epsilon} (1 - x_2^2 x_3)^{2\epsilon} f(x_1, \dots, x_4) \quad (3.74)$$

$$\times (1 - x_2^2 x_3 + x_4 \bar{x}_1 + x_1 x_2 x_4 - x_2^2 x_3 x_4)^{-2\epsilon} (1 - x_2^2 x_3 - x_1 + x_1 x_2)^{-2\epsilon}.$$

The numerical convergence we find with this strategy is also comparable to our former approaches to factorise this integral.

3.4 Line singularities

A line singularity arises when two or more variables of integration must lie on a hyper contour of the region of integration to create the singularity.

A simple example is given by the integral

$$I = \int_0^1 dx_1 dx_2 \frac{f(x_1, x_2)}{|x_1 - x_2|^{1-\epsilon}}, \quad (3.75)$$

where the singularity is located along the line $x_1 = x_2$. This line singularity may be factorised with sector decomposition. Inserting

$$1 = \theta(x_1 - x_2) + \theta(x_2 - x_1) \quad (3.76)$$

and then mapping $x_2 \mapsto x_1 x_2$ in the first and $x_1 \mapsto x_1 x_2$ in the second sector yields

$$I = \int_0^1 dx_1 dx_2 f(x_1, x_1 x_2) x_1^\epsilon \bar{x}_2^{-1+\epsilon} + \int_0^1 dx_1 dx_2 f(x_1 x_2, x_2) x_2^\epsilon \bar{x}_1^{-1+\epsilon}. \quad (3.77)$$

The reason why the sector decomposition works here is because it splits the region of integration along the line $x_1 = x_2$. Therefore the line singularity is mapped onto the upper boundary of each of the new sectors. We are not aware of trick which allows to factorise a line singularity without splitting the integrand, nevertheless a non-linear mapping can be applied to shrink the line singularity into a single point. Mapping $x_1 \mapsto \alpha(x_1, x_2, \bar{x}_2)$ yields

$$I = \int_0^1 dx_1 dx_2 x_2^\epsilon \bar{x}_2^\epsilon (1 - 2x_1)^{-1+\epsilon} (\bar{x}_1 \bar{x}_2 + x_1 x_2)^{-1-\epsilon} f(\alpha(x_1, x_2, \bar{x}_2), x_2). \quad (3.78)$$

This contains a singularity at $x = 1/2$, in order to map this back to the boundary we would have to insert

$$1 = \theta\left(x_1 - \frac{1}{2}\right) + \theta\left(\frac{1}{2} - x_1\right),$$

thereby also creating two sectors. And so there is no apparent gain in using a non-linear mapping to factorise a line singularity.

3.5 Conclusion

In this chapter we first reviewed the subtraction method for factorised singularities. We then introduced overlapping singularities, discussed the two-variable case in some depth and introduced the notion of active and passive singularities by focusing on two simple example integrals displaying these features.

The subtraction method for overlapping singularities was discussed and applied to a simple example integral. An alternative to the subtraction method is a method of factorisation. We illustrated the method of sector decomposition on our two examples, showing that the algorithm of sector decomposition worked irrespective of singularities being active or passive. As an alternative to sector decomposition we introduced a non-linear mapping. We demonstrated that with non-linear mappings a proliferation of integrals can be avoided. Further, we showed that the use of non-linear mappings, in contrast to sector decomposition, is sensitive to whether a singularity is active or passive. As a rule of thumb, we established that only active singularities should be remapped. We gave a number of useful identities which could be used to factorise certain denominator structures and demonstrated the connection of our non-linear mapping with Feynman parameters. Furthermore we remarked that this non-linear mapping could be used to derive analytic continuation identities for hypergeometric functions. Finally the method was demonstrated on a more complicated example containing several entangled overlapping singularities. In particular we showed three different ways in which this example integral could be factorised systematically with non-linear mappings.

Chapter 4

Factorising singular loop integrals with non-linear mappings

In this section we shall use the method of non-linear mappings to factorise some of the most singular one- and two-loop integrals. At one-loop we will consider the massless one-loop box with both, sector decomposition and non-linear mappings. This will serve as a demonstration of how the latter can avoid a proliferation of integrals. We will further consider a one-loop box containing two adjacent external masses. As a final example, we will consider the two-loop massless non-planar triangle, and use non-linear mappings to derive a fully factorised integral representation for it.

4.1 The massless one-loop box with sector decomposition

Let us consider the one-loop box scalar integral,

$$I = \int \frac{d^d k}{i\pi^{\frac{d}{2}}} \frac{1}{k^2(k+p_1)^2(k+p_1+p_2)^2(k+p_1+p_2+p_3)^2}. \quad (4.1)$$

The corresponding Feynman parametrisation reads,

$$I = \int_0^1 dx_1 \dots dx_4 \delta(1 - x_1 - \dots - x_4) f(x_1, \dots, x_4) \quad (4.2)$$

with

$$f(x_1, \dots, x_4) \equiv \frac{\Gamma(2 + \epsilon)}{[-sx_1x_3 - tx_2x_4 - i0]^{2+\epsilon}}. \quad (4.3)$$

To avoid creating poles at the upper limit of the x_i integrations we first apply the method of primary sectors [11], which solves the delta-constraint of a Feynman integral by decomposing into primary sectors as follows

$$I = \int dx \int_0^1 \left(\prod_i dx_i \right) \delta\left(1 - \sum x_i\right) f(\{x_i\}) \sum_i \delta(x_i - x) \prod_{j \neq i} \theta(x_i - x_j). \quad (4.4)$$

We now rescale

$$x_k = y_k x \quad (4.5)$$

and perform the x integration. This yields

$$I = \Gamma(2 + \epsilon) \int_0^1 dy_1 \dots dy_4 \left(\sum_i y_i \right)^{2\epsilon} \frac{\sum_i \delta(1 - y_i)}{[-sy_1y_3 - ty_2y_4 - i0]^{2+\epsilon}}. \quad (4.6)$$

All terms in the sum can be computed in exactly the same fashion. For convenience, although not necessary, we use the special symmetry of this problem, $y_1 \leftrightarrow y_3$ and $y_2 \leftrightarrow y_4$, and cast the integral as

$$\begin{aligned} I &= 2\Gamma(2 + \epsilon) \int_0^1 dy_1 dy_2 dy_3 (1 + y_1 + y_2 + y_3)^{2\epsilon} \\ &\quad \times \left\{ [-sy_1 - ty_2y_3]^{-2-\epsilon} + [-ty_1 - sy_2y_3]^{-2-\epsilon} \right\} \end{aligned} \quad (4.7)$$

We observe that the integral becomes singular in the following instances

$$y_1 = 0 \text{ and } (y_2 = 0 \text{ or } y_3 = 0). \quad (4.8)$$

We now apply sector decomposition to factorize the entangled singularity structure. We multiply the integrand by

$$\begin{aligned} 1 &= \theta(y_1 - y_2) + \theta(y_2 - y_1) (\theta(y_2y_3 - y_1) + \theta(y_1 - y_2y_3)) \\ &= \theta(y_1 - y_2) + \theta(y_2 - y_1)\theta(y_2y_3 - y_1) + \theta(y_2 - y_1)\theta(y_1 - y_2y_3). \end{aligned} \quad (4.9)$$

In each of the three sectors of the above equation we rescale the smallest variables with respect to the large ones, mapping the boundaries of the sectors to the unit

cube. Specifically,

$$\theta(y_2 y_3 - y_1) : \quad y_1 \rightarrow y_1 y_2 y_3, \quad (4.10)$$

$$\theta(y_2 - y_1) \theta(y_1 - y_2 y_3) : \quad y_1 \rightarrow y_1 y_2 \text{ and } y_3 \rightarrow y_3 y_1, \quad (4.11)$$

$$\theta(y_1 - y_2) : \quad y_2 \rightarrow y_2 y_1. \quad (4.12)$$

This allows us to obtain a representation for the one-loop box,

$$I = I_1 + I_2 + I_3, \quad (4.13)$$

with a simple, factorised singularity structure:

$$\begin{aligned} I_1 = & 2 \Gamma(2 + \epsilon) \int_0^1 dy_1 dy_2 dy_3 (1 + y_1 y_2 y_3 + y_2 + y_3)^{2\epsilon} \\ & \times \{ [-s y_1 - t]^{-2-\epsilon} + [-t y_1 - s]^{-2-\epsilon} \} (y_2 y_3)^{-1-\epsilon}, \end{aligned} \quad (4.14)$$

$$\begin{aligned} I_2 = & 2 \Gamma(2 + \epsilon) \int_0^1 dy_1 dy_2 dy_3 (1 + y_1 y_2 + y_2 + y_3 y_1)^{2\epsilon} \\ & \times \{ [-s - t y_3]^{-2-\epsilon} + [-t - s y_3]^{-2-\epsilon} \} (y_2 y_1)^{-1-\epsilon}, \end{aligned} \quad (4.15)$$

$$\begin{aligned} I_3 = & 2 \Gamma(2 + \epsilon) \int_0^1 dy_1 dy_2 dy_3 (1 + y_1 + y_2 y_1 + y_3)^{2\epsilon} \\ & \times \{ [-s - t y_2 y_3]^{-2-\epsilon} + [-t - s y_2 y_3]^{-2-\epsilon} \} y_1^{-1-\epsilon}. \end{aligned} \quad (4.16)$$

The resulting integrals I_1, I_2, I_3 of sector decomposition can all be expanded in ϵ using the subtraction method.

4.2 The massless one-loop box with non-linear mappings

Let us write eq.(4.14) as

$$I = F(s, t) + F(t, s), \quad (4.17)$$

where

$$F(s, t) = 2 \Gamma(2 + \epsilon) \int_0^1 dy_1 dy_2 dy_3 (1 + y_1 + y_2 + y_3)^{2\epsilon} [-s y_1 - t y_2 y_3]^{-2+\epsilon}. \quad (4.18)$$

The singularity structure is of the same type as eq.(3.47), and can be factorised efficiently with the mapping

$$y_1 \mapsto \beta \left(y_1, \frac{ty_2y_3}{s} \right). \quad (4.19)$$

We obtain

$$\begin{aligned} F(s, t) &= 2 \Gamma(2 + \epsilon) \int_0^1 dy_1 dy_2 dy_3 (y_2 y_3 t)^{-1-\epsilon} [-s - ty_2 y_3]^{-1-\epsilon} \\ &\quad \times (1 + \beta(y_1, ty_2 y_3 / (s y_1)) + y_2 + y_3)^{2\epsilon} \end{aligned} \quad (4.20)$$

All the singularities arising from the loop integration are now factorised and subtractable. Let us remark that it is not necessary to apply a primary sector decomposition in the first place. This may be advantageous when using sector decomposition, since it implies that all singularities are located at the origin. When using non-linear mappings on the other hand, singularities present at both boundaries are a welcome feature, since they often allow the use of the identity eq.(3.46). Let us demonstrate this by solving the delta constraint in eq.(4.2) with the following parameterisation:

$$\begin{aligned} x_1 &= y_1 \\ x_2 &= \bar{y}_1 y_2 \\ x_3 &= \bar{y}_1 \bar{y}_2 y_3 \\ x_4 &= \bar{y}_1 \bar{y}_2 \bar{y}_3. \end{aligned} \quad (4.21)$$

The box integral may then be expressed as

$$F(s, t) = \Gamma(2 + \epsilon) \int_0^1 dy_1 dy_2 dy_3 (\bar{y}_1)^{-\epsilon} (\bar{y}_2)^{-1-\epsilon} [-s y_1 y_3 - t \bar{y}_1 y_2 \bar{y}_3]^{-2-\epsilon}. \quad (4.22)$$

We observe that the identity of eq.(3.46) should be applicable and map

$$y_3 \mapsto \alpha(y_3, -t \bar{y}_1 y_2, -s y_1),$$

which results in

$$F(s, t) = \Gamma(2 + \epsilon) \int_0^1 dy_1 dy_2 dy_3 (\bar{y}_1)^{-1-2\epsilon} (s t y_1 y_2 \bar{y}_2)^{-1-\epsilon} [-s y_1 \bar{y}_3 - t \bar{y}_1 y_2 y_3]^\epsilon. \quad (4.23)$$

An interesting complication arises here. While all the singularities appear to be factorised, the purely finite term $[-sy_1\bar{y}_3 - t\bar{y}_1y_2y_3]^\epsilon$ is not subtractable at the limit $y_1 = 0 = y_2$. The problem can in fact be cured with the γ -mapping. Mapping $(y_1, y_2) \mapsto \gamma(y_1, y_2)$ yields the now fully factorised and subtractable result

$$F(s, t) = \Gamma(2 + \epsilon) \int_0^1 dy_1 dy_2 dy_3 (sty_1\bar{y}_1y_2\bar{y}_2)^{-1-\epsilon} [-sy_2\bar{y}_3 - t\bar{y}_2y_3]^\epsilon. \quad (4.24)$$

In comparison to the result of eq.(4.20), this result is much more compact. Furthermore the y_1 integration can be done trivially and yields just a simple $B(-\epsilon, -\epsilon)$. We also saw that the identity eq.(3.46) must be applied with care and can create non-subtractable numerator functions. As was already demonstrated in section 3.3.7, a γ mapping could also be applied here to obtain a subtractable result.

4.3 The one-loop box with two external masses

Let us now consider the box which has two adjacent external masses. This is of course less singular than the purely massless box, but the denominator structure is considerably more complicated and one may therefore question whether the non-linear mapping can be used efficiently to factorise such structures. The standard Feynman parametrisation of this integral reads

$$I = \int_0^1 \left(\prod_{i=1}^4 dx_i \right) \frac{\delta(\sum_i x_i - 1)}{[x_1x_3s + x_2x_4t + x_1x_2m_1^2 + x_2x_3m_2^2]^{2+\epsilon}}. \quad (4.25)$$

We shall now use the projective mapping,

$$x_i \mapsto \frac{x_i A_i}{\sum_j x_j A_j}, \quad (4.26)$$

used also by 'tHooft [23]. Under this mapping the measure transforms as

$$\int_0^1 \left(\prod_{i=1}^n dx_i \right) \delta\left(\sum_i x_i - 1\right) \mapsto \int_0^1 \left(\prod_{i=1}^n dx_i \right) \delta\left(\sum_i x_i - 1\right) \frac{\prod_i A_i}{\left[\sum_j x_j A_j\right]^n}. \quad (4.27)$$

Essentially this is nothing but the n -dimensional generalisation of our non-linear α -mapping. The box integral then becomes

$$I = \int_0^1 \left(\prod_{i=1}^4 dx_i A_i \right) \frac{\delta(\sum_i x_i - 1) (\sum_i x_i A_i)^{2\epsilon}}{[x_1 x_3 s A_1 A_3 + x_2 x_4 t A_2 A_4 + x_1 x_2 m_1^2 A_1 A_2 + x_2 x_3 m_2^2 A_2 A_3]^{2+\epsilon}}. \quad (4.28)$$

We can remove all kinematical dependences from the numerator by choosing [26]

$$A_1 A_3 = \frac{1}{s}, \quad A_2 A_4 = \frac{1}{t}, \quad A_1 A_2 = \frac{1}{m_1^2}, \quad A_2 A_3 = \frac{1}{m_2^2}. \quad (4.29)$$

This choice has the following unique solutions for the A_i :

$$A_1 = \frac{m_2}{\sqrt{s} m_1}, \quad A_2 = \frac{\sqrt{s}}{m_1 m_2}, \quad A_3 = \frac{m_1}{\sqrt{s} m_2}, \quad A_4 = \frac{m_1 m_2}{\sqrt{s} t}. \quad (4.30)$$

We should remark that this choice is only possible for all A_i positive, and we are thus working in the Euclidean regime where $s, t > 0$. The integral becomes

$$I = \int_0^1 \left(\prod_{i=1}^4 dx_i A_i \right) \frac{\delta(\sum_i x_i - 1) (\sum_i x_i A_i)^{2\epsilon}}{[x_1 x_3 + x_2 (x_4 + x_1 + x_3)]^{2+\epsilon}}. \quad (4.31)$$

Let us now solve the δ -constraint as follows

$$\begin{aligned} x_1 &= \bar{y}_1 y_2, \\ x_3 &= \bar{y}_1 \bar{y}_2 y_3, & x_2 &= y_1, \\ x_4 &= \bar{y}_1 \bar{y}_2 \bar{y}_3. \end{aligned} \quad (4.32)$$

This results in

$$I = \left(\prod_{i=1}^4 A_i \right) \int_0^1 dy_1 dy_2 dy_3 \bar{y}_1^{-\epsilon} \bar{y}_2^{-\epsilon} \frac{(\sum_i x_i A_i)^{2\epsilon}}{[\bar{y}_1 y_2 \bar{y}_2 y_3 + y_1]^{2+\epsilon}}. \quad (4.33)$$

We can factorise the remaining overlapping singularity with

$$y_1 \mapsto \alpha(y_1, y_2 \bar{y}_2 y_3, 1). \quad (4.34)$$

Due to a remarkable conspiracy, the Jacobian of this transformation is cancelled entirely and we end up with

$$I = \left(\prod_{i=1}^4 A_i \right) \int_0^1 dy_1 dy_2 dy_3 (\bar{y}_1 \bar{y}_2)^{-\epsilon} (y_2 y_3)^{-1-\epsilon} \left(\sum_i \tilde{x}_i A_i \right)^{2\epsilon}, \quad (4.35)$$

where

$$\begin{aligned} \tilde{x}_1 &= \bar{y}_1 y_2, \\ \tilde{x}_3 &= \bar{y}_1 \bar{y}_2 y_3, & \tilde{x}_2 &= y_1 y_2 \bar{y}_2 y_3, \\ \tilde{x}_4 &= \bar{y}_1 \bar{y}_2 \bar{y}_3. \end{aligned} \quad (4.36)$$

This result is fully factorised and subtractable.

4.4 The non-planar massless two-loop triangle

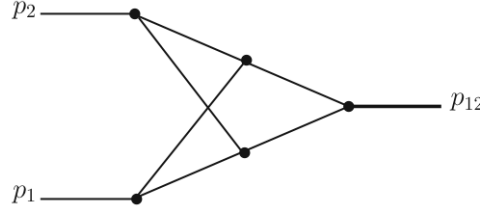


Figure 4.1: The massless non-planar two-loop triangle with one massive external leg

A convenient Feynman parametrisation for the non-planar massless two-loop triangle, see Fig 4.1, reads

$$\text{Xtri} = \Gamma(2 + 2\epsilon) \int_0^1 dx_1 dx_2 dx dy dz \frac{z \bar{z}^{-1-\epsilon} y^{1+\epsilon} \bar{y}^{-1-\epsilon}}{[x \bar{x} + yz(x - x_1)(x - x_2)]^{2+2\epsilon}}. \quad (4.37)$$

First we rearrange the denominator into a positive definite form. We find

$$\text{Xtri} = \Gamma(2 + 2\epsilon) \int_0^1 dx_1 dx_2 dx dy dz \frac{z \bar{z}^{-1-\epsilon} y^{1+\epsilon} \bar{y}^{-1-\epsilon}}{[x \bar{x}(1 - yz) + yz(x \bar{x}_1 \bar{x}_2 + \bar{x} x_1 x_2)]^{2+2\epsilon}}. \quad (4.38)$$

In this form it is apparent that y and z always appear as a product inside the denominator. We can use the mapping $(z, y) \mapsto \gamma^{-1}(y, z)$ to shrink this product

into a single parameter of integration, this yields

$$\text{Xtri} = \Gamma(2 + 2\epsilon) \int_0^1 dx_1 dx_2 dx dy dz \frac{y^{1+\epsilon} (z\bar{z})^{-1-\epsilon} \bar{y}^{-1-2\epsilon}}{[x\bar{x}\bar{y} + y(x\bar{x}_1\bar{x}_2 + \bar{x}x_1x_2)]^{2+2\epsilon}}. \quad (4.39)$$

The denominator structure is now of the type $yA_1 + \bar{y}A_2$. Eq.(4.20) therefore suggests the mapping

$$y \mapsto \alpha(y, x\bar{x}, x\bar{x}_1\bar{x}_2 + \bar{x}x_1x_2). \quad (4.40)$$

This results in

$$\begin{aligned} \text{Xtri} = & \Gamma(2 + 2\epsilon) \int_0^1 dx_1 dx_2 dx_3 dy dz y^{1+\epsilon} \bar{y}^{-1-2\epsilon} (z\bar{z})^{-1-\epsilon} (x\bar{x})^{-\epsilon} \\ & \times \left\{ x\bar{x}y + \bar{y}(x\bar{x}_1\bar{x}_2 + \bar{x}x_1x_2) \right\}^{3\epsilon} [x\bar{x}_1\bar{x}_2 + \bar{x}x_1x_2]^{-2-4\epsilon}. \end{aligned} \quad (4.41)$$

The singular denominator (in square brackets) is now of the form $xA + \bar{x}B$ allowing us to repeat the *Spiel* with the mapping

$$x \mapsto \alpha(x, x_1x_2, \bar{x}_1\bar{x}_2). \quad (4.42)$$

We then obtain

$$\begin{aligned} I = & \Gamma(2 + 2\epsilon) \int_0^1 dx_1 dx_2 dx dy dz y^{1+\epsilon} \bar{y}^{-1-2\epsilon} (z\bar{z})^{-1-\epsilon} (x\bar{x})^{-\epsilon} \\ & \times (x_1\bar{x}_1)^{-1-2\epsilon} (x_2\bar{x}_2)^{-1-2\epsilon} \left\{ x\bar{x}y + \bar{y}(xx_1x_2 + \bar{x}\bar{x}_1\bar{x}_2) \right\}^{3\epsilon}, \end{aligned} \quad (4.43)$$

which is fully factorised and subtractable. Indeed we could easily perform the z -integration which leads to a pre-factor of $B(-\epsilon, -\epsilon)$, but for the purpose of demonstration we perform a completely numerical evaluation of the above with standard subtractions. Numerically we then obtain

$$\begin{aligned} \text{Xtri} = & \Gamma(2 + 2\epsilon) \left[\frac{1}{\epsilon^4} - \frac{2.00001(8)}{\epsilon^3} - \frac{9.1598(7)}{\epsilon^2} - \frac{11.73(3)}{\epsilon} + 9.13(1) \right. \\ & \left. + 90.2(1)\epsilon + 312.4(2)\epsilon^2 + 863.2(7)\epsilon^3 + 2164(2)\epsilon^4 + 5169(6)\epsilon^5 + \mathcal{O}(\epsilon^6) \right], \end{aligned} \quad (4.44)$$

which agrees with the known analytic result [70]. For the numerical evaluation we used the partial fraction identity eq.(3.4), this creates eight separate terms. However the symmetry of the integrand allows to regroup these into two non-equal integrals.

This is to be compared to 64 integrals which are created when sector decomposition is used to factorise the integrand.

4.5 Conclusion

We have demonstrated the method of non-linear mappings on three loop integrals, namely the massless one-loop box, the two adjacent massive box and the massless non-planar two-loop triangle. We find that the non-linear mappings can be used very efficiently to factorise the singularities of all three integrals, without the need to split the integrals. In comparison to the sector decomposition approach we save a factor of three in the number of different independent integrals for the one-loop box and a factor of 32 for the non-planar two-loop triangle.

Chapter 5

Real corrections to the hadronic production of massive states

Singularities in phase space integrals are encountered when two or more final state massless particles become indistinguishable from each other. This means either that at least one particle's energy vanishes, or that at least two particles become collinear to each other. When considering LO jet cross-sections, for example the hadronic production of two gluons, it is therefore necessary to demand these gluons to be distinguishable (or resolved) such that they may not become too soft or too collinear to each other or to the beam. Such requirements can be efficiently implemented via a jet algorithm.

Beyond LO un-resolved emissions must also be taken into account to ensure the cancellation of singularities between real and virtual corrections. Given a suitable phase space parametrisation on the unit hypercube we can handle these singularities with simple subtractions.

The latter, together with QCD factorisation, is also the basis of FKS subtraction [18, 19, 20], which formulates a subtraction scheme for NLO real emissions. Other schemes in particular the Catani-Seymour dipoles [21, 22] make use of counter-terms, such as dipoles, whose singular limits resemble those of the physical amplitudes. The counter-terms are first subtracted from the real emission part, then integrated over the singular phase space of the real emission, and finally added to the virtual contributions in their integrated form. This procedure therefore allows for a purely analytic cancellation of poles. Subtraction schemes therefore do not directly rely on an explicit factorisation of the singularities, instead the poles in ϵ are retrieved via an analytic integration of these counter-terms. Several schemes exist which generalize

the subtraction ideas to NNLO. Quite general is the Antenna subtraction scheme [42, 43, 44, 45, 46] which uses simpler physical amplitudes to build their subtraction terms, this makes an analytical evaluation feasible with loop integration techniques via cut-propagators. A scheme, which aims at a yet more general subtraction, using dipoles as counter-terms, is under development [47, 48, 49, 50, 51]. Further ideas were developed [52, 53, 54].

However, the first fully differential NNLO calculations were accomplished using sector decomposition [35, 36, 37, 38, 39, 40]. The original approach was as follows. First, a suitable decomposition of the squared amplitude in terms of topologically different denominator structures is performed. For each denominator structure, a suitable phase-space parametrisation is then used, which factorises the singularities of that denominator with the help of sector decomposition.

In the meantime a new approach has been proposed [71, 72, 73], which merges the subtraction idea of FKS with a factorisation of the singularities via sector decomposition. But there is an essential difference between the latter developments and the original approach with sector decomposition. This new approach does not intend a decomposition into different singularity structures on the squared amplitude level, rather its approach is to first sector decompose the entire phase-space in such a way that all possible singularity structures are factorised. Further it then substitutes the singular limits of the matrix element, known from QCD factorization, at the corresponding points of subtraction.

The latter substitution of the singular limits was not trivial to accomplish with the former method of topology separation. This is mainly because QCD factorisation works on the amplitude squared level rather than on the diagram level, where the different singular topologies are identified.

We will present yet another approach to double real emission which is based also on a topology decomposition of the amplitude, however instead of using sector decomposition for the factorisation of the singularities, we will use non-linear mappings to achieve a more economical factorisation, and save on the number of integrals, which have to be integrated independently. We will first review the case of single real emission at NLO, before moving to the case of double real emission. This will serve as both an introduction, as well as a preparation for the complexity which exists at NNLO.

5.1 Notational setup for the NNLO partonic cross section

Let us consider a LO process where n massive particles with momenta p_i and masses $p_i^2 = m_i^2$, where $i = 1..n$, are produced in a collision of two massless partons of momenta q_1 and q_2 . Momentum conservation then yields

$$q_1 + q_2 = \sum_{i=1}^n p_i. \quad (5.1)$$

In the partonic center of mass frame we can parameterise the momenta of the incoming partons as follows

$$q_1 = \frac{\sqrt{s}}{2} n^+, \quad q_2 = \frac{\sqrt{s}}{2} n^- \quad (5.2)$$

where $n^\pm = (1, 0, 0, \pm 1)$ are light cone vectors and $s = (q_1 + q_2)^2$ is the partonic center of mass energy. The fully differential hadronic cross section at NNLO may be written as

$$\begin{aligned} \sigma_{2 \rightarrow n+X}[\mathcal{J}] &= \sigma_{2 \rightarrow n}^{(0)}[\mathcal{J}] + \left(\frac{\alpha_s}{\pi}\right) \left(\sigma_{2 \rightarrow n+1}^{(0)}[\mathcal{J}] + \sigma_{2 \rightarrow n}^{(1)}[\mathcal{J}]\right) \\ &+ \left(\frac{\alpha_s}{\pi}\right)^2 \left(\sigma_{2 \rightarrow n+2}^{(0)}[\mathcal{J}] + \sigma_{2 \rightarrow n+1}^{(1)}[\mathcal{J}] + \sigma_{2 \rightarrow n}^{(2)}[\mathcal{J}]\right) + \mathcal{O}(\alpha_s^3), \end{aligned} \quad (5.3)$$

where X shall collectively stand for QCD radiation in the final state and the notation is such that $\sigma_{2 \rightarrow n+r}^{(l)}[\mathcal{J}]$ corresponds to the l th order correction with r emitted particles in the final state. The fully differential cross section $\sigma_{2 \rightarrow n+X}[\mathcal{J}]$ is a functional of the jet function \mathcal{J} , through which arbitrary infra-red safe final state phase space cuts can be implemented. We shall denote the momenta of the r unresolved particles as $q_{i=3..2+r}$. Here $\alpha_s = \alpha_s(\mu)$ shall denote the $\overline{\text{MS}}$ renormalised strong coupling constant. The fully differential LO partonic cross section is

$$\sigma_{2 \rightarrow n}^{(0)}[\mathcal{J}] = \frac{1}{2s} \int d\Phi_n |\mathcal{A}_{2 \rightarrow n}^{(0)}|^2 \mathcal{J}_n \quad (5.4)$$

At NLO we must also include one-loop corrections (the *virtual*) and the emissions of a massless parton at tree-level (the *real*):

$$\begin{aligned}\sigma_{2 \rightarrow n}^{(1)}[\mathcal{J}] &= \frac{1}{2s} \int d\Phi_n |\mathcal{A}_{2 \rightarrow n}^{(1)}|^2 \mathcal{J}_n \\ \sigma_{2 \rightarrow n+1}^{(0)}[\mathcal{J}] &= \frac{1}{2s} \int d\Phi_{n+1} |\mathcal{A}_{2 \rightarrow n+1}^{(0)}|^2 \mathcal{J}_{n+1}.\end{aligned}\tag{5.5}$$

At NNLO *double virtual*, *real-virtual* and *double real* corrections must be considered, these are

$$\begin{aligned}\sigma_{2 \rightarrow n}^{(2)}[\mathcal{J}] &= \frac{1}{2s} \int d\Phi_n |\mathcal{A}_{2 \rightarrow n}^{(2)}|^2 \mathcal{J}_n, \\ \sigma_{2 \rightarrow n+1}^{(1)}[\mathcal{J}] &= \frac{1}{2s} \int d\Phi_{n+1} |\mathcal{A}_{2 \rightarrow n+1}^{(1)}|^2 \mathcal{J}_{n+1}, \\ \sigma_{2 \rightarrow n+2}^{(0)}[\mathcal{J}] &= \frac{1}{2s} \int d\Phi_{n+2} |\mathcal{A}_{2 \rightarrow n+2}^{(0)}|^2 \mathcal{J}_{n+2},\end{aligned}\tag{5.6}$$

respectively. Here $|\mathcal{A}_{n+r}^{(l)}|^2$ shall denote the coefficient of the l th order correction to a squared spin averaged and summed amplitude of the $2 \rightarrow n+r$ process. Further we introduced the notation

$$\mathcal{J}_{n+r} = \mathcal{J}(\{p_{i=1..n}, q_{i=3..2+r}\})\tag{5.7}$$

which shall denote the $n+r$ final state jet function, through which we will implement any infra-red safe final state phase space cuts. The phase space volumes here are defined in a similar fashion as

$$\Phi_{n+r} = \Phi_{n+r}(\sqrt{s}; m_1, \dots, m_n, \underbrace{0, \dots, 0}_r).\tag{5.8}$$

Lorentz invariants shall be defined through scalar products of the vectors

$$\begin{aligned}p_{i_1 \dots i_n} &= p_{i_1} + \dots + p_{i_n} \\ q_{i_1 \dots i_n} &= \tau_{i_1} q_{i_1} + \dots + \tau_{i_n} q_{i_n}\end{aligned}\tag{5.9}$$

where

$$\tau_i = \begin{cases} -1 & \text{if } i = 1, 2 \\ +1 & \text{if } i > 2 \end{cases}\tag{5.10}$$

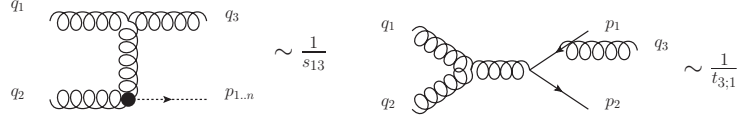


Figure 5.1: Singular Feynman diagrams for single real emissions

as

$$u_{i_1 \dots i_n} = (p_{i_1 \dots i_n})^2, \quad s_{i_1 \dots i_n} = (q_{i_1 \dots i_n})^2 \quad (5.11)$$

and

$$t_{i_1 \dots i_n; j_1, \dots, j_m} = (q_{i_1 \dots i_n} + p_{j_1 \dots j_m})^2 - (m_{j_1}^2 + \dots + m_{j_m}^2). \quad (5.12)$$

At times we shall also use the angle functions

$$y_{ij} = \frac{1 - \cos \theta_{ij}}{2}, \quad \text{where} \quad \cos \theta_{ij} = \frac{\vec{q}_i \cdot \vec{q}_j}{|\vec{q}_i| |\vec{q}_j|} \quad (5.13)$$

and

$$y_{i;j} = \frac{1 - \cos \theta_{i;j}}{2}, \quad \text{where} \quad \cos \theta_{i;j} = \frac{\vec{q}_i \cdot \vec{p}_j}{|\vec{q}_i| |\vec{p}_j|}. \quad (5.14)$$

The energies or zero components of the momenta q_i shall be denoted by E_i . We will not often need the energies of the momenta p_i and shall denote them by p_i^0 to avoid confusion with the energies of q_i .

5.2 Single real emission for massive final states

The possible singular invariants may be identified most easily when working with energy and angle variables and are

$$\begin{aligned} s_{13} &= (q_1 - q_3)^2 = -\sqrt{s} E_3 (1 - \cos \theta_{13}) \\ s_{23} &= (q_2 - q_3)^2 = -\sqrt{s} E_3 (1 + \cos \theta_{13}) \end{aligned} \quad (5.15)$$

and

$$t_{3;i} = (q_3 + p_i)^2 - m_i^2 = 2E_3 p_i^0 (1 - v_i \cos \theta_{3;i}), \quad i = 1..n, \quad (5.16)$$

where $v_i = \frac{|\vec{p}_i|}{p_i^0}$ is the velocity of the massive particle i . Diagrams corresponding to these singularities are depicted in Figure 5.1. Soft singularities are therefore present in s_{13}, s_{23} and $t_{3;i}$, while collinear singularities are present only in s_{13} and s_{23} since as long as $m_i^2 > 0$ further collinear singularities in the invariants $t_{3;i}$ are shielded by

the fact that $|v_i| < 1$. The singularities may therefore be factorised in terms of the energy and angle of q_3 and are independent of the momenta p_i . It is then convenient to factorise the $n + 1$ particle phasespace as follows

$$\Phi_{n+1}(\sqrt{s}; m_1, \dots, m_n, 0) = \int \frac{du_{1..n}}{2\pi} \Phi_2(\sqrt{s}; 0, \sqrt{u_{1..n}}) \Phi_n(\sqrt{u_{1..n}}; m_1, \dots, m_n). \quad (5.17)$$

where

$$(m_1 + \dots + m_n)^2 \leq u_{1..n} \leq s. \quad (5.18)$$

See also Figure 5.2. It is then clear that when the center of mass energy $u_{1..n}$ of the massive particles equals the total partonic center of mass energy s , that no energy is left over and q_3 must become soft. This limit is therefore uniquely specified when

$$\bar{z} = 1 - z = 1 - \frac{u_{1..n}}{s} \rightarrow 0. \quad (5.19)$$

In the case $n = 1$ of only a single massive particle being produced (e.g. W,Z or single Higgs production), the above still holds. The $2 \rightarrow 1$ phase space is

$$\Phi_1(\sqrt{u_1}; m_1) = 2\pi\delta(u_1 - m_1^2), \quad (5.20)$$

which precisely kills the integral over u_1 and the soft singularity occurs as

$$\bar{z} = 1 - z = 1 - \frac{m_1^2}{s} \rightarrow 0. \quad (5.21)$$

We shall see in the next sections that this variable can always be used to control the maximum soft singularity which occurs. Let us now parametrise the 2 particle

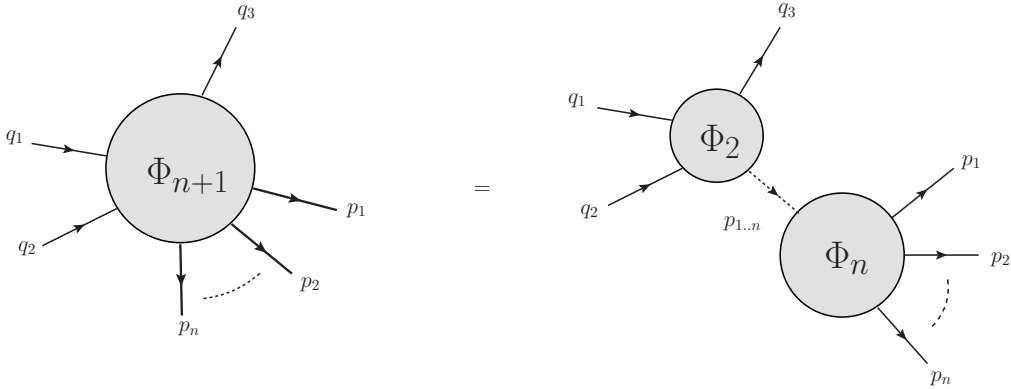


Figure 5.2: Phase space factorisation: q_i are massless particles while p_i are massive.

phase-space volume

$$\begin{aligned} \Phi_2(\sqrt{s}; 0, \sqrt{u_{1..n}}) &= \int \frac{d^d q_3}{(2\pi)^{d-1}} \delta^+(q_3^2) \frac{d^d p_{1..n}}{(2\pi)^{d-1}} \delta^+(p_{1..n}^2 - u_{1..n}) \\ &\times (2\pi)^d \delta^{(d)}(q_1 + q_2 - q_3 - p_{1..n}). \end{aligned} \quad (5.22)$$

The d -dimensional delta function may be used to integrate out the momentum $p_{1..n}$. The 4-vector q_3 may then be parametrised in terms of the energy E_3 and a further angle through the following change of variables

$$d^d q_3 \delta(q_3^2) = \frac{1}{2} dE_3 E_3^{d-3} d\Omega^{(d-1)}. \quad (5.23)$$

Here

$$\Omega^{(d)} = \frac{2\pi^{\frac{d}{2}}}{\Gamma(\frac{d}{2})} \quad (5.24)$$

is the volume of the unit sphere in d -dimensions. We can extract a further angle via the identity

$$d\Omega^{(d-1)} = d\Omega^{(d-2)} d\cos\theta_{13} (\sin\theta_{13})^{d-4}. \quad (5.25)$$

It is convenient to parameterise $\cos\theta_{13} = 2y_{13} - 1$, such that y_{13} is situated in $[0, 1]$. Solving the remaining delta function for the energy yields

$$E_3 = \frac{\sqrt{s\bar{z}}}{2}, \quad (5.26)$$

which indeed vanishes in the limit $\bar{z} \rightarrow 0$. We end up with the following parametrisation of the phase space:

$$\Phi_2(\sqrt{s}; 0, \sqrt{sz}) = \frac{1}{8\pi} \frac{(4\pi)^\epsilon}{\Gamma(1-\epsilon)} s^{-\epsilon} \bar{z}^{1-2\epsilon} \int_0^1 dy_{13} [y_{13}\bar{y}_{13}]^{-\epsilon}, \quad (5.27)$$

with the Lorentz invariants taking the simple form

$$\begin{aligned} s_{13} &= -s\bar{z}y_{13}, \\ s_{23} &= -s\bar{z}\bar{y}_{13}. \end{aligned} \quad (5.28)$$

All singular propagators s_{13} , s_{23} and $t_{3;i}$ are therefore factorised nicely and may be dealt with using simple subtractions.

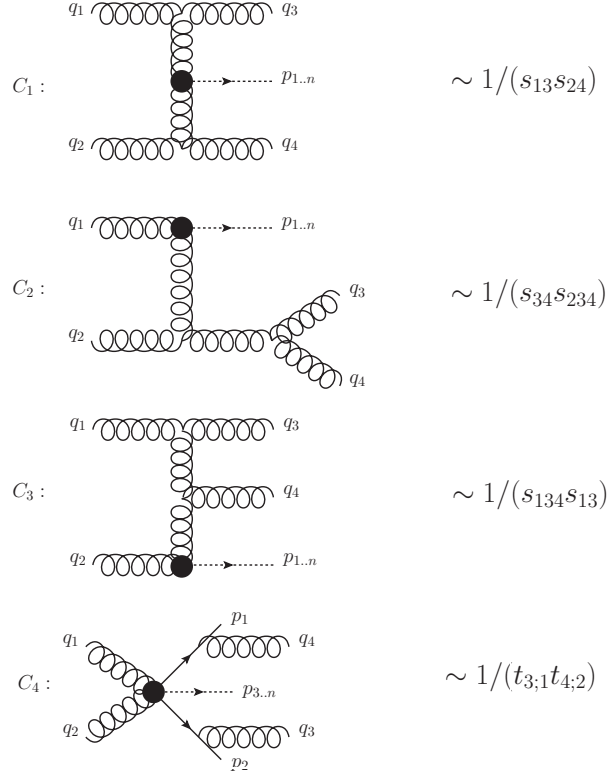


Figure 5.3: The most singular topologies: C_1, C_2, C_3, C_4

5.3 Double real emissions for massive final states

Infrared singularities can occur in this double real emission phase-space whenever q_3 and/or q_4 become soft or collinear to q_1 , q_2 or to each other. The situation is therefore considerably more complicated than for single real emissions.

For the case of double real radiation to the production of a color singlet (e.g. Higgs, W , $Z, \gamma\gamma$, WW or ZZ production) potentially singular propagators can be summarized as

$$\begin{aligned}
 s_{34} &= 2q_3 \cdot q_4 \\
 s_{13} &= -2q_1 \cdot q_3 \\
 s_{23} &= -2q_2 \cdot q_3 \\
 s_{14} &= -2q_1 \cdot q_4 \\
 s_{24} &= -2q_2 \cdot q_4
 \end{aligned} \tag{5.29}$$

and

$$\begin{aligned}s_{134} &= (q_3 + q_4 - q_1)^2 = s_{34} + s_{13} + s_{14} \\ s_{234} &= (q_3 + q_4 - q_2)^2 = s_{34} + s_{23} + s_{24}.\end{aligned}\tag{5.30}$$

Note that s_{123} , s_{124} are bounded from below. Further soft singularities can be found if there are colored massive particles in the final state, which radiate off soft gluons. One can then also get the following possibly singular denominators:

$$\begin{aligned}t_{3;i} &= 2q_3 \cdot p_i \\ t_{4;i} &= 2q_4 \cdot p_i\end{aligned}\tag{5.31}$$

as well as

$$t_{34;i} = (q_3 + q_4 + p_k)^2 - m_k^2 = s_{34} + t_{3;i} + t_{4;i}.\tag{5.32}$$

for $i \geq 1$. These denominators only contain soft singularities as was the case for the single real emissions. Whenever some heavy colored state radiates off two gluons we now also get the denominator $t_{34;i}$, it can only become singular in the double soft limit when $E_3 = 0 = E_4$. However the double soft limit will always be factorized as we will show in the next section.

Not all singular propagators can appear at the same time. We can identify the most singular denominator structures, by considering typical Feynman Diagrams. The most singular diagrams which one could expect are those where radiation is emitted from the initial state particles. We illustrate their propagator structure using diagrams containing gluons in Fig. 5.3, diagrams containing massless quarks contain of course the same propagator structures. Diagrams whose propagator structure can be related to the ones in Fig.5.3 by a simple interchange of q_3 with q_4 or of q_1 with q_2 will also fall into the same topology. By considering square and interference terms of the topologies C_1, C_2 and C_3 , we obtain the list of integrals depicted in Table 5.3.

Here $d\Phi_3$ is the differential double emission phase space element for $2 + n$ final state particles, and $N(\{s_{ij}\})$ is in general a finite function of the kinematical invariants. The topology C_4 contains only soft singularities similar to those in C_1 . The topologies $C_4 \otimes C_4$ and $C_4 \otimes C_1$ are, therefore, easier than $C_1 \otimes C_1$. They can be treated exactly like $C_1 \otimes C_1$ and we will not discuss them in what follows.

Table 5.1: The most singular integrals to double real emission of massive final states

Topology	Most singular integrals
$C_1 \otimes C_1$	$\int \frac{d\Phi_3 N(\{s_{ij}\})}{(s_{13}s_{24})^2} \quad \int \frac{d\Phi_3 N(\{s_{ij}\})}{s_{13}s_{23}s_{14}s_{24}}$
$C_2 \otimes C_2$	$\int \frac{d\Phi_3 N(\{s_{ij}\})}{(s_{34}s_{134})^2} \quad \int \frac{d\Phi_3 N(\{s_{ij}\})}{s_{34}^2 s_{134}s_{234}}$
$C_3 \otimes C_3$	$\int \frac{d\Phi_3 N(\{s_{ij}\})}{(s_{13}s_{134})^2} \quad \int \frac{d\Phi_3 N(\{s_{ij}\})}{s_{13}s_{23}s_{134}s_{234}} \quad \int \frac{d\Phi_3 N(\{s_{ij}\})}{s_{13}s_{24}s_{134}s_{234}}$
$C_1 \otimes C_2$	$\int \frac{d\Phi_3 N(\{s_{ij}\})}{s_{34}s_{234}s_{13}s_{24}}$
$C_1 \otimes C_3$	$\int \frac{d\Phi_3 N(\{s_{ij}\})}{s_{134}s_{13}s_{23}s_{14}} \quad \int \frac{d\Phi_3 N(\{s_{ij}\})}{s_{134}s_{13}^2 s_{14}}$
$C_2 \otimes C_3$	$\int \frac{d\Phi_3 N(\{s_{ij}\})}{s_{34}s_{134}^2 s_{13}} \quad \int \frac{d\Phi_3 N(\{s_{ij}\})}{s_{34}s_{134}s_{234}s_{23}}$
$C_4 \otimes C_1$	$\int \frac{d\Phi_3 N(\{s_{ij}\})}{t_{3;i}t_{4;j}s_{13}s_{14}}$
$C_4 \otimes C_2$	$\int \frac{d\Phi_3 N(\{s_{ij}\})}{t_{3;i}t_{4;j}s_{34}s_{134}}$
$C_4 \otimes C_3$	$\int \frac{d\Phi_3 N(\{s_{ij}\})}{t_{3;i}t_{4;j}s_{13}s_{134}}$
$C_4 \otimes C_4$	$\int \frac{d\Phi_3 N(\{s_{ij}\})}{t_{3;i}^2 t_{4;j}^2} \quad \int \frac{d\Phi_3 N(\{s_{ij}\})}{t_{3;i}t_{4;j}t_{3;j}t_{4;i}}$

5.3.1 Factorisation of the double emission phase space

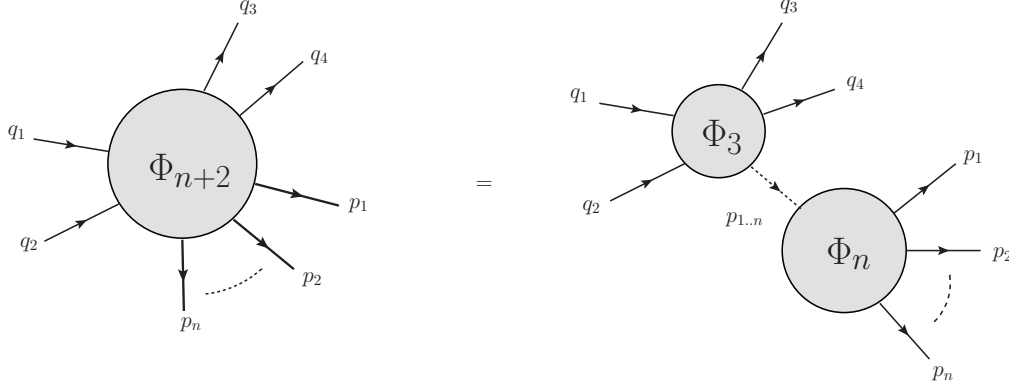


Figure 5.4: Double real phase space factorisation

It does not appear to be possible to find phase space parametrisations which completely factorise all singularities, without splitting the phase space into a number of integrals via sector decomposition. Nevertheless, different parametrisations of the phase-space can factorize different sets of kinematic invariants. We will derive two such parametrisations which allow for a more convenient numerical evaluation of diverse diagrams, according to their topology.

Similarly to the NLO case, we factorize the double real phase space into a 3-particle phase space times an n -particle phase space as follows

$$\Phi_{n+2}(\sqrt{s}; m_1, \dots, m_n, 0, 0) = \int \frac{du_{1..n}}{2\pi} \Phi_3(\sqrt{s}; 0, 0, \sqrt{u_{1..n}}) \Phi_n(\sqrt{u_{1..n}}; m_1, \dots, m_n). \quad (5.33)$$

This is depicted graphically in Figure 5.4. The double soft singularity will then appear when

$$\bar{z} \equiv 1 - \frac{u_{1..n}}{s} \rightarrow 0. \quad (5.34)$$

The fact that the double soft singularity can always be factorised then follows from the fact that it is controlled by the single parameter z .

In the following we will assume that one can parametrise the n -particle phase space $d\Phi_n$, and we will focus on the phase-space of the potentially unresolved massless partons $d\Phi_3$.

5.3.2 Energies and angles parametrisation

Since infra-red singularities are due to vanishing energies and angles, it appears to be rather natural to use these variables to parametrise the real emission phase-space. Indeed, already at NLO we saw that this choice lead us to a fully factorised parametrisation. As our first attempt we shall therefore pursue a similar path here as well. The three particle phase space element $d\Phi_3$ is defined as

$$\begin{aligned} d\Phi_3(\sqrt{s}; 0, 0, \sqrt{u_{1..n}}) &= (2\pi)^{3-2d} d^d q_3 \delta^{(+)}(q_3^2) d^d q_4 \delta^{(+)}(q_4^2) \\ &\times d^d Q \delta^{(+)}(Q^2 - u_{1..n}) \delta^{(d)}(q_1 + q_2 - q_3 - q_4 - Q). \end{aligned} \quad (5.35)$$

We proceed as in the case of the single real emission by integrating out $Q = p_{1..n}$ and using that $d^d q \delta^{(+)}(q^2) = dE E^{d-3} d\Omega^{(d-1)}/2$. We then obtain the measure in terms of energies and angles:

$$\begin{aligned} d\Phi_3(\sqrt{s}; 0, 0, \sqrt{u_{1..n}}) &= (2\pi)^{3-2d} \frac{1}{4} d\Omega_3^{(d-1)} d\Omega_4^{(d-1)} dE_3 dE_4 (E_3 E_4)^{d-3} \\ &\times \delta^{(+)}(s - u_{1..n} - 2\sqrt{s}(E_3 + E_4) + 2E_3 E_4 (1 - \cos \theta_{34})). \end{aligned} \quad (5.36)$$

The remaining δ -constraint can be solved in a number of ways. We could integrate out $u_{1..n}$ or $\cos \theta_{34}$, but $u_{1..n}$ controls the double soft limit and we would like to keep this feature. If we would integrate out $\cos \theta_{34}$ we would have to choose this parameter as a parameter of integration by pulling it out of either $d\Omega_3$ or $d\Omega_4$, the solid angles of q_3 and q_4 . Picking one would also break the same symmetry. Alternatively we can integrate out E_3 or E_4 . This may lead to a nice parametrisation but we desire a more symmetric parametrisation of the two energies. We therefore make the following *Ansatz*:

$$\begin{aligned} E_3 &= \frac{1}{2} \sqrt{s} \bar{z} x_1 \kappa \\ E_4 &= \frac{1}{2} \sqrt{s} \bar{z} \bar{x}_1 \kappa. \end{aligned} \quad (5.37)$$

The energy constraint may then be written as a quadratic equation in κ

$$\xi \kappa^2 - \kappa + 1 = 0, \quad \text{with} \quad \xi = x_1 \bar{x}_1 \bar{z} y_{34}, \quad (5.38)$$

where y_{34} is defined in eq.(5.13). The positive energy solution is

$$\kappa = \frac{1 - \sqrt{1 - 4\xi}}{2\xi} \in [1, 2). \quad (5.39)$$

In the limit $\xi \rightarrow 0$ this function behaves as

$$\lim_{\xi \rightarrow 0} \kappa = 1 + \xi + 2\xi^2 + 5\xi^3 + \mathcal{O}(\xi^4) \quad (5.40)$$

and is therefore well behaved in this limit. The double soft limit now appears when $z \rightarrow 1$, and does not overlap with the single soft singularities which are now nicely separated in phase-space at $x_1 = 0$ and $x_1 = 1$. After this transformation the phase space volume becomes

$$d\Phi_3 = 2^{-4}(2\pi)^{3-2d} d\Omega_3^{(d-1)} d\Omega_4^{(d-1)} dx_1 \left(\frac{\bar{z}\kappa^2}{2-\kappa} \right) \left(\frac{s\bar{z}^2\kappa^2 x_1 \bar{x}_1}{4} \right)^{d-3}. \quad (5.41)$$

Having solved the energy constraint we must still classify the angles. It is convenient to choose the z-axis as the direction of q_1 and we can directly parametrise the angles which q_3 and q_4 make with the z-axis. At last we parametrize the azimuthal angle, ϕ , between q_3 and q_4 in the x-y plane. This leads to the following expressions of the differential solid angles

$$\begin{aligned} d\Omega_3^{(d-1)} &= d\Omega_3^{(d-2)} d\cos\theta_3 (\sin\theta_3)^{d-4} \\ d\Omega_4^{(d-1)} &= d\Omega_4^{(d-3)} d\cos\theta_4 (\sin\theta_4)^{d-4} d\cos\phi (\sin\phi)^{d-5}. \end{aligned} \quad (5.42)$$

Suppressing any extra dimensional components our 4-vectors are then fully parametrized as $q_3 = E_3(1, \sin\theta_3, 0, \cos\theta_3)$ and $q_4 = E_4(1, \sin\theta_4 \sin\phi, \sin\theta_4 \cos\phi, \cos\theta_4)$. Mapping the remaining angles linearly, i.e. $\cos\theta_3 = 2x_3 - 1$, $\cos\theta_4 = 2x_4 - 1$ and $\phi = x_2\pi$, one obtains

$$\begin{aligned} \int d\Phi_3 &= \frac{(2\pi)^{-3+2\epsilon}}{16\Gamma(1-2\epsilon)} \int_0^1 dx_1 dx_2 dx_3 dx_4 \left(\frac{s\bar{z}^3\kappa^4 x_1 \bar{x}_1}{2-\kappa} \right) \\ &\quad \times (s^2 \bar{z}^4 \kappa^4 x_1^2 \bar{x}_1^2 x_3 \bar{x}_3 x_4 \bar{x}_4 \sin^2(\pi x_2))^{-\epsilon} \end{aligned} \quad (5.43)$$

The following lists the propagators of massless partons in this parameterization:

$$\begin{aligned}
s_{13} &= -s\bar{z}\kappa x_1 x_3 \\
s_{23} &= -s\bar{z}\kappa x_1 \bar{x}_3 \\
s_{14} &= -s\bar{z}\kappa \bar{x}_1 x_4 \\
s_{24} &= -s\bar{z}\kappa \bar{x}_1 \bar{x}_4
\end{aligned} \tag{5.44}$$

and

$$\begin{aligned}
s_{34} &= s\bar{z}^2 \kappa^2 x_1 \bar{x}_1 \tilde{x}_{34} \\
s_{134} &= s\bar{z}\kappa [\bar{z}\kappa x_1 \bar{x}_1 \tilde{x}_{34} - x_1 x_3 - \bar{x}_1 x_4] \\
s_{234} &= s\bar{z}\kappa [\bar{z}\kappa x_1 \bar{x}_1 \tilde{x}_{34} - x_1 \bar{x}_3 - \bar{x}_1 \bar{x}_4]
\end{aligned} \tag{5.45}$$

where

$$\tilde{x}_{34} = x_3 \bar{x}_4 + x_4 \bar{x}_3 - 2 \cos(x_2 \pi) \sqrt{x_3 \bar{x}_3 x_4 \bar{x}_4} \tag{5.46}$$

and

$$\kappa = \frac{1 - \sqrt{1 - 4\bar{z}x_1\bar{x}_1\tilde{x}_{34}}}{2\bar{z}x_1\bar{x}_1\tilde{x}_{34}}. \tag{5.47}$$

The angle between q_3 and q_4 is related to

$$\tilde{x}_{34} = \frac{1 - \cos \theta_{34}}{2} = \frac{1 - \cos \theta_3 \cos \theta_4 - \cos \phi \sin \theta_3 \sin \theta_4}{2}. \tag{5.48}$$

This expression exposes the weak point of this parametrisation: it gives rise to an overlapping line singularity when $\phi = 0$ and $\theta_3 = \theta_4$ i.e. when q_3 is parallel to q_4 . Nevertheless the above construction can be used to fully subtract all phase space integrals which do not contain singularities in \tilde{x}_{34} , i.e. which do not contain s_{34}, s_{134}, s_{234} .

Let us now analyse the singularities in this parametrisations. While s_{13}, s_{23}, s_{14} and s_{24} are fully factorized, there is an overlapping line singularity in s_{34} when $\tilde{x}_{34} = 0$. Furthermore there are overlapping singularities in s_{134} and s_{234} . For s_{134} there are 3 different possibilities

$$\begin{aligned}
a) & x_3 = 0 \quad \text{and} \quad x_4 = 0 \\
b) & x_3 = 0 \quad \text{and} \quad x_1 = 1 \\
c) & x_4 = 0 \quad \text{and} \quad x_1 = 0
\end{aligned} \tag{5.49}$$

while for s_{234} the singularities are located at

$$\begin{aligned} a) & x_3 = 1 \quad \text{and} \quad x_4 = 1 \\ b) & x_3 = 1 \quad \text{and} \quad x_1 = 1 \\ c) & x_4 = 1 \quad \text{and} \quad x_1 = 0. \end{aligned} \tag{5.50}$$

We can now apply this parametrisation to all integrals of type $C_1 \otimes C_1, C_3 \otimes C_3$ and $C_1 \otimes C_3$.

Line singularities in the energy and angles parametrisation

One can use a non-linear transformation to get rid of the overlapping structure in \tilde{x}_{34} [35]. A convenient way to derive such a mapping is remapping \tilde{x}_{34} from $\tilde{x}_{34}^- = \tilde{x}_{34}(\phi = 0)$ to $\tilde{x}_{34}^+ = \tilde{x}_{34}(\phi = 1)$ using

$$\tilde{x}_{34} = \frac{\tilde{x}_{34}^- \tilde{x}_{34}^+}{\tilde{x}_{34}^+ - x_2(\tilde{x}_{34}^+ - \tilde{x}_{34}^-)}. \tag{5.51}$$

It is then apparent that \tilde{x}_{34} will vanish whenever \tilde{x}_{34}^- or \tilde{x}_{34}^+ will, for any value of x_2 . The overlapping line singularity is then re-expressed into just a line singularity. To aid numerical stability we perform the mapping $x_2 \rightarrow (1 - \cos(x_2\pi))/2$, such that \tilde{x}_{34} becomes

$$\tilde{x}_{34} = \frac{(x_3 - x_4)^2}{x_3\bar{x}_4 + x_4\bar{x}_3 + 2\cos(x_2\pi)\sqrt{x_3\bar{x}_3x_4\bar{x}_4}}. \tag{5.52}$$

This is in fact identical to the mapping in [71]. The phase space volume then becomes

$$\begin{aligned} \Phi_3 = & \frac{(2\pi)^{-3+2\epsilon}}{16\Gamma(1-2\epsilon)} \int_0^1 dx_1 dx_2 dx_3 dx_4 \left(\frac{s\bar{z}^3 \kappa^4 x_1 \bar{x}_1}{2 - \kappa} \right) \\ & \times \left(s^2 \bar{z}^4 \kappa^4 x_1^2 \bar{x}_1^2 x_3 \bar{x}_3 x_4 \bar{x}_4 \sin^2(\pi x_2) \right)^{-\epsilon} \left(\frac{\tilde{x}_{34}}{|x_3 - x_4|} \right)^{1-2\epsilon}. \end{aligned} \tag{5.53}$$

To factorize the line singularity in s_{34} (at $x_3 = x_4$) we are forced to split the integration region in two, separating $x_3 < x_4$ from $x_4 < x_3$.

5.3.3 A more general κ parameterisation

Writing

$$\begin{aligned} y_1 &= x_1 x_3 & y_3 &= \bar{x}_1 x_4 \\ y_2 &= x_1 \bar{x}_3 & y_4 &= \bar{x}_1 \bar{x}_4, \end{aligned} \quad (5.54)$$

it is clear that $\sum_i y_i = 1$. This observation allows us to generalise the energies and angle parameterisation of the previous section, as follows

$$\begin{aligned} \int d\Phi_3 &= \frac{(2\pi)^{-3+2\epsilon}}{16\Gamma(1-2\epsilon)} \int_0^1 dx_2 \left(\prod_{i=1}^4 dy_i \right) \delta \left(\sum_{i=1}^4 y_i - 1 \right) \\ &\times \left(\frac{s \bar{z}^3 \kappa^4}{2 - \kappa} \right) \left(s^2 \bar{z}^4 \kappa^4 \sin^2(\pi x_2) \prod_{i=1}^4 y_i \right)^{-\epsilon}. \end{aligned} \quad (5.55)$$

In the following we list the propagators of massless partons in this parameterization:

$$\begin{aligned} s_{13} &= -s \bar{z} \kappa y_1 \\ s_{23} &= -s \bar{z} \kappa y_2 \\ s_{14} &= -s \bar{z} \kappa y_3 \\ s_{24} &= -s \bar{z} \kappa y_4 \end{aligned} \quad (5.56)$$

and

$$s_{34} = s \kappa^2 \bar{z}^2 (y_1 y_4 + y_2 y_3 + 2 \cos(\pi x_2) \sqrt{y_1 y_4 y_2 y_3}). \quad (5.57)$$

This allows to derive a whole class of possibly nice parameterisations. We can, for example, solve the δ -constraint using

$$\begin{aligned} y_1 &= x_1 x_3 & y_2 &= \bar{x}_1 x_4 \\ y_3 &= x_1 \bar{x}_3 & y_4 &= \bar{x}_1 \bar{x}_4. \end{aligned} \quad (5.58)$$

The parameterisation for s_{134} and s_{234} then read

$$\begin{aligned} s_{134} &= s \bar{z} \kappa \left[\bar{z} \kappa (x_1^2 x_3 \bar{x}_3 + \bar{x}_1^2 x_4 \bar{x}_4 + 2 x_1 \bar{x}_1 \cos(\pi x_2) \sqrt{x_3 \bar{x}_3 x_4 \bar{x}_4}) - x_1 \right], \\ s_{234} &= s \bar{z} \kappa \left[\bar{z} \kappa (x_1^2 x_3 \bar{x}_3 + \bar{x}_1^2 x_4 \bar{x}_4 + 2 x_1 \bar{x}_1 \cos(\pi x_2) \sqrt{x_3 \bar{x}_3 x_4 \bar{x}_4}) - \bar{x}_1 \right]. \end{aligned} \quad (5.59)$$

For s_{134} there overlapping singularities are now located at,

$$\begin{aligned} a) x_4 = 0 \quad \text{and} \quad x_1 = 0 \\ b) x_4 = 1 \quad \text{and} \quad x_1 = 0, \end{aligned} \tag{5.60}$$

while for s_{234} the overlapping singularities are located at:

$$\begin{aligned} a) x_3 = 0 \quad \text{and} \quad x_1 = 1 \\ b) x_3 = 1 \quad \text{and} \quad x_1 = 1 \end{aligned} \tag{5.61}$$

5.3.4 Hierarchical parameterization

Since in the energy and angles parameterization the invariants s_{34}, s_{134}, s_{234} had line and overlapping singularities, it is worth having a second parameterization which factorizes these, but may not factorize the others. Our second parameterization closely resembles the features of the rapidity parameterization published in [36], however it is somewhat simpler. In this parameterization the three particle phase space element $d\Phi_3$ is first factorized into a product of two 2-particle phase spaces

$$d\Phi_3(\sqrt{s}; 0, 0, \sqrt{u_{1..n}}) = \int \frac{ds_{34}}{2\pi} d\Phi_2(\sqrt{s}; \sqrt{s_{34}}, \sqrt{u_{1..n}}) d\Phi_2(\sqrt{s_{34}}; 0, 0), \tag{5.62}$$

with

$$\begin{aligned} d\Phi_2(\sqrt{s}; \sqrt{s_{34}}, \sqrt{u_{1..n}}) &= (2\pi)^{2-d} d^d Q \delta^{(+)}(Q^2 - u_{1..n}) \\ &\quad \times d^d \tilde{Q} \delta^{(+)}(\tilde{Q}^2 - s_{34}) \delta^d(q_1 + q_2 - \tilde{Q} - Q) \end{aligned} \tag{5.63}$$

and

$$d\Phi_2(\sqrt{s_{34}}; 0, 0) = (2\pi)^{2-d} d^d q_3 \delta^{(+)}(q_3^2) d^d q_4 \delta^{(+)}(q_4^2) \delta^d(\tilde{Q} - q_3 - q_4). \tag{5.64}$$

Parameterisation of $d\Phi_2(\sqrt{s}; \sqrt{s_{34}}, \sqrt{u_{1..n}})$

Integrating out Q we obtain

$$d\Phi_2(\sqrt{s}; \sqrt{s_{34}}, \sqrt{u_{1..n}}) = d^d p_{34} \delta(\tilde{Q}^2 - s_{34}) \delta((p_1 + p_2 - \tilde{Q})^2 - u_{1..n}). \tag{5.65}$$

We rewrite $d^d \tilde{Q}$ in terms of energy $E_{\tilde{Q}}$, transverse momentum \tilde{Q}_\perp and the z-momentum component \tilde{Q}_z and use the two delta functions to eliminate $E_{\tilde{Q}}$ and

\tilde{Q}_\perp . This yields

$$E_{\tilde{Q}} = \frac{1}{2\sqrt{s}}(s + s_{34} - u_{1..n}) \quad (5.66)$$

and

$$\tilde{Q}_\perp = \sqrt{E_{\tilde{Q}}^2 - (\tilde{Q}_z)^2 - s_{34}} \quad (5.67)$$

We then introduce the integration variable s_{134} through the identity

$$1 = \int ds_{134} \delta(s_{134} - (p_1 - \tilde{Q})^2) \quad (5.68)$$

and use this new constraint to eliminate \tilde{Q}_z as

$$\tilde{Q}_z = E_{\tilde{Q}} + \frac{s_{134} - s_{34}}{\sqrt{s}}. \quad (5.69)$$

The phase space measure then becomes

$$d\Phi_2(\sqrt{s}; \sqrt{s_{34}}, \sqrt{u_{1..n}}) = (2\pi)^{2-d} \frac{1}{4s} d\Omega^{d-2} (\tilde{Q}_\perp)^{d-4} ds_{134}. \quad (5.70)$$

We use the condition $\tilde{Q}_\perp \geq 0$ to find the physical region for s_{34} and s_{134} . This yields the conditions

$$\begin{aligned} 0 &\leq s_{34} \leq \frac{s_{134}(s + s_{134} - u_{1..n})}{s_{134} - u_{1..n}} \\ 0 &\geq s_{134} \geq (u_{1..n} - s). \end{aligned} \quad (5.71)$$

Parametrisation of $d\Phi_2(\sqrt{s_{34}}; 0, 0)$

$d\Phi_2(\sqrt{s_{34}}; 0, 0)$ can be parameterised in terms of the invariants s_{13} and s_{23} yielding

$$d\Phi_2(\sqrt{s_{34}}; 0, 0) = (2\pi)^{2-d} \frac{1}{8\tilde{Q}_\perp s} ds_{13} ds_{23} d\Omega^{d-3} [(p_3)_\perp \sin \phi]^{d-5} \quad (5.72)$$

where ϕ is the angle between $(p_3)_\perp$ and \tilde{Q}_\perp . We fulfil the constraint $(p_3)_\perp \sin \phi \geq 0$ to find the limits of integration for s_{13} and then for s_{23} .

Hierarchical parametrisation of $d\Phi_3(\sqrt{s}, 0, 0, \sqrt{u_{1..n}})$

Parameterizing s_{134} , s_{34} , s_{13} and s_{23} linearly between their corresponding limits of integration, as described above, we arrive at the following parameterisation of the

phase space measure

$$\int d\Phi_3 = \frac{(2\pi)^{-3+2\epsilon}}{16\Gamma(1-2\epsilon)} \int_0^1 dx_1 dx_2 dx_3 dx_4 \left(\frac{s\bar{z}^3 x_1 \bar{x}_1}{z + x_1 \bar{z}} \right) \left(\frac{s^2 \bar{z}^4 x_1^2 \bar{x}_1^2 x_2 \bar{x}_2 x_3 \bar{x}_3 \sin^2(\pi x_4)}{z + x_1 \bar{z}} \right)^{-\epsilon}. \quad (5.73)$$

The invariants in this parameterization are

$$\begin{aligned} s_{34} &= \frac{s\bar{z}^2 x_1 \bar{x}_1 x_2}{z + x_1 \bar{z}} \\ s_{134} &= -s\bar{z} x_1 \\ s_{234} &= -s\bar{z} \bar{x}_1 \left[\frac{z + x_1 \bar{x}_2 \bar{z}}{z + x_1 \bar{z}} \right] \\ s_{23} &= -s\bar{z} \bar{x}_1 x_3 \\ s_{24} &= -s\bar{z} \bar{x}_1 \bar{x}_3 \end{aligned} \quad (5.74)$$

and

$$\begin{aligned} s_{13} &= -s\bar{z} x_1 \left[x_3 \bar{x}_2 + \frac{x_2 \bar{x}_3}{z + x_1 \bar{z}} - 2 \cos(\pi x_4) \sqrt{\frac{x_2 \bar{x}_2 x_3 \bar{x}_3}{z + x_1 \bar{z}}} \right] \\ s_{14} &= -s\bar{z} x_1 \left[\bar{x}_3 \bar{x}_2 + \frac{x_2 x_3}{z + x_1 \bar{z}} + 2 \cos(\pi x_4) \sqrt{\frac{x_2 \bar{x}_2 x_3 \bar{x}_3}{z + x_1 \bar{z}}} \right]. \end{aligned}$$

We see that the only invariants which are not factorized are s_{13} and s_{14} . The variable s_{13} contains overlapping singularities at $x_3 = 0 = x_2$ and $x_3 = 1 = x_2$ as well as an overlapping line singularity at $x_4 = 0, x_1 = 1, x_3 = x_2$, while s_{14} contains overlapping singularities at $x_3 = 0, x_2 = 1$ and $x_3 = 1, x_2 = 1$ as well as an overlapping line singularity at $x_4 = 1, x_1 = 1, x_3 = 1 - x_2$.

Line singularities in the hierarchical parameterization

Let us consider the expressions

$$\frac{J(p_1, p_2, p_3, p_4)}{s_{13}s_{24}}, \quad \frac{J(p_1, p_2, p_3, p_4)}{s_{13}s_{23}} \quad (5.75)$$

with $J(p_1, p_2, p_3, p_4)$ a finite numerator function. They both contain a line singularity due to s_{13} in the denominator. We now use the partial fractioning identities,

$$\frac{1}{s_{13}s_{24}} = \frac{1}{s_{13}s_{234} + s_{134}s_{24}} \left(\frac{s_{134}}{s_{13}} + \frac{s_{234}}{s_{24}} \right), \quad (5.76)$$

$$\frac{1}{s_{13}s_{23}} = \frac{1}{s_{13}s_{234} + s_{23}s_{134}} \left(\frac{s_{134}}{s_{13}} + \frac{s_{234}}{s_{23}} \right). \quad (5.77)$$

The term $s_{13}s_{234} + s_{134}s_{24}$ has an overlapping singularity at $x_3 = 1 = x_2$, while the term $s_{13}s_{234} + s_{134}s_{23}$ has an overlapping singularity at $x_3 = 0 = x_2$. Then we exchange $1 \leftrightarrow 2$ and $3 \leftrightarrow 4$ in the term containing s_{13} to rotate the line singularity out, i.e.

$$\frac{J(p_1, p_2, p_3, p_4)}{s_{13}s_{24}} = \frac{J(p_1, p_2, p_3, p_4) + J(p_2, p_1, p_4, p_3)}{s_{13}s_{234} + s_{134}s_{24}} \frac{s_{234}}{s_{24}} \quad (5.78)$$

$$\frac{J(p_1, p_2, p_3, p_4)}{s_{13}s_{23}} = \frac{J(p_1, p_2, p_3, p_4) + J(p_2, p_1, p_3, p_4)}{s_{13}s_{234} + s_{23}s_{134}} \frac{s_{234}}{s_{23}}. \quad (5.79)$$

and we are left with just overlapping singularities, which can be treated as explained in the following section. This trick was first discovered by Frank Petriello [74] and it has been used in the implementation of the program FEHIP described in [36], it has been also been used in the evaluation of double real counterterms in [51].

5.3.5 Numerical evaluation of double-real radiation phase-space integrals

In this section, we present a numerical evaluation of the phase-space integrals we presented in Table 5.3. To evaluate our integrals numerically we choose the point ($s = 1, z = 0.1$). We will only consider the integrals to $\mathcal{O}(\epsilon^0)$.

Topology $C_1 \otimes C_1$

1. The integral

$$I_{11a} = \int \frac{d\Phi_3}{s_{13}s_{23}s_{14}s_{24}} \quad (5.80)$$

fully factorizes in the energies and angles parameterization (Section 5.3.2), we obtain

$$I_{11a} = 0.09400(2) + \frac{0.010951(4)}{\epsilon} - \frac{0.0035586(5)}{\epsilon^2} - \frac{0.001119844946(1)}{\epsilon^3}. \quad (5.81)$$

2. The integral

$$I_{11b} = \int d\Phi_3 \frac{(s_{34}s - s_{14}s_{23})^2}{s_{13}^2 s_{24}^2} \quad (5.82)$$

with the numerator structure as in [36], factorizes in the energies and angles

parameterization (Section 5.3.2), we get

$$I_{11b} = 0.023885(3) + \frac{0.0041606(3)}{\epsilon} + \frac{0.00036930(4)}{\epsilon^2}. \quad (5.83)$$

Topology $C_2 \otimes C_2$

1. The integral

$$I_{22a} = \int \frac{d\Phi_3 N(\{s_{ij}\})}{(s_{34}s_{134})^2} \quad (5.84)$$

factorizes in the hierarchical parameterization (Section 5.3.4). The numerator function has the scaling behavior $N(\{s_{ij}\}) \sim s_{34}s_{134}$ [36]. We obtain

$$I_{22a} = \int \frac{d\Phi_3}{s_{34}s_{134}} = 0.0011728(1) - \frac{0.00050726(1)}{\epsilon} - \frac{0.000125982556(0)}{\epsilon^2}. \quad (5.85)$$

2. The integral

$$I_{22b} = \int \frac{d\Phi_3 N(\{s_{ij}\})}{s_{34}^2 s_{134} s_{234}} \quad (5.86)$$

factorizes in the hierarchical parameterization (Section 5.3.4). The numerator scales as $N(\{s_{ij}\}) \sim s_{34}$. We obtain

$$I_{22b} = \int \frac{d\Phi_3}{s_{34}s_{134}s_{234}} = -0.0015003(2) + \frac{0.00112726(5)}{\epsilon} + \frac{0.000279961236(1)}{\epsilon^2}. \quad (5.87)$$

Topology $C_3 \otimes C_3$

1. The integral

$$I_{33a} = \int d\Phi_3 \frac{(s_{34}s_{134} - s_{14}s_{23})^2}{s_{234}^2 s_{24}^2} \quad (5.88)$$

factorizes in the hierarchical parameterization (section 5.3.4). The numerator structure can be found in [36]. We obtain

$$I_{33a} = -0.003841(2) + \frac{0.0007814(4)}{\epsilon} + \frac{0.00018465(1)}{\epsilon^2}. \quad (5.89)$$

2. The integral

$$I_{33b} = \int \frac{d\Phi_3}{s_{134}s_{234}s_{13}s_{23}} \quad (5.90)$$

neither factorizes in energies and angles nor in the hierarchical parameterization. We use the hierarchical parameterization (section 5.3.4), since fewer over-

lapping singularities are present there. Using partial fractions, as described in section 5.3.4 we can rewrite the integral as

$$I_{33b} = \int \frac{2d\Phi_3}{s_{23}s_{134}(s_{134}s_{23} + s_{234}s_{13})}. \quad (5.91)$$

This contains the following substructure

$$\frac{1}{x_3} \frac{1}{x_3 A + x_2 \bar{x}_3 B + C \sqrt{x_2 \bar{x}_2 x_3 \bar{x}_2}} \quad (5.92)$$

with A, B, C finite. This becomes singular when $x_3 = 0 = x_2$ where x_3 is active. We factorize this singularity by applying

$$x_3 \mapsto \alpha(x_3, x_2, 1) \quad (5.93)$$

and obtain

$$I_{33b} = 0.023155(3) + \frac{0.0076371(1)}{\epsilon} + \frac{0.00007730(6)}{\epsilon^2} - \frac{0.000279961236(1)}{\epsilon^3}. \quad (5.94)$$

3. The integral

$$I_{33c} = \int \frac{d\Phi_3}{s_{134}s_{234}s_{13}s_{24}} \quad (5.95)$$

is similar to I_{33b} in the hierarchical parameterization (Section 5.3.4). Partial fractioning as before we get

$$I_{33c} = \int \frac{2d\Phi_3}{s_{24}s_{134}(s_{134}s_{24} + s_{234}s_{13})}. \quad (5.96)$$

This contains the substructure

$$\frac{1}{\bar{x}_3} \frac{1}{\bar{x}_3 \bar{x}_2 A + \bar{x}_3 x_2 B + C \sqrt{x_2 \bar{x}_2 x_3 \bar{x}_3}} \quad (5.97)$$

with A, B, C finite. This becomes singular when $\bar{x}_3 = 0 = \bar{x}_2$ with \bar{x}_3 being active. We disentangle this singularity by applying

$$\bar{x}_3 \mapsto \alpha(\bar{x}_3, \bar{x}_2, 1) \quad (5.98)$$

We then obtain

$$I_{33c} = 0.12567(9) - \frac{0.03645(1)}{\epsilon} - \frac{0.018566(1)}{\epsilon^2} + \frac{0.002799612364(0)}{\epsilon^3}. \quad (5.99)$$

Topology $C_1 \otimes C_3$

1. The integral

$$I_{13a} = \int d\Phi_3 \frac{(s_{34}s - s_{14}s_{23})^2}{s_{234}s_{24}^2s_{13}} \quad (5.100)$$

with the numerator structure as in [36]. The singularities factorize in energies and angles. We immediately obtain

$$I_{13a} = -0.0040885(4) - \frac{0.00036930(1)}{\epsilon}. \quad (5.101)$$

2. The integral

$$I_{13b} = \int d\Phi_3 \frac{N(\{s_{ij}\})}{s_{134}s_{13}s_{14}s_{23}} \quad (5.102)$$

has a quadratic divergence due to the term $s_{134}s_{13}s_{14}$. This means that $N(\{s_{ij}\}) \sim \{s_{134}, s_{13}, s_{14}\}$. Such that

$$I_{13b} = \left\{ \int \frac{d\Phi_3}{s_{13}s_{14}s_{23}}, \int \frac{d\Phi_3}{s_{134}s_{14}s_{23}} \right\} \quad (5.103)$$

the first of which is a sub-topology of C_1^2 while the second is a sub-topology of C_3^2 .

Topology $C_1 \otimes C_2$

1. The integral

$$I_{12} = \int \frac{d\Phi_3 N(\{s_{ij}\})}{s_{34}s_{234}s_{13}s_{24}} \quad (5.104)$$

has a quadratic divergence due to the term $s_{34}s_{234}s_{24}$. The numerator can have the following scalings: $N(\{s_{ij}\}) \sim \{s_{34}, s_{234}, s_{24}\}$. We therefore consider the following possibilities

$$I_{12} = \left\{ \int \frac{d\Phi_3}{s_{34}s_{13}s_{24}}, \int \frac{d\Phi_3}{s_{34}s_{234}s_{13}}, \int \frac{d\Phi_3}{s_{234}s_{13}s_{24}} \right\} \quad (5.105)$$

The last of these is a sub-topology of C_3^2 and does not merit further attention. We will evaluate the other two in the hierarchical parameterization. For

$$I_{12a} = \int \frac{d\Phi_3}{s_{34}s_{13}s_{24}} \quad (5.106)$$

we use the same strategy as we used for I_{33c} . We obtain

$$I_{12a} = 0.07115(1) + \frac{0.006996(1)}{\epsilon} - \frac{0.0029912(1)}{\epsilon^2} - \frac{0.000839883709(0)}{\epsilon^3}. \quad (5.107)$$

The integral

$$I_{12b} = \int \frac{d\Phi_3}{s_{34}s_{234}s_{13}} \quad (5.108)$$

factorizes in the hierarchical parameterization. We obtain

$$I_{12b} = 0.0198554(9) + \frac{0.0023667(2)}{\epsilon} - \frac{0.00088965(4)}{\epsilon^2} - \frac{0.000279961236(1)}{\epsilon^3}. \quad (5.109)$$

Topology $C_2 \otimes C_3$

1. The integral

$$I_{23a} = \int \frac{d\Phi_3 N(\{s_{ij}\})}{s_{34}s_{234}^2 s_{23}} \quad (5.110)$$

factorizes in the hierarchical parameterization, but carries a cubic divergence in $\bar{x}_1 \sim s_{234}$. Taking $N(\{s_{ij}\}) \sim s_{234}^2$, we get

$$I_{23a} = \int \frac{d\Phi_3}{s_{34}s_{23}} \quad (5.111)$$

which just is a sub-topology of I_{12a} . While other numerators are possible these do not give different singularity structures.

2. The integral

$$I_{23a} = \int \frac{d\Phi_3 N(\{s_{ij}\})}{s_{34}s_{134}s_{234}s_{23}} \quad (5.112)$$

factorizes in the hierarchical parameterization, but carries a quadratic divergence in $\bar{x}_1 \sim s_{234}$. A minimal choice for the numerator is $N(\{s_{ij}\}) \sim s_{234}$ in which case we recover I_{22b} . Hence no new singularity structures can be obtained from this topology.

Topologies $C_2 \otimes C_4$ and $C_3 \otimes C_4$

We will now consider interferences of C_4 with C_2 and C_3 . One can evaluate these interferences in the energies and angles parameterization. In the following we will use $t_{13} \sim E_3 \sim (s_{13} + s_{23})$ and $t_{24} \sim E_4 \sim (s_{14} + s_{24})$.

1. Topology $C_2 \otimes C_4$:

The integral

$$I_{24} = \int \frac{d\Phi_3}{s_{34}s_{134}(s_{13} + s_{23})(s_{14} + s_{24})} \quad (5.113)$$

has the following singularity structure

$$\frac{1}{x_1\bar{x}_1(x_3 - x_4)} \frac{1}{Ax_1\bar{x}_1(x_3 - x_4)^2 + Bx_1x_3 + C\bar{x}_1x_4} \quad (5.114)$$

in the energy and angle parameterization after the mapping (see 5.3.2) is applied. We first split the integration region into two sectors which we define as $x_3 < x_4$ (sector 1) and $x_4 < x_3$ (sector 2). After this sector decomposition we are still left with overlapping singularities at $x_3 = 0 = \bar{x}_1$ in sector 1 and at $x_4 = 0 = x_1$ in sector 2. These can be disentangled using

$$\bar{x}_1 \mapsto \alpha(\bar{x}_1, x_3, 1) \quad (5.115)$$

in sector 1 and

$$x_1 \mapsto \alpha(x_1, x_4, 1) \quad (5.116)$$

in sector 2. We then obtain

$$I_{24} = -0.006956(3) - \frac{0.0010708(3)}{\epsilon} + \frac{0.00065900(1)}{\epsilon^2} + \frac{0.000207378694(0)}{\epsilon^3}. \quad (5.117)$$

2. Topology $C_3 \otimes C_4$:

The integral

$$I_{34} = \int \frac{d\Phi_3}{s_{13}s_{134}(s_{13} + s_{23})(s_{14} + s_{24})} \quad (5.118)$$

has the following singularity structure

$$\frac{1}{x_1x_3} \frac{1}{Ax_1\bar{x}_1(x_3 - x_4)^2 + Bx_1x_3 + C\bar{x}_1x_4}. \quad (5.119)$$

It contains no line singularity but several overlapping ones located at $x_3 = 0 = x_4$, $x_4 = 0 = x_1$ and at $x_3 = 0, \bar{x}_1 = 0$. To separate the two singularities we first

partial fraction the soft singularities by multiplying by $1 = x_1 + \bar{x}_1$. We then treat the two terms with different non-linear transformations. For the first term we apply the mapping

$$x_3 \mapsto \alpha(x_3, x_4 \bar{x}_1, 1) \quad (5.120)$$

since x_3 is the only active singularity, it is clear that we had to remap it. The second term is more difficult, since both x_3 and x_1 are now active. We apply the following sequence of mappings:

First let

$$x_3 \mapsto \alpha(x_3, x_4, 1) \quad (5.121)$$

and then

$$\begin{aligned} x_1 &\mapsto \alpha(x_1, \bar{x}_3, 1) \\ x_4 &\mapsto \alpha(x_4, \bar{x}_3, 1) \end{aligned} \quad (5.122)$$

We obtain

$$I_{34} = -0.32519(4) - \frac{0.048942(2)}{\epsilon} - \frac{0.0062917(3)}{\epsilon^2} - \frac{0.000559922473(3)}{\epsilon^3}. \quad (5.123)$$

5.4 On the dimensionality of the massive LO n -particle phase space in higher order calculations

The dimension of the massive LO n -particle phase-space, which we explicitly factored out also for real and double real corrections, can always be taken as strictly 4 dimensional. This appears to be intuitively clear, since there are no singularities associated to any of the kinematical variables of the n massive particles.

We can prove this statement more rigorously. Let us write the NNLO contribution

to the partonic cross section as

$$\begin{aligned}
\sigma_{2 \rightarrow n+x}^{\text{NNLO}} &= \sigma_{2 \rightarrow n}^{(2)}[\mathcal{J}] + \sigma_{2 \rightarrow n+1}^{(1)}[\mathcal{J}] + \sigma_{2 \rightarrow n+2}^{(0)}[\mathcal{J}] \\
&= \frac{1}{2s} \left[\int d\Phi_n |\mathcal{A}_{2 \rightarrow n}^{(2)}|^2 \mathcal{J}_n \right. \\
&\quad + \int d\Phi_{n+1} |\mathcal{A}_{2 \rightarrow n+1}^{(1)}|^2 \mathcal{J}_{n+1} \\
&\quad \left. + \int d\Phi_{n+2} |\mathcal{A}_{2 \rightarrow n+2}^{(0)}|^2 \mathcal{J}_{n+2} \right].
\end{aligned} \tag{5.124}$$

Now we apply the phase space factorisation of the single and double real emission phase space measures to obtain

$$\begin{aligned}
\sigma_{2 \rightarrow n+x}^{\text{NNLO}} &= \frac{1}{2s} \int \frac{du_{1..n}}{2\pi} \int d\Phi_n \left[(2\pi) \delta(u_{1..n} - s) |\mathcal{A}_{2 \rightarrow n}^{(2)}|^2 \mathcal{J}_n \right. \\
&\quad \left. + \int d\Phi_2 |\mathcal{A}_{2 \rightarrow n+1}^{(1)}|^2 \mathcal{J}_{n+1} + \int d\Phi_3 |\mathcal{A}_{2 \rightarrow n+2}^{(0)}|^2 \mathcal{J}_{n+2} \right].
\end{aligned} \tag{5.125}$$

Let us now assume that all re-normalisation procedures, both UV and initial state collinear, have already been carried out. It may not be trivial that one can do this for the initial state collinear singularities, but it can always be done by introducing explicit counter-terms on the amplitude squared level. The expression in the square bracket of eq.(5.125) must then be finite. This follows straight from the condition of infra-red safety, which essentially states that, in the event of a singularity of a real emission, the $n + r$ particle jet function must reduce to an $n + r - 1$ jet function. In the most singular configurations at NNLO, those which require cancellations between double-virtual, real-virtual and double-real corrections, we then have that $\mathcal{J}_{n+2}, \mathcal{J}_{n+1} \rightarrow \mathcal{J}_n$. We can interpret this as the statement that IR singularities cancel locally in the phase-space of the n massive particles.

It follows that for any infra-red safe observable, the expression in the square bracket is a finite real number plus terms of order ϵ , for every allowed configuration of the n massive momenta $\{p_i\}$. Then there is no problem in taking the limit $d \rightarrow 4$ already now, and to perform the integration over $d\Phi_n$ in four dimensions only. Furthermore, this statement is not limited to NNLO, but is true to all orders in perturbation theory, by the same argument.

5.5 Conclusions

In this chapter we developed a method for double real emissions to massive final states in hadronic collisions. This method is based in particular on two phase-space parametrisations with which many of the singular invariants are in a factorised form. By considering the most singular propagator structures which may occur in all possible Feynman diagrams we derived a list of the most singular denominators, which could appear. For each of these integrals it was then demonstrated how an efficient factorisation could be achieved using mostly non-linear mappings and in some cases partial fraction identities to avoid possible line-singularities. For the scenario of gluon emissions off massive coloured particles, it is more beneficial to use the energy and angle parametrisation, this is the only case in which a sector decomposition must be partially applied. To proof our concept we evaluated all singular integrals numerically.

Chapter 6

Real corrections to $1 \rightarrow 2$ massless decays

There exist a number phenomenologically important processes of $1 \rightarrow 2$ decays (e.g. $(Z, H) \rightarrow q\bar{q}, W \rightarrow u\bar{d}, \dots$), which may be very well approximated by taking the 2 decay products as massless. In this chapter we shall develop a general approach towards tackling single and double real emissions corrections to such processes using the tool of non-linear mappings. When considering double real emission corrections to a $1 \rightarrow 2$ decay process, the production of two further massless particles in the final state must be considered. At NNLO this results in phase-space integrals with up to 4 massless particles in the final state.

We should remark that the more general subtraction schemes which we mentioned in the beginning of Chapter 5 should also be applicable in this scenario. In fact a more difficult problem, the NNLO corrections to the $1 \rightarrow 3$ decay: $\gamma^* \rightarrow jjj$, was tackled using the Antenna subtraction scheme, but remains to this day the only complete differential computation which has been accomplished within this scheme.

6.1 Notational setup for $1 \rightarrow 2$ decays at NNLO

Let us denote the momenta of the final state massless particles by p_i , where $i \in \{1, 2, 3, 4\}$, and the momentum of the decaying massive particle as Q . Momentum conservation then gives

$$Q = \sum_{i=1}^4 p_i. \tag{6.1}$$

We define the Lorentz invariants such that they correspond to singular propagators appearing in the corresponding Feynman diagrams, normalised to the only physical scale Q^2 :

$$\begin{aligned} s_{ij} &= \frac{(p_i + p_j)^2}{Q^2}, & i, j \in \{1, 2, 3, 4\}, \quad i \neq j \\ s_{ijk} &= \frac{(p_i + p_j + p_k)^2}{Q^2}, & i, j, k \in \{1, 2, 3, 4\}, \quad i \neq j, j \neq k, k \neq i. \end{aligned} \quad (6.2)$$

All of these invariants may become singular in some limit.

At NNLO the fully differential decay width may be written as

$$\begin{aligned} \Gamma_{1 \rightarrow 2+X}[\mathcal{J}] &= \Gamma_{1 \rightarrow 2}^{(0)}[\mathcal{J}] + \left(\frac{\alpha_s}{\pi}\right) \left(\Gamma_{1 \rightarrow 2}^{(1)} + \Gamma_{1 \rightarrow 3}^{(0)}[\mathcal{J}]\right) \\ &+ \left(\frac{\alpha_s}{\pi}\right)^2 \left(\Gamma_{1 \rightarrow 2}^{(2)}[\mathcal{J}] + \Gamma_{1 \rightarrow 3}^{(1)}[\mathcal{J}] + \Gamma_{1 \rightarrow 4}^{(0)}[\mathcal{J}]\right) + \mathcal{O}(\alpha_s^3). \end{aligned} \quad (6.3)$$

Here the notation is such that $\Gamma_{1 \rightarrow n+r}^{(l)}[\mathcal{J}]$ corresponds to the l th order correction with r emitted particles in the final state. The fully differential LO partonic decay rate is then

$$\Gamma_{1 \rightarrow 2}^{(0)}[\mathcal{J}] = \frac{1}{\sqrt{Q^2}} \int d\Phi_2 |\mathcal{A}_{1 \rightarrow 2}^{(0)}|^2 \mathcal{J}_2. \quad (6.4)$$

At NLO we must also include virtual and real corrections:

$$\begin{aligned} \Gamma_{1 \rightarrow 2}^{(1)}[\mathcal{J}] &= \frac{1}{\sqrt{Q^2}} \int d\Phi_2 |\mathcal{A}_{1 \rightarrow 2}^{(1)}|^2 \mathcal{J}_2 \\ \Gamma_{1 \rightarrow 3}^{(0)}[\mathcal{J}] &= \frac{1}{\sqrt{Q^2}} \int d\Phi_3 |\mathcal{A}_{1 \rightarrow 3}^{(0)}|^2 \mathcal{J}_3 \end{aligned} \quad (6.5)$$

At NNLO double virtual, real-virtual and double-real emissions must be included:

$$\begin{aligned} \Gamma_{1 \rightarrow 2}^{(2)}[\mathcal{J}] &= \frac{1}{\sqrt{Q^2}} \int d\Phi_2 |\mathcal{A}_{1 \rightarrow 2}^{(2)}|^2 \mathcal{J}_2 \\ \Gamma_{1 \rightarrow 3}^{(1)}[\mathcal{J}] &= \frac{1}{\sqrt{Q^2}} \int d\Phi_3 |\mathcal{A}_{1 \rightarrow 3}^{(1)}|^2 \mathcal{J}_3 \\ \Gamma_{1 \rightarrow 4}^{(0)}[\mathcal{J}] &= \frac{1}{\sqrt{Q^2}} \int d\Phi_4 |\mathcal{A}_{1 \rightarrow 4}^{(0)}|^2 \mathcal{J}_4. \end{aligned} \quad (6.6)$$

Here we used the shorthand notation $\mathcal{J}_n = \mathcal{J}(\{p_{i=1..n}\})$ to denote the jet function of the n -particle final state. With $\Phi_n = \Phi_n(\sqrt{Q^2}; 0, \dots, 0)$ we denote the massless n -particle phase space volume and with $|\mathcal{A}_{1 \rightarrow n}^{(l)}|^2$ the l th order correction to the

squared, spin summed and averaged matrix element.

6.2 A $1 \rightarrow 2$ phase space parametrisation

The $1 \rightarrow 2$ phase-space is trivial, since in the center of mass frame, the 2 decay products are back to back. The phase- space volume is therefore

$$\Phi_2^d = \int d\Phi_2^d = \frac{1}{(2\pi)^{d-2}} \frac{\Omega_{d-1}}{2^{d-1}} (Q^2)^{-\epsilon} = \frac{1}{8\pi} \frac{(Q^2)^{-\epsilon} (4\pi)^\epsilon \Gamma(1-\epsilon)}{\Gamma(2-2\epsilon)}. \quad (6.7)$$

6.3 A $1 \rightarrow 3$ phase space parametrisation

We use the following parametrisation for the $1 \rightarrow 3$ phase space:

$$\Phi_3 = \frac{\Phi_2(Q^2)^{1-2\epsilon}}{(4\pi)^{d/2} \Gamma(1-\epsilon)} \int_0^1 dx_1 dx_2 (x_1 \bar{x}_1 x_2)^{-\epsilon} \bar{x}_2^{1-2\epsilon}. \quad (6.8)$$

The invariants take the simple form:

$$\begin{aligned} s_{12} &= x_2 \\ s_{13} &= \bar{x}_2 x_1 \\ s_{23} &= \bar{x}_2 \bar{x}_1 \end{aligned} \quad (6.9)$$

The most singular Feynman diagram is depicted in Figure 6.1. Considering the

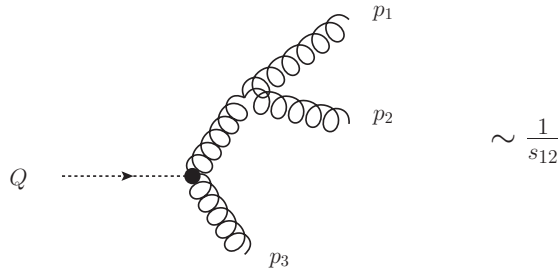


Figure 6.1: Most singular Feynman diagrams in real emissions to $1 \rightarrow 2$ massless decays

expressions which the invariants take in this parametrisation it is clear that all interferences and squares of this topology are always factorised.

6.4 A $1 \rightarrow 4$ phase space parametrisation

We parameterize the phase space for the $1 \rightarrow 4$ processes as follows:

$$\Phi_4(Q; 0, 0, 0, 0) = N_4 \int_0^1 dx_1 dx_2 dx_3 dx_4 dx_5 [x_1 \bar{x}_1 \bar{x}_2]^{1-2\epsilon} [x_2 x_3 \bar{x}_3 x_4 \bar{x}_4]^{-\epsilon} [\sin(x_5 \pi)]^{-2\epsilon} \quad (6.10)$$

where

$$N_4 = \frac{(Q^2)^{2-3\epsilon} 2^{-13+8\epsilon} \pi^{-4+3\epsilon} (1-2\epsilon)}{\Gamma(3/2-\epsilon)^2 \Gamma(1-\epsilon)}. \quad (6.11)$$

The invariants in this parameterization are

$$\begin{aligned} s_{234} &= x_1 \\ s_{34} &= x_1 x_2 \\ s_{23} &= x_1 \bar{x}_2 x_4 \\ s_{24} &= x_1 \bar{x}_2 \bar{x}_4 \\ s_{12} &= \bar{x}_1 \bar{x}_2 \bar{x}_3 \\ s_{134} &= x_2 + x_3 \bar{x}_1 \bar{x}_2 \end{aligned} \quad (6.12)$$

and

$$\begin{aligned} s_{13} &= \bar{x}_1 [x_4 x_3 + x_2 \bar{x}_3 \bar{x}_4 + 2 \cos(x_5 \pi) \sqrt{x_2 x_3 \bar{x}_3 x_4 \bar{x}_4}] \\ s_{14} &= \bar{x}_1 [x_3 \bar{x}_4 + x_2 \bar{x}_3 x_4 - 2 \cos(x_5 \pi) \sqrt{x_2 x_3 \bar{x}_3 x_4 \bar{x}_4}]. \end{aligned} \quad (6.13)$$

This parameterization is very similar to the ones used in [75, 35].

In the following section we shall describe how to factorise the singularities of the most singular topologies using the above parametrisation with the non-linear mapping. In contrast to our strategy for double real emissions in hadronic production processes we shall here demonstrate the power of non-linear mappings by factorising all singularities in a single parametrisation. Due to the large discrete symmetry group S_4 of the massless 4 particle phase space only a small number of maximally singular integrals must be considered independently. We depict typical Feynman diagrams which correspond to maximally singular phase-space integrals in Figure 6.2.

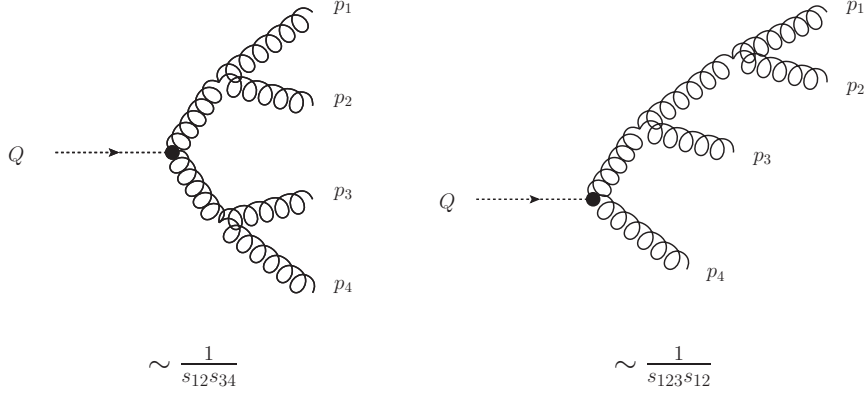


Figure 6.2: Most singular Feynman Diagrams in $1 \rightarrow 2$ massless Decays

6.5 Integration of most singular double-real integrals

In this section we show how the most singular double emission phase space integrals can be factorized with non-linear transformations. We begin the discussion with an integral with four singular denominators,

$$I_1[J] = \int d\Phi_4 \frac{J(p_1, p_2, p_3, p_4)}{s_{12}s_{34}s_{123}s_{234}}. \quad (6.14)$$

where the function J represents a non singular function of the partonic momenta, composed of numerators in the squared matrix elements and the infrared-safe observable \mathcal{J} . We disentangle the overlapping singularities using

$$\bar{x}_3 \mapsto \alpha(\bar{x}_3, x_4, 1), \quad (6.15)$$

After this transformation all remaining singularities are integrable. The expansion in ϵ is then straightforward with simple subtractions. For the special case $J = 1$, we obtain

$$I_1[J = 1] = N_4 \left[61.76(2) + \frac{8.554(2)}{\epsilon} - \frac{0.1710(2)}{\epsilon^2} + \frac{0.34657(2)}{\epsilon^3} + \frac{0.25}{\epsilon^4} \right]. \quad (6.16)$$

Other integrals may be mapped to I_1 of Eq. 6.14 with a relabeling of the partonic momenta. For example, the integral

$$I_1 = \int d\Phi_4 \frac{J(p_1, p_2, p_3, p_4)}{s_{14}s_{23}s_{134}s_{234}}, \quad (6.17)$$

which has an apparently more complicated singularity structure due to s_{14} in the denominator, is transformed to the integral of Eq. 6.14 by exchanging p_2 and p_4 .

A second class of integrals has the following denominator structure:

$$I_2[J] = \int d\Phi_4 \frac{J(p_1, p_2, p_3, p_4)}{s_{13}s_{23}s_{134}s_{234}} \quad (6.18)$$

Notice, that the integrand is singular not only at the boundaries of the integration variables x_i , but it also develops a “line singularity” inside the integration volume. We eliminate this by casting the integral in the form

$$I_2[J] = \int d\Phi_4 \frac{(J(p_1, p_2, p_3, p_4) + J(p_2, p_1, p_3, p_4))s_{24}}{s_{23}s_{134}s_{234}(s_{13}s_{24} + s_{14}s_{23})}. \quad (6.19)$$

It is easy to see that Eq. 6.19 is equivalent to $I_2[J]$, by exchanging the momenta $p_1 \leftrightarrow p_2$ in the term with $J(p_2, p_1, p_3, p_4)$. The denominator

$$\begin{aligned} s_{13}s_{24} + s_{14}s_{23} = x_1\bar{x}_1\bar{x}_2 \Big[& 2x_3x_4\bar{x}_4 + x_2\bar{x}_3(x_4^2 + \bar{x}_4^2) \\ & + 2\cos(\pi x_5)(1 - 2x_4)\sqrt{x_2x_3\bar{x}_3x_4\bar{x}_4} \Big] \end{aligned} \quad (6.20)$$

is only singular at the boundaries of the integration region. Applying the following sequence of mappings

$$\begin{aligned} x_2 &\mapsto \alpha(x_2, x_3, 1) \\ x_4 &\mapsto \alpha(x_4, x_2\bar{x}_3, 1) \\ x_2 &\mapsto \alpha(x_2, \bar{x}_1, 1) \end{aligned} \quad (6.21)$$

leads to a factorized form. Numerically we then obtain

$$I_2[J=1] = N_4 \left[-201.16(3) - \frac{68.426(4)}{\epsilon} - \frac{12.027(8)}{\epsilon^2} + \frac{1.0397(1)}{\epsilon^3} + \frac{0.75}{\epsilon^4} \right]. \quad (6.22)$$

A last class of singular integrals with four denominators is:

$$\begin{aligned}
I_3 [J] &= \int d\Phi_4 \frac{J(p_1, p_2, p_3, p_4)}{s_{13}s_{23}s_{14}s_{24}} \\
&= \int d\Phi_4 \frac{J(p_1, p_3, p_2, p_4)}{s_{12}s_{34}s_{14}s_{23}} \\
&= \int d\Phi_4 \frac{(J(p_1, p_3, p_2, p_4) + J(p_2, p_4, p_1, p_3))s_{24}}{s_{34}s_{12}s_{23}(s_{13}s_{23} + s_{14}s_{24})}.
\end{aligned} \tag{6.23}$$

The term in parenthesis in the last denominator is given by

$$\begin{aligned}
s_{13}s_{23} + s_{14}s_{24} &= x_1\bar{x}_1\bar{x}_2 \left[2x_2\bar{x}_3x_4\bar{x}_4 + x_3(x_4^2 + \bar{x}_4^2) \right. \\
&\quad \left. + 2\cos(\pi x_5)(2x_4 - 1)\sqrt{x_2x_3\bar{x}_3x_4\bar{x}_4} \right]
\end{aligned} \tag{6.24}$$

We let $dI_3 = x_2dI_3 + \bar{x}_2dI_3$ and apply

$$\begin{aligned}
x_2 &\mapsto \alpha(x_2, x_3, 1) \\
x_{3,4} &\mapsto \alpha(x_{3,4}, \bar{x}_2, 1)
\end{aligned} \tag{6.25}$$

to \bar{x}_2dI_3 and

$$x_4 \mapsto \alpha(x_4, x_3, 1) \tag{6.26}$$

to x_2dI_3 . After these transformations, both integrals have only factorized singularities and can be evaluated numerically. We obtain:

$$I_3 [J = 1] = N_4 \left[-292.54(4) - \frac{217.030(9)}{\epsilon} - \frac{52.768(2)}{\epsilon^2} + \frac{6.9314(3)}{\epsilon^3} + \frac{5}{\epsilon^4} \right]. \tag{6.27}$$

Other integrals with four denominators are mapped to $I_{1,2,3}[J]$ with simple relabeling of the partonic momenta. Integrals with fewer denominators are simpler and the non-linear mappings for them are obvious upon inspection. One case which requires special attention arises when a denominator is raised to the second power in the squares of diagrams where a gluon splits into a $q\bar{q}$ or gg pair, as has already been discussed in the literature (see, for example, [36, 76]). These quadratic singularities are fake. A combination of terms, such as

$$\frac{1}{s_{34}^2} \left(\frac{s_{14}}{s_{134}} - \frac{s_{24}}{s_{234}} \right)^2 \tag{6.28}$$

is the one which emerges in the physical matrix elements. After a non-linear mapping

$$x_2 \rightarrow \alpha(x_2, x_3, 1) \tag{6.29}$$

to factorize an overlapping singularity, the integrand is also free of quadratic singularities in the integration variables x_i .

6.6 Conclusion

In this chapter we developed a strategy to tackle real emission integrals for $1 \rightarrow 2$ massless decay processes at NNLO. The major challenge here was to tackle the double real emission integrals, very complicated overlapping singularity structures are encountered here. In order to factorise these singularities we employed the method of non-linear mappings. With the aid of partial fractions it was found that all singularities can be factorised with this technique. We presented numerical results for the most singular of these integrals and checked these against known analytic results in the literature.

Chapter 7

The $H \rightarrow b\bar{b}$ decay width

Direct searches and electroweak precision tests suggest that a Standard Model Higgs boson is light, and that it should decay predominantly into a bottom quark ($b\bar{b}$) pair. Inclusive searches at the LHC of a Higgs resonance in the bottom-pair invariant mass distribution are unfortunately hampered by a very large QCD background. Direct searches are therefore focusing on other decay channels, such as $H \rightarrow \gamma\gamma$, with a much smaller branching ratio. In view of this, perturbative corrections to the $H \rightarrow b\bar{b}$ decay are most interesting for the inclusive rate, due to its contribution to the total decay width and the branching ratios of other decays. A remarkable effort has been made for a precise calculation of $\Gamma_{H \rightarrow b\bar{b}}$ and now QCD corrections are known to $\mathcal{O}(\alpha_s^4)$ [77, 78, 79, 80, 81, 82, 83, 84, 85].

Recently, confidence has grown that the $H \rightarrow b\bar{b}$ decay can be observed at the LHC directly in events where the Higgs boson is produced in association with a massive vector boson (W, Z) [86] or a $t\bar{t}$ pair [87]. Backgrounds from $t\bar{t}, V + jj$ and multi-jet production are challenging. However, the excellent b -jet tagging of the ATLAS and CMS detectors as well as sophisticated selections of jet events described in [86, 87], render these channels hopeful, as explicitly demonstrated by the ATLAS collaboration in a full detector simulation analysis for the ZH case [88]. For this channel, further suppression of the background can be obtained with the sub-jet algorithms of [89].

These search strategies rely on a selection of phase space corners which are rich in potential Higgs events. An accurate modeling of QCD radiation is necessary in order to assess the efficiency of these selections. This motivates the computation of the fully differential $H \rightarrow b\bar{b}$ decay at NNLO in perturbative QCD.

7.1 Notation and set-up

We compute the partial width $\Gamma_{H \rightarrow b\bar{b}X}[\mathcal{J}]$ through NNLO in perturbative QCD for any infrared safe observable \mathcal{J} , such as an appropriate jet-algorithm, in the decay of a Higgs boson to a pair of bottom-quarks,

$$H \rightarrow b + \bar{b} + X. \quad (7.1)$$

In our calculation we consider only the Higgs boson to couple to a bottom quarks with a bare Yukawa coupling strength $y_b^B = \frac{m_b^B}{v}$. Due to the largely different mass of the Higgs boson, m_H , and the small bottom-quark mass, m_b , we treat the latter as independent of the Yukawa coupling and set it to zero in matrix elements and phase space integrals. In addition, we neglect top-quarks both in virtual corrections and in the renormalization procedure and consider $n_f = 5$ light quark flavors. For the renormalization of UV divergences we work in the $\overline{\text{MS}}$ -scheme where the bare couplings, $y_b^B = \frac{m_b^B}{v}$, and $g_s^B = \sqrt{4\pi\alpha_s^B}$, are related to their renormalized counterparts by the relations introduced in chapter 2. These considerations lead us to use the Lagrangian

$$\mathcal{L} = \mathcal{L}_{\text{QCD}}|_{n_f=5, m_i=0} - y_b H \bar{b} b \quad (7.2)$$

to effectively describe the interactions of this process. We shall use a notation similar to the one introduced in Chapter 6, with $Q = p_H$ and $Q^2 = m_H^2$. We write the fully differential $H \rightarrow b\bar{b}$ decay rate as

$$\begin{aligned} \Gamma_{H \rightarrow b\bar{b}+X}[\mathcal{J}] &= y_b^2 \left[\Gamma_{H \rightarrow b\bar{b}}^{(0)}[\mathcal{J}] + \left(\frac{\alpha_s}{\pi} \right) \left(\Gamma_{H \rightarrow b\bar{b}}^{(0)}[\mathcal{J}] + \Gamma_{H \rightarrow b\bar{b}j}^{(1)}[\mathcal{J}] \right) \right. \\ &\quad \left. + \left(\frac{\alpha_s}{\pi} \right)^2 \left(\Gamma_{H \rightarrow b\bar{b}}^{(2)}[\mathcal{J}] + \Gamma_{H \rightarrow b\bar{b}j}^{(1)}[\mathcal{J}] + \Gamma_{H \rightarrow b\bar{b}jk}^{(0)}[\mathcal{J}] \right) + \mathcal{O}(\alpha_s^3) \right]. \end{aligned} \quad (7.3)$$

At LO we must consider

$$\Gamma_{H \rightarrow b\bar{b}}^{(0)}[\mathcal{J}] = \frac{1}{2m_H} \int d\Phi_2 \left| \mathcal{A}_{H \rightarrow b\bar{b}}^{(0)} \right|^2 \mathcal{J}_2 \quad (7.4)$$

At NLO we include real and virtual corrections

$$\begin{aligned} \Gamma_{H \rightarrow b\bar{b}}^{(1)}[\mathcal{J}] &= \frac{1}{2m_H} \int d\Phi_2 \left| \mathcal{A}_{H \rightarrow b\bar{b}}^{(1)} \right|^2 \mathcal{J}_2 \\ \Gamma_{H \rightarrow b\bar{b}j}^{(0)}[\mathcal{J}] &= \frac{1}{2m_H} \int d\Phi_3 \left| \mathcal{A}_{H \rightarrow b\bar{b}g}^{(0)} \right|^2 \mathcal{J}_3. \end{aligned} \quad (7.5)$$

At NNLO we include double virtual, real-virtual and double real emissions

$$\begin{aligned}
\Gamma_{H \rightarrow b\bar{b}}^{(2)}[\mathcal{J}] &= \frac{1}{2m_H} \int d\Phi_2 \left| \mathcal{A}_{H \rightarrow b\bar{b}}^{(2)} \right|^2 \mathcal{J}_2 \\
\Gamma_{H \rightarrow b\bar{b}j}^{(1)}[\mathcal{J}] &= \frac{1}{2m_H} \int d\Phi_3 \left| \mathcal{A}_{H \rightarrow b\bar{b}j}^{(1)} \right|^2 \mathcal{J}_3 \\
\Gamma_{H \rightarrow b\bar{b}jk}^{(0)}[\mathcal{J}] &= \frac{1}{2m_H} \int d\Phi_4 \left(\left| \mathcal{A}_{H \rightarrow b\bar{b}q\bar{q}}^{(0)} \right|^2 \mathcal{J}_4 \right. \\
&\quad \left. + \frac{1}{2!} \left| \mathcal{A}_{H \rightarrow b\bar{b}gg}^{(0)} \right|^2 \mathcal{J}_4 + \frac{1}{2!2!} \left| \mathcal{A}_{H \rightarrow b\bar{b}b\bar{b}}^{(0)} \right|^2 \mathcal{J}_4 \right).
\end{aligned} \tag{7.6}$$

Regarding the analytic continuations of complex functions presented in this chapter the positive “epsilon prescription” must be used, since all occurring mass scales are external, i.e.

$$m_H^2 \rightarrow m_H^2 + i\varepsilon, \quad s_{ij} \rightarrow s_{ij} + i\varepsilon. \tag{7.7}$$

where ε is a small positive parameter.

7.2 Squared amplitudes

In this section we present the square of the scattering amplitudes needed for the computation of the $H \rightarrow b\bar{b}$ decay width through $\mathcal{O}(\alpha_s^2)$. These can be derived with modern methods for computing Feynman diagrams and have been ingredients of many prior calculations. For example, the same matrix elements enter the calculation of the NNLO total cross-section $b\bar{b} \rightarrow H$ [90]. We have made an independent computation and present them here for completeness. For the generation of the matrix elements we used QGRAF [91]. For further symbolic manipulations, such as color and Dirac algebra, we used FORM [92] and MAPLE [93]. We reduced one and two-loop amplitudes to master integrals using the method of integration by parts [94, 95] and the Laporta algorithm [96] with AIR [97].

7.2.1 Decay to two partons

For the process

$$H(p_H) \rightarrow b(p_1) + \bar{b}(p_2)$$

we require up to 2-loop corrections. The tree-level coefficient is simply

$$\left| \mathcal{A}_{H \rightarrow b\bar{b}}^{(0)} \right|^2 = 2N m_H^2, \quad (7.8)$$

the one-loop coefficient is

$$\left| \mathcal{A}_{H \rightarrow b\bar{b}}^{(1)} \right|^2 = \left| \mathcal{A}_{H \rightarrow b\bar{b}}^{(0)} \right|^2 C_F \left[\Re \left(\left(\frac{\mu^2}{-m_H^2} \right)^\epsilon \right) f_\epsilon + \frac{3}{2\epsilon} \right]$$

with

$$f_\epsilon = (1 - \epsilon)^2 \frac{\Gamma(1 + \epsilon) \Gamma(-\epsilon)^2}{\Gamma(2 - 2\epsilon)} e^{\gamma_\epsilon}. \quad (7.9)$$

The NNLO contribution is

$$\left| \mathcal{A}_{H \rightarrow b\bar{b}}^{(2)} \right|^2 = \left| \mathcal{A}_{H \rightarrow b\bar{b}}^{(0)} \right|^2 \left(\left| \mathcal{A}_{H \rightarrow b\bar{b}}^{VV} \right|^2 + \left| \mathcal{A}_{H \rightarrow b\bar{b}}^{V^2} \right|^2 \right), \quad (7.10)$$

where

$$\left| \mathcal{A}_{H \rightarrow b\bar{b}}^{V^2} \right|^2 = C_F^2 \left[\left| \frac{\mu^2}{-m_H^2} \right|^{2\epsilon} f_\epsilon^2 + \frac{3}{\epsilon} \Re \left(\left(\frac{\mu^2}{-m_H^2} \right)^\epsilon \right) f_\epsilon + \frac{9}{4\epsilon^2} \right]. \quad (7.11)$$

corresponds to the one-loop squared amplitude and

$$\left| \mathcal{A}_{H \rightarrow b\bar{b}}^{VV} \right|^2 = \sum_{k=0}^4 \frac{\left| \mathcal{A}_{-k}^{VV} \right|^2}{\epsilon^k} + \mathcal{O}(\epsilon) \quad (7.12)$$

corresponds to the two-loop amplitude interfered with the tree amplitude. The coefficients are given by

$$\begin{aligned} \left| \mathcal{A}_0^{VV} \right|^2 &= \left[\frac{1}{6} l_H^4 + \frac{13}{72} l_H^3 + \left(-6\zeta_2 - \frac{31}{36} \right) l_H^2 + \left(-\frac{55}{108} - \frac{61}{24} \zeta_2 - \frac{7}{6} \zeta_3 \right) l_H \right. \\ &\quad \left. + \frac{455}{162} + \frac{377}{72} \zeta_2 + \frac{263}{16} \zeta_4 - \frac{47}{36} \zeta_3 \right] C_F^2 + \left[-\frac{1}{36} n_f l_H^3 + \frac{5}{36} n_f l_H^2 \right. \\ &\quad \left. + \frac{1}{27} (9\zeta_2 - 7) n_f l_H - \frac{1}{648} (495\zeta_2 - 18\zeta_3 - 200) n_f \right] C_F \end{aligned}$$

$$\begin{aligned}
& + \left[\frac{11}{72} l_H^3 + \left(\frac{1}{4} \zeta_2 - \frac{67}{72} \right) l_H^2 + \left(-\frac{13}{4} \zeta_3 - \frac{11}{6} \zeta_2 + \frac{121}{108} \right) l_H \right. \\
& \left. + \frac{701}{144} \zeta_2 - \zeta_4 - \frac{467}{648} + \frac{151}{72} \zeta_3 \right] C_F N^{-1} \\
|\mathcal{A}_{-1}^{VV}|^2 &= \left(-\frac{1}{3} l_H^3 + \frac{3}{8} l_H^2 + \left(6\zeta_2 + \frac{31}{36} \right) l_H - \frac{13}{4} \zeta_2 + \frac{7}{12} \zeta_3 - \frac{491}{864} \right) C_F^2 \\
& + \left(-\frac{5}{36} n_f l_H + \frac{1}{432} (54\zeta_2 + 65) n_f \right) C_F \\
& + \left(\left(-\frac{1}{4} \zeta_2 + \frac{67}{72} \right) l_H - \frac{11}{16} \zeta_2 + \frac{13}{8} \zeta_3 - \frac{961}{864} \right) C_F N^{-1} \\
|\mathcal{A}_{-2}^{VV}|^2 &= \left(-3\zeta_2 - \frac{5}{3} l_H + \frac{1}{2} l_H^2 + \frac{217}{144} \right) C_F^2 \\
& + \left(\frac{1}{12} n_f l_H - \frac{1}{18} n_f \right) C_F + \left(\frac{1}{8} \zeta_2 - \frac{11}{24} l_H + \frac{2}{9} \right) C_F N^{-1} \\
|\mathcal{A}_{-3}^{VV}|^2 &= \left(\frac{17}{8} - \frac{1}{2} l_H \right) C_F^2 - \frac{1}{8} C_F n_f + \frac{11}{16} \frac{C_F}{N} \\
|\mathcal{A}_{-4}^{VV}|^2 &= \frac{1}{4} C_F^2
\end{aligned} \tag{7.13}$$

with $l_H = \ln \left(\frac{\mu^2}{m_H^2} \right)$.

7.2.2 Decay to three partons

For the process

$$H(p_H) \rightarrow b(p_1) + \bar{b}(p_2) + g(p_3)$$

we require up to 1-loop corrections. The tree contribution can be expressed as

$$|\mathcal{A}_{H \rightarrow b\bar{b}g}^{(0)}|^2 = 8\pi^2 S_\epsilon^{-1} |\mathcal{A}_{H \rightarrow b\bar{b}}^{(0)}|^2 \hat{P}_{qq} \left(\frac{s_{12}}{m_H^2} \right) \left[\frac{1}{s_{13}} + \frac{1}{s_{23}} \right] \tag{7.14}$$

where

$$\hat{P}_{qq}(z) = C_F \left[\frac{1+z^2}{1-z} - \epsilon(1-z) \right] \tag{7.15}$$

is the quark gluon splitting kernel. The one-loop correction can be expressed as

$$\begin{aligned}
\left| \mathcal{A}_{H \rightarrow b\bar{b}g}^{(1)} \right|^2 = & -2\pi^2 (\mu^2 e^{\gamma_E})^\epsilon S_\epsilon^{-1} \times \left\{ \left(8 \frac{(s_{23} + s_{13})^2 \epsilon^2}{s_{23}s_{13}} \right. \right. \\
& + 4 \frac{(s_{23} + s_{13})^2 \epsilon}{s_{23}s_{13}} + \frac{-12 s_{12}^2 - 12 m_H^4 + 8 s_{12} m_H^2}{s_{23}s_{13}} + \frac{4 s_{12}^2 + 4 m_H^4}{\epsilon s_{13}s_{23}} \Big) C_F \text{Bub}(s_{12}) \\
& + \left[\left(8 + 4 \frac{(s_{23} + s_{13})(s_{23} + m_H^2) \epsilon^2}{(s_{13} + s_{12}) s_{23}} - 4 \frac{(s_{12}s_{23} + 3 s_{23}s_{13} - s_{23}^2 + m_H^4) \epsilon}{(s_{13} + s_{12}) s_{23}} \right) N C_F^2 \right. \\
& + \left(4 \frac{(s_{23} + s_{13})(2 s_{23} + s_{13}) \epsilon^2}{s_{23}s_{13}} - 4 \frac{(s_{12}s_{13} - s_{23}^2 - s_{13}^2) \epsilon}{s_{23}s_{13}} \right. \\
& \left. \left. - 4 \frac{2 s_{12}^2 + s_{23}^2 + s_{23}s_{13} + s_{13}^2 + 2 m_H^4}{s_{23}s_{13}} + 4 \frac{s_{12}^2 + m_H^4}{\epsilon s_{13}s_{23}} \right) C_F \right] \text{Bub}(s_{23}) + (1 \leftrightarrow 2) \\
& + \left[\left(-8 \frac{(s_{23} + s_{13}) m_H^2 (2 s_{23}s_{13} + s_{12}s_{23} + s_{12}s_{13}) \epsilon^2}{s_{13}s_{23}(s_{23} + s_{12})(s_{13} + s_{12})} \right. \right. \\
& + \frac{(8 m_H^8 - 8 s_{12}^2 s_{13}^2 + 16 s_{23}^2 s_{13}^2 - 8 s_{23}^2 s_{12}^2 + 8 s_{12}^4 - 8 s_{13}^3 m_H^2 - 8 s_{23}^3 m_H^2) \epsilon}{s_{13}s_{23}(s_{23} + s_{12})(s_{13} + s_{12})} \\
& \left. \left. - 8 \frac{2 s_{12}^2 + 3 s_{23}s_{13} + s_{23}^2 + s_{13}^2 + 2 m_H^4}{s_{23}s_{13}} + 8 \frac{s_{12}^2 + m_H^4}{\epsilon s_{13}s_{23}} \right) N C_F^2 \right. \\
& + \left(-8 \frac{(s_{23} + s_{13})^2 \epsilon^2}{s_{23}s_{13}} - 4 \frac{(s_{23}^2 + s_{13}^2) \epsilon}{s_{23}s_{13}} + 4 \frac{2 s_{12}^2 + s_{23}^2 + s_{23}s_{13} + s_{13}^2 + 2 m_H^4}{s_{23}s_{13}} \right. \\
& \left. - 4 \frac{s_{12}^2 + m_H^4}{\epsilon s_{13}s_{23}} \right) C_F \Big] \text{Bub}(m_H^2) + \left[2 \frac{s_{12}s_{13}(s_{23} + s_{13}) \epsilon^2}{s_{23}} \right. \\
& + 2 \frac{s_{12}(s_{23} + s_{13})^2 \epsilon}{s_{23}} - 2 \frac{s_{12}(s_{12}^2 + m_H^4)}{s_{23}} \Big] C_F \text{Box}(s_{12}, s_{13}, m_H^2) + (1 \leftrightarrow 2) \\
& + \left[((-12 s_{23}s_{13} - 4 s_{23}^2 - 4 s_{13}^2) \epsilon + 4 s_{12}^2 + 4 m_H^4) N C_F^2 \right. \\
& + ((-6 s_{23}s_{13} - 2 s_{23}^2 - 2 s_{13}^2) \epsilon + 2 s_{12}^2 + 2 m_H^4) C_F \Big] \text{Box}(s_{13}, s_{23}, m_H^2) \Big\} \\
& - \frac{1}{\epsilon} \left(\frac{3C_F}{2} + \frac{11C_A}{12} - \frac{T_F n_f}{3} \right) \left| \mathcal{A}_{H \rightarrow b\bar{b}g}^{(0)} \right|^2. \tag{7.16}
\end{aligned}$$

There are only two different master integrals which appear here. The bubble

$$\text{Bub}(s_{23}) = \int \frac{d^d k}{i\pi^{\frac{d}{2}}} \frac{1}{k^2(k + p_2 + p_3)^2} = \frac{\Gamma(1 + \epsilon)\Gamma(1 - \epsilon)^2}{\epsilon\Gamma(2 - 2\epsilon)} (-s_{23})^{-\epsilon} \tag{7.17}$$

as well as the following box integral

$$\text{Box}(s_{23}, s_{34}, m_H^2) = \int \frac{d^d k}{i\pi^{\frac{d}{2}}} \frac{1}{k^2(k+p_2)^2(k+p_2+p_3)^2(k+p_2+p_3+p_4)^2}. \quad (7.18)$$

which can be expressed to all orders in ϵ in terms of hypergeometric functions

$$\begin{aligned} \text{Box}(s, t, M^2) = & \frac{2\Gamma(1+\epsilon)\Gamma(1-\epsilon)^2}{\epsilon^2\Gamma(1-2\epsilon)} \frac{1}{st} \left[-(-M^2)^{-\epsilon} {}_2F_1\left(1, -\epsilon; 1-\epsilon; -\frac{uM^2}{st}\right) \right. \\ & \left. + (-t)^{-\epsilon} {}_2F_1\left(1, -\epsilon; 1-\epsilon; -\frac{u}{s}\right) + (-s)^{-\epsilon} {}_2F_1\left(1, -\epsilon; 1-\epsilon; -\frac{u}{t}\right) \right] \end{aligned} \quad (7.19)$$

with $u = M^2 - s - t$. This result is well known, nevertheless we provide an independent derivation in Appendix C.

7.2.3 Decay to four partons

For the decay to four partons we need

$$H(p_H) \rightarrow b(p_1) + \bar{b}(p_2) + i(p_3) + j(p_4), \quad (ij) \in \{(q\bar{q}), (b\bar{b}), (gg)\} \quad (7.20)$$

at tree-level. The $H \rightarrow b\bar{b}q\bar{q}$ amplitude can be expressed as

$$\left| \mathcal{A}_{H \rightarrow b\bar{b}q\bar{q}}^{(0)} \right|^2 = (2\pi)^4 S_\epsilon^{-2} (2NC_F) A(p_1, p_2, p_3, p_4). \quad (7.21)$$

For two $b\bar{b}$ pairs in the final state we obtain

$$\begin{aligned} \left| \mathcal{A}_{H \rightarrow b\bar{b}b\bar{b}}^{(0)} \right|^2 = & (2\pi)^4 S_\epsilon^{-2} \\ & \times \left\{ 2NC_F [A(p_1, p_2, p_3, p_4) + A(p_1, p_4, p_3, p_2) + A(p_3, p_2, p_1, p_4) + A(p_3, p_4, p_1, p_2)] \right. \\ & \left. + 2C_F [B(p_1, p_2, p_3, p_4) + B(p_3, p_4, p_1, p_2) + B(p_4, p_3, p_2, p_1) + B(p_2, p_1, p_4, p_3)] \right\} \end{aligned} \quad (7.22)$$

where

$$\begin{aligned}
A(p_1, p_2, p_3, p_4) = & \\
& 2 \left[\frac{2(1-\epsilon)}{s_{34}} - (1+\epsilon) \left(\frac{1}{s_{134}} + \frac{1}{s_{234}} \right) + m^2(\epsilon-1) \left(\frac{1}{s_{134}^2} + \frac{1}{s_{234}^2} \right) \right. \\
& + \frac{s_{13} - s_{14} - 2(s_{24} + m^2) - \epsilon(s_{13} + s_{14})}{s_{234}s_{34}} - \frac{2m^2}{s_{34}^2} \left(\frac{s_{14}}{s_{134}} - \frac{s_{24}}{s_{234}} \right)^2 \\
& + \frac{s_{23} - s_{24} - 2(s_{14} + m^2) - \epsilon(s_{23} + s_{24})}{s_{134}s_{34}} - \frac{2m^2}{s_{34}^2} \left(\frac{s_{14}}{s_{134}} - \frac{s_{24}}{s_{234}} \right)^2 \\
& \left. + 2 \frac{m^4 + m^2(s_{14} + s_{24}) + (s_{14} + s_{24})^2}{s_{134}s_{34}s_{234}} + 2 \frac{(1+\epsilon)m^2 + s_{34} + 2(s_{14} + s_{24})}{s_{134}s_{234}} \right]. \quad (7.23)
\end{aligned}$$

The form factor $B(p_1, p_2, p_3, p_4)$ is presented in Appendix A. The squared amplitude corresponding to the Higgs decaying into a $b\bar{b}$ plus two extra gluons can be expressed as

$$\left| \mathcal{A}_{H \rightarrow b\bar{b}gg}^{(0)} \right|^2 = (2\pi)^4 S_\epsilon^{-2} \left[C_F A_{Hb\bar{b}gg} + N C_F^2 B_{Hb\bar{b}gg} + C_F (1 + 2N C_F) C_{Hb\bar{b}gg} \right] \quad (7.24)$$

where

$$\begin{aligned}
A_{Hb\bar{b}gg} &= A_{Hb\bar{b}gg}^{(0)} + \epsilon A_{Hb\bar{b}gg}^{(1)} + \epsilon^2 A_{Hb\bar{b}gg}^{(2)} \\
B_{Hb\bar{b}gg} &= B_{Hb\bar{b}gg}^{(0)} + \epsilon B_{Hb\bar{b}gg}^{(1)} + \epsilon^2 B_{Hb\bar{b}gg}^{(2)} \\
C_{Hb\bar{b}gg} &= C_{Hb\bar{b}gg}^{(0)} + \epsilon C_{Hb\bar{b}gg}^{(1)}. \quad (7.25)
\end{aligned}$$

The form factors $A_{Hb\bar{b}gg}^{(i)}$, $B_{Hb\bar{b}gg}^{(i)}$ and $C_{Hb\bar{b}gg}^{(i)}$ can be found in Appendix A.

7.3 Integration over phase-space

For the integration over phase-space we use the techniques developed in Chapter 6. While these are fully sufficient for the integrations of the single and double real, complications arise with the integration over the real-virtual contribution. We will discuss this issue in the next section.

7.4 Integration of the real-virtual

In the one loop amplitude for $H \rightarrow b\bar{b}g$ we will face integrals like

$$\int d\Phi_3 \frac{{}_2F_1(1, -\epsilon; 1 - \epsilon; -\frac{s_{23}}{s_{13}})}{s_{23}s_{13}} \quad (7.26)$$

Since the numerator in this case is not well defined for $s_{23}, s_{13} \rightarrow 0$, we can not simply apply the plus-prescription of eq.(3.7) to extract the singularities. To tackle this difficulty we use Euler's integral representation of the hypergeometric function, and apply a non-linear mapping to disentangle an overlapping singularity of the integration variable in the hypergeometric representation and the phase space variables which generate s_{13}, s_{23} . Defining

$$F(z) = \int_0^1 dx_3 \frac{x_3^{-1-\epsilon}}{1 + zx_3} = \frac{{}_2F_1(1, -\epsilon; 1 - \epsilon; -z)}{-\epsilon} \quad (7.27)$$

we apply the transformation,

$$x_3 \mapsto \beta(x_3, z^{-1}) \quad (7.28)$$

which yields

$$F(z) = (1+z)^\epsilon \int_0^1 dx_3 x_3^{-1-\epsilon} \left(1 - \frac{x_3 z}{1+z}\right)^\epsilon. \quad (7.29)$$

This representation of the hypergeometric function has finite values at the points where we need to make a subtraction,

$$\begin{aligned} {}_2F_1(-\epsilon, -\epsilon; 1 - \epsilon; 0) &= 1 \\ {}_2F_1(-\epsilon, -\epsilon; 1 - \epsilon; 1) &= \Gamma(1 + \epsilon)\Gamma(1 - \epsilon), \end{aligned} \quad (7.30)$$

and we can obtain the Laurent expansion in ϵ of the real-virtual contribution easily with a “plus-prescription” subtraction. For non-special values of the kinematic variables the ϵ -expansion of the hypergeometric function reads:

$${}_2F_1(-\epsilon, -\epsilon; 1 - \epsilon; z) = (1-z)^\epsilon \left(1 - \epsilon \log(1-z) - \sum_{k=2}^{\infty} \epsilon^k \text{Li}_k\left(\frac{z}{z-1}\right)\right). \quad (7.31)$$

The mapping of Eq. 7.28 simply re-derives a well known identity

$${}_2F_1(a, b; c; z) = (1-z)^{-b} {}_2F_1\left(c-a, b; c; \frac{z}{z-1}\right), \quad (7.32)$$

and there would be no need of it had we started with the following representation of the box master integral:

$$\begin{aligned}
\text{Box}(u, t, M^2) = & \frac{2\Gamma(1+\epsilon)\Gamma(1-\epsilon)^2}{\epsilon^2\Gamma(1-2\epsilon)}(ut)^{-1-\epsilon} \\
& \times \left[(-t-s)^\epsilon {}_2F_1\left(-\epsilon, -\epsilon; 1-\epsilon; \frac{s}{t+s}\right) \right. \\
& + (-u-s)^\epsilon {}_2F_1\left(-\epsilon, -\epsilon; 1-\epsilon; \frac{s}{u+s}\right) \\
& \left. - (-M^2)^{-\epsilon}(ut+sM^2)^\epsilon {}_2F_1\left(-\epsilon, -\epsilon; 1-\epsilon; \frac{sM^2}{ut+sM^2}\right) \right]
\end{aligned} \tag{7.33}$$

On the other hand, more complicated master integrals for one-loop amplitudes do not always have representations in terms of hypergeometric functions with known expansions in ϵ and variable limits. However, it is always possible to derive a Feynman representation or a hypergeometric representation (via a Mellin-Barnes representation) for them and attempt a direct numerical evaluation of the combined phase space and virtual multiple integral using non-linear transformations to factorize the singularities. We have compared the two approaches:

1. Numerically evaluate the coefficients of the Laurent expansion for the two-dimensional phase space integral after we express the loop amplitude and its hypergeometric functions in terms of polylogarithms,
2. Numerically evaluate the coefficients of the Laurent expansion for the three-dimensional combined phase space and loop integral.

We find that the three-dimensional numerical integration is as fast as the two-dimensional numerical integration where we require the evaluation of polylogarithmic functions.

7.5 Numerical results

In this section we present our numerical results for the decay rate $\Gamma_{H \rightarrow b\bar{b}X}[\mathcal{J}]$ for selected infrared safe observables \mathcal{J} . We select the value of the renormalization scale $\mu = m_H$. First, we compute the inclusive decay width. Our numerical result is,

$$\Gamma_{H \rightarrow b\bar{b}}^{NNLO} = \Gamma_{H \rightarrow b\bar{b}}^{LO} \left[1 + \left(\frac{\alpha_s}{\pi}\right) 5.6666(4) + \left(\frac{\alpha_s}{\pi}\right)^2 29.14(2) + \mathcal{O}(\alpha_s^3) \right] \tag{7.34}$$

with

$$\Gamma_{H \rightarrow b\bar{b}}^{LO} = \frac{y_b^2 m_H N}{4\pi}. \quad (7.35)$$

This is in agreement with the known result [77]

$$\Gamma_{H \rightarrow b\bar{b}}^{NNLO} = \Gamma_{H \rightarrow b\bar{b}}^{LO} \left[1 + \left(\frac{\alpha_s}{\pi} \right) 5.66666666.. + \left(\frac{\alpha_s}{\pi} \right)^2 29.146714.. + \mathcal{O}(\alpha_s^3) \right]. \quad (7.36)$$

With our numerical program, we can compute the decay rate for arbitrary infrared-safe observables. As an example we present our results for the 2,3 and 4 jet rates using the JADE algorithm [98] with parameter $y_{cut} = 0.01$:

$$\begin{aligned} \Gamma_{H \rightarrow b\bar{b}}^{LO}(4\text{Jets}) &= \Gamma_{H \rightarrow b\bar{b}}^{LO} \left[+ \left(\frac{\alpha_s}{\pi} \right)^2 94.1(1) + \mathcal{O}(\alpha_s^3) \right] \\ \Gamma_{H \rightarrow b\bar{b}}^{NLO}(3\text{Jets}) &= \Gamma_{H \rightarrow b\bar{b}}^{LO} \left[+ \left(\frac{\alpha_s}{\pi} \right) 19.258(4) + \left(\frac{\alpha_s}{\pi} \right)^2 241(2) + \mathcal{O}(\alpha_s^3) \right] \\ \Gamma_{H \rightarrow b\bar{b}}^{NNLO}(2\text{Jets}) &= \Gamma_{H \rightarrow b\bar{b}}^{LO} \left[1 - \left(\frac{\alpha_s}{\pi} \right) 13.591(6) - \left(\frac{\alpha_s}{\pi} \right)^2 307(2) + \mathcal{O}(\alpha_s^3) \right] \end{aligned} \quad (7.37)$$

We have checked that our results for the jet-rates indeed add up to the inclusive rate for general y_{cut} values to cross-check our implementation.

In Fig. 7.1, we present the leading jet energy, E_{max} , in the rest frame of the Higgs boson, for events with two jets ($y_{cut} = 0.1$). This is a new result which can only be obtained with a fully differential NNLO calculation and cannot be inferred from the inclusive decay width and NLO calculations. At leading order, $E_{max} = \frac{m_H}{2}$. At higher orders, there is a range of jet energies which are kinematically allowed. We choose a value of $\alpha_s(m_Z) = 0.118$ at the Z boson mass and evolve consistently through LO, NLO and NNLO up to the Higgs boson mass, which we then assumed to be $m_H = 120\text{GeV}$.

7.6 Conclusions

In this chapter, we presented a first physical application of a new method for the factorization of overlapping singularities in phase space and loop integrations. We computed the fully differential decay width of a Higgs boson to a bottom-quark pair. We computed the required tree, one-loop and two-loop amplitudes with standard Feynman diagrammatic methods.

We applied non-linear mappings to factorize all overlapping singularities in all real-virtual and double-real integrations. Consequently, we perform the expansion of

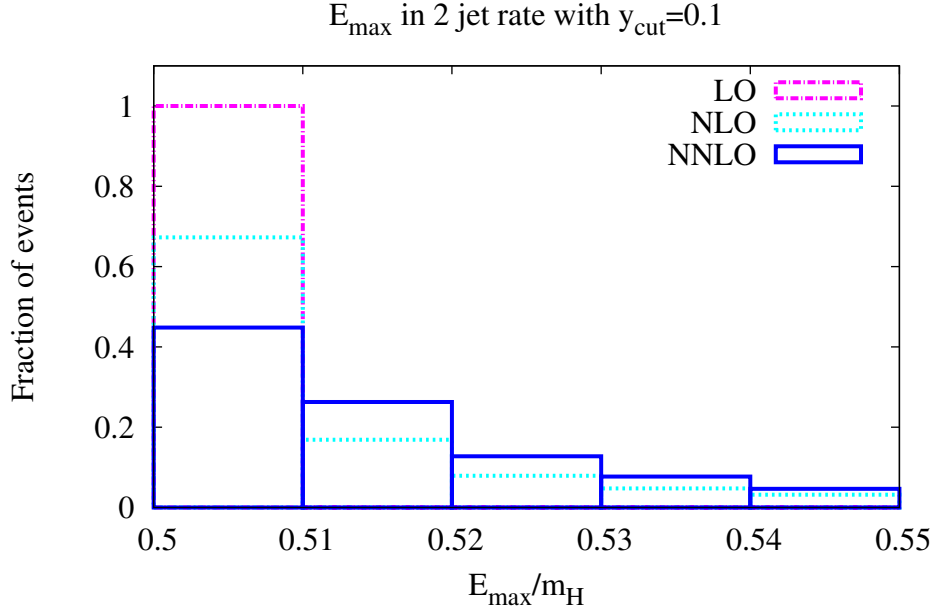


Figure 7.1: The energy spectrum of the leading jet in the decay $H \rightarrow b\bar{b}$ in the rest frame of the Higgs boson through NNLO. The jet clustering is performed with the JADE algorithm with $y_{\text{cut}} = 0.1$.

all integrals in the dimensional regulator ϵ with simple subtractions. The formalism allows for the computation of the decay rate for arbitrary physical observables.

We verify that we can reproduce the known results for the NNLO inclusive decay width and compute the differential two, three and four jet rates with the JADE algorithm. We also present the leading jet energy distributions, a new result that cannot be inferred from previous calculations. In the future, we will interface our NNLO Monte-Carlo to Monte-Carlo programs for the production of a Higgs boson.

Chapter 8

Hadronic $b\bar{b} \rightarrow H$ production

The dominant production channel in the SM, but also in all non-fermiophobic models of new physics, is single Higgs hadroproduction. Within the SM, Higgs production is dominated by gluon fusion, since the alternative mechanism of quark annihilation is severely suppressed by the small Yukawa coupling of bottom and light quarks to the Higgs boson. However, if the Higgs sector is non-minimal, as is the case in any two-Higgs-doublet model (among which the MSSM is the most studied example), the Yukawa coupling to down-type quarks is enhanced by a factor of $\tan\beta$ (the ratio of the vacuum expectation values of the two doublets) and the contribution of the $b\bar{b} \rightarrow H$ process becomes significant. Furthermore, the production cross section through gluon fusion decreases due to the enhanced, negative top-bottom interference diagrams. In such a scenario, the production of a Higgs boson via $b\bar{b}$ pairs contributes much more than in the SM, and a detailed description of this process is desirable. In other BSM models, for example in models with dynamically generated Yukawa couplings [99, 100] both the bottom and the charm quarks have enhanced couplings to the Higgs boson and charm annihilation becomes important as well.

The experimental searches are currently focused on measuring an enhanced production rate via bottom annihilation in the $\tau^+\tau^-$ decay channel with the MSSM as the default BSM model [101, 102]. There are, moreover, several studies on measuring single Higgs decaying to bottom quarks in more generic models in which bottom annihilation is the dominant production channel, using, for example, three b-tagged jets [103, 104], or measuring the ratio of three heavy (c- or b-) jet events to three b-jet events to discriminate between classes of models with two Higgs doublets [105].

Bottom quark annihilation has been the subject of much theoretical discussion

in the last decade due to the freedom in treating the initial state bottom quarks. Bottom quarks lie in an intermediate mass range between the non-perturbative regime of the proton mass and the typical scale of a hard scattering event at the LHC. One can retain their small mass in the calculation, and exclude them from the proton constituents (four flavor scheme – 4FS) or treat them as massless partons with their own parton distribution functions (five flavor scheme – 5FS). In the 4FS the inclusive cross section develops large logarithms $\sim \log(\frac{m_b}{m_H})$ due to the collinear production of b-quarks which is regulated by the bottom mass. In the 5FS these logarithms are re-summed to all orders by the DGLAP evolution inside the bottom PDFs, for all scales up to the factorisation scale adopted in the calculation. The consequent improved convergence of the perturbative expansion is an advantage of the 5FS approach, but at the same time it renders the 5FS prediction very sensitive to the choice of factorisation scale. It has been realized that if the factorisation scale is set to low values $\sim m_H/4$, both the 5FS and the 4FS predictions for the inclusive cross sections agree with each other within their respective uncertainties [106, 107, 108], and there is an open discussion as to how one would combine information from both approaches [109, 110].

In the 4FS, the lowest order process is $gg \rightarrow b\bar{b}H$ which begins at order α_s^2 in the QCD perturbative expansion and is known at next-to-leading-order (NLO) in QCD [111, 112, 113, 114]. The process $bg \rightarrow bH$, which starts at order α_s , has also been studied at NLO in QCD [115] and with electroweak (EW) corrections [116]. In the 5FS the lowest process is $b\bar{b} \rightarrow H$. Hence the LO 4FS process where a non-collinear bottom pair is observable, is reached for the first time at NNLO in the 5FS. The inclusive cross section, in the 5FS, of $b\bar{b} \rightarrow H$ is known at NNLO in QCD [90] as well as at NLO EW [117]. NNNLO threshold re-summed soft and collinear terms are also known [118] and the transverse momentum distribution of the Higgs boson has been studied with re-summation techniques [119, 120]. Also known at NNLO are the zero, one and two jet rates and related distributions [121], quantities which can be obtained already from the differential H+jet computation at NLO [122] in combination with the fully inclusive NNLO cross section.

8.1 Notation and set-up

8.1.1 The hadronic cross section

We consider the following hadronic process

$$P_1 + P_2 \rightarrow H + X, \quad (8.1)$$

where P_1, P_2 are the incoming hadrons, H denotes the Higgs boson and X generically denotes surplus QCD radiation in the final state. The Higgs boson is assumed to couple only to bottom quarks via the SM Yukawa interaction. Assuming the usual factorisation, the fully exclusive hadronic cross section can be written as

$$\sigma_{P_1 P_2 \rightarrow H+X}[\mathcal{J}] = \sum_{i_1, i_2} \int_0^1 dx_1 dx_2 \theta(x_1 x_2 - \tau) f_{i_1}(x_1) f_{i_2}(x_2) \sigma_{i_1 i_2 \rightarrow HX}[\mathcal{J}], \quad (8.2)$$

where the $f_i(x)$ denote the bare (unrenormalized) parton distribution functions (PDFs) in the 5FS, x_1 and x_2 are the usual Bjorken- x momentum fractions of the partons i_1 and i_2 respectively, and $\tau = \frac{m_H^2}{S}$, where m_H^2 is the (on-shell) mass of the Higgs boson and S is the square of the total center of mass (CoM) energy of the colliding hadrons. A number of different parametrisations and some performance tests are given in Appendix B. By $\sigma_{i_1 i_2 \rightarrow HX}$ we denote the partonic cross section for the processes

$$i_1(q_1) + i_2(q_2) \rightarrow H(p_H) + X(i_3(q_3), i_4(q_4), \dots), \quad i_{1,2,3,\dots} \in S_{\text{partons}} \quad (8.3)$$

where the set of partons is defined as

$$S_{\text{partons}} := \{\bar{b}, \bar{q}, g, q, b\}. \quad (8.4)$$

We are denoting with q the whole set of light quarks u, d, s and c collectively. This is convenient since the process under consideration is not sensitive to their flavour. The PDFs we have inserted in eq.(8.2) are bare and still have to be rewritten in terms of the renormalized PDFs. This step will introduce collinear counter terms which cancel initial state collinear singularities which remain even after all real and virtual corrections have been added. This cancellation is achieved fully numerically in our calculation, we will discuss it in Appendix 8.4.

8.1.2 The partonic cross section

For the computation of the partonic cross section we shall use the notation introduced in Chapter 5, with the Higgs boson being the single massive particle with momentum $p_1 = p_H$ and mass $m_1^2 = m_H^2$.

Expanding the partonic cross section to NNLO in QCD we obtain

$$\begin{aligned} \sigma_{ij \rightarrow HX}[\mathcal{J}] = & y_b^2 \left[\sigma_{ij \rightarrow H}^{(0)}[\mathcal{J}] + \frac{\alpha_s}{\pi} \left(\sigma_{ij \rightarrow H}^{(1)}[\mathcal{J}] + \sum_{k \in S_{\text{partons}}} \sigma_{ij \rightarrow Hk}^{(0)}[\mathcal{J}] \right) \right. \\ & + \left(\frac{\alpha_s}{\pi} \right)^2 \left(\sigma_{ij \rightarrow H}^{(2)}[\mathcal{J}] + \sum_{k \in S_{\text{partons}}} \sigma_{ij \rightarrow Hk}^{(1)}[\mathcal{J}] + \sum_{k,l \in S_{\text{partons}}} \sigma_{ij \rightarrow Hkl}^{(0)}[\mathcal{J}] \right) \\ & \left. + \mathcal{O}(\alpha_s^3) \right]. \end{aligned} \quad (8.5)$$

Here $y_b = y_b(\mu)$ and $\alpha_s = \alpha_s(\mu)$ are the $\overline{\text{MS}}$ renormalized bottom Yukawa and strong couplings, with 5 active flavors as in Chapter 7. We set the dimensional regularisation scale μ to be equal to both the renormalisation and factorisation scales, μ_R and μ_F . Separation of the two scales can be achieved via the relations given in section D.

The LO partonic cross section is defined as

$$\sigma_{ij \rightarrow H}^{(0)}[\mathcal{J}] = \frac{1}{2s} \int d\Phi_1 \left| \mathcal{A}_{ij \rightarrow H}^{(0)} \right|^2 \mathcal{J}_1 \quad (8.6)$$

At NLO we encounter *virtual* and *real* corrections

$$\begin{aligned} \sigma_{ij \rightarrow H}^{(1)}[\mathcal{J}] &= \frac{1}{2s} \int d\Phi_1 \left| \mathcal{A}_{ij \rightarrow H}^{(1)} \right|^2 \mathcal{J}_1 \\ \sigma_{ij \rightarrow Hk}^{(0)}[\mathcal{J}] &= \frac{1}{2s} \int d\Phi_2 \left| \mathcal{A}_{ij \rightarrow Hk}^{(0)} \right|^2 \mathcal{J}_2. \end{aligned} \quad (8.7)$$

At NNLO *double virtual*, *real-virtual* and *double real* corrections must be considered

$$\begin{aligned} \sigma_{ij \rightarrow H}^{(2)}[\mathcal{J}] &= \frac{1}{2s} \int d\Phi_1 \left| \mathcal{A}_{ij \rightarrow H}^{(2)} \right|^2 \mathcal{J}_1 \\ \sigma_{ij \rightarrow Hk}^{(1)}[\mathcal{J}] &= \frac{1}{2s} \int d\Phi_2 \left| \mathcal{A}_{ij \rightarrow Hk}^{(1)} \right|^2 \mathcal{J}_2 \\ \sigma_{ij \rightarrow Hkl}^{(0)}[\mathcal{J}] &= \frac{1}{2s} \int d\Phi_3 \left| \mathcal{A}_{ij \rightarrow Hkl}^{(0)} \right|^2 \mathcal{J}_3. \end{aligned} \quad (8.8)$$

8.2 Squared amplitudes

In this section we discuss the squared amplitudes required. Using the discrete symmetries of the squared amplitudes we are able to considerably reduce the number of independent channels, which need to be implemented separately. These symmetries are due to the charge invariance of all the $ij \rightarrow HX$ amplitudes (exchanging $q \leftrightarrow \bar{q}$ or $b \leftrightarrow \bar{b}$ leaves the squared amplitudes invariant). For $2 \rightarrow 1$ processes we only need to consider the $b\bar{b}$ channel

$$\left| \mathcal{A}_{ij \rightarrow H}^{(l=0,1,2)} \right|^2 = \begin{cases} \left| \mathcal{A}_{b\bar{b} \rightarrow H}^{(l)} \right|^2 & \text{if } (i, j) \in \{(b, \bar{b}), (\bar{b}, b)\} \\ 0 & \text{otherwise} \end{cases} \quad (8.9)$$

When one unresolved parton is found in the final state, also gluons must be considered in the initial state:

$$\sum_k \left| \mathcal{A}_{ij \rightarrow Hk}^{(l=0,1)} \right|^2 = \begin{cases} \left| \mathcal{A}_{b\bar{b} \rightarrow Hg}^{(l)} \right|^2 & \text{if } (i, j) \in \{(b, \bar{b}), (\bar{b}, b)\} \\ \left| \mathcal{A}_{bg \rightarrow Hb}^{(l)} \right|^2 & \text{if } (i, j) \in \{(b, g), (\bar{b}, g)\} \\ \left| \mathcal{A}_{gb \rightarrow Hb}^{(l)} \right|^2 & \text{if } (i, j) \in \{(g, b), (g, \bar{b})\} \\ 0 & \text{otherwise} \end{cases} \quad (8.10)$$

For two unresolved partons in the final state yet more channels open up:

$$\sum_{k,l} \left| \mathcal{A}_{ij \rightarrow Hkl}^{(0)} \right|^2 = \begin{cases} \frac{1}{2!} \left| \mathcal{A}_{bb \rightarrow ggH}^{(0)} \right|^2 + \left| \mathcal{A}_{b\bar{b} \rightarrow b\bar{b}H}^{(0)} \right|^2 \\ + (n_f - 1) \left| \mathcal{A}_{b\bar{b} \rightarrow q\bar{q}H}^{(0)} \right|^2 & \text{if } (i,j) \in \{(b, \bar{b}), (\bar{b}, b)\} \\ \left| \mathcal{A}_{q\bar{q} \rightarrow b\bar{b}H}^{(0)} \right|^2 & \text{if } (i,j) \in \{(q, \bar{q}), (\bar{q}, q)\} \\ \left| \mathcal{A}_{qb \rightarrow qbH}^{(0)} \right|^2 & \text{if } (i,j) \in \{(q, b), (\bar{q}, b), (q, \bar{b}), (\bar{q}, \bar{b})\} \\ \left| \mathcal{A}_{bq \rightarrow bqH}^{(0)} \right|^2 & \text{if } (i,j) \in \{(b, q), (\bar{b}, q), (b, \bar{q}), (\bar{b}, \bar{q})\} \\ \left| \mathcal{A}_{bg \rightarrow bgH}^{(0)} \right|^2 & \text{if } (i,j) \in \{(b, g), (\bar{b}, g)\} \\ \left| \mathcal{A}_{gb \rightarrow gbH}^{(0)} \right|^2 & \text{if } (i,j) \in \{(g, b), (g, \bar{b})\} \\ \left| \mathcal{A}_{gg \rightarrow b\bar{b}H}^{(0)} \right|^2 & \text{if } (i,j) = (g, g) \\ \frac{1}{2!} \left| \mathcal{A}_{bb \rightarrow bbH}^{(0)} \right|^2 & \text{if } (i,j) \in \{(b, b), (\bar{b}, \bar{b})\} \\ 0 & \text{otherwise} \end{cases} \quad (8.11)$$

All the above amplitudes can in fact be obtained from the decay amplitudes $\left| \mathcal{A}_{H \rightarrow b\bar{b}}^{(l=0,1,2)} \right|^2$, $\left| \mathcal{A}_{H \rightarrow b\bar{b}g}^{(l=0,1)} \right|^2$, $\left| \mathcal{A}_{H \rightarrow b\bar{b}gg}^{(0)} \right|^2$, $\left| \mathcal{A}_{H \rightarrow b\bar{b}bb}^{(0)} \right|^2$, $\left| \mathcal{A}_{H \rightarrow b\bar{b}q\bar{q}}^{(0)} \right|^2$ by crossing external legs between the initial and final state, and multiplying with the corresponding averaging factors. A factor of minus one must be included when crossing a fermion line.

8.3 Details on the calculation

In order to perform the required phase-space integrations over the real emission phase space, we will use the technology we developed in Chapter 5. As was already mentioned there, our strategy is fully applicable also to the case $n = 1$ where the LO phase-space,

$$\Phi_{2 \rightarrow 1}(\sqrt{s}, m_H) = 2\pi \delta(s - m_H^2), \quad (8.12)$$

yields a further constraint on the Bjorken-x integration variables. In this special case the phase-space factorisation of the real-emission phase-spaces from the leading order phase-space becomes obsolete, since the real emission phase-spaces already cover the entire phase-space.

Non-trivial problems are encountered when integrating over the phase space of the unresolved parton in the real-virtual contribution. In Chapter 7 we found that

hypergeometric argument transformations can be applied to extract potentially singular factors from the hypergeometric functions, which express the box-function. We outline how this approach can be applied in section 8.3.1.

While our methods of chapter 5 are fully sufficient to factorise all singularities, we will go one step further here and perform a separation of purely soft and hard contributions to $\sigma_{b\bar{b} \rightarrow HX}$. Since this procedure is fully process independent and holds at all orders, we shall carry out this separation for a generic cross-section σ in section 8.3.2. In our case, the correspondence is $\sigma = \sigma_{b\bar{b} \rightarrow HX}$, since other initial state channels must vanish in this limit. We will present the explicit soft limit of $\sigma_{b\bar{b} \rightarrow HX}$ at NNLO in section 8.3.2.

8.3.1 Analytic continuations for the real-virtual

The box integrals we encounter in this amplitude are entirely expressible in terms of Gauss' hypergeometric function ${}_2F_1(1, -\epsilon, 1 - \epsilon, z)$ where z can be in any of the three sets S_{fine} , S_{inv} and S_{nl} :

$$\begin{aligned} S_{fine} &= \left\{ \frac{-s_{13}}{s_{12}}, \frac{-s_{23}}{s_{12}} \right\}, & S_{inv} &= \left\{ \frac{-s_{12}}{s_{13}}, \frac{-s_{12}}{s_{23}} \right\}, \\ S_{nl} &= \left\{ \frac{-s_{13}}{s_{23}}, \frac{-s_{23}}{s_{13}}, \frac{-s_{12}m_H^2}{s_{13}s_{23}}, \frac{-s_{13}m_H^2}{s_{23}s_{12}}, \frac{-s_{23}m_H^2}{s_{12}s_{13}} \right\}. \end{aligned} \quad (8.13)$$

When attempting a direct subtraction of the singularities present due to the real emission, the points of subtraction overlap with singular points of the hypergeometric functions which express the box integral. In section 7.4 it was found that, in order to circumvent this difficulty, one can apply transformations on the argument of the functions. Since here we are no longer in the euclidean regime of this amplitude, the required transformations are different than in section 7.4. Analyzing integral representations, we find that we have to apply the following identities:

- If $z \in S_{fine}$ the soft-collinear limits are well defined.
- If $z \in S_{nl}$ we apply

$${}_2F_1(a, b; c; z) \mapsto (1 - z)^{-b} {}_2F_1\left(c - a, b; c; \frac{z}{z - 1}\right).$$

- If $z \in S_{inv}$ we employ the argument inversion,

$${}_2F_1(a, b; c; z) \mapsto \frac{\Gamma(b-a)\Gamma(c){}_2F_1(a, a-c+1; a-b+1; \frac{1}{z})}{\Gamma(b)\Gamma(c-a)(-z)^a} + \frac{\Gamma(a-b)\Gamma(c){}_2F_1(b, b-c+1; b-a+1; \frac{1}{z})}{\Gamma(a)\Gamma(c-b)(-z)^b}. \quad (8.14)$$

After these transformations are applied, the singularities corresponding to the real emission are factorized and sub-tractable. In order to obtain the final Laurent expansion in ϵ we employ the library `HypExp` [123] to expand the hypergeometric functions in terms of polylogarithms.

8.3.2 Separation of Soft and Hard

Let us loosely define the soft contribution σ_S to σ as the sum of the leading order contribution, all purely virtual contributions plus the limit of all real emissions in which the unresolved partons are all simultaneously soft. We wish to separate this soft contribution (σ_S) to the partonic cross section (σ), from the hard contribution (σ_H), such that

$$\sigma = \sigma_S + \sigma_H. \quad (8.15)$$

This would allow for a fully analytic treatment of σ_S , while σ_H must, as far as external kinematics are concerned, be treated numerically. Let us re-introduce the variable

$$z = \frac{m_H^2}{s_{12}}. \quad (8.16)$$

Then the soft limit of all real emission amplitudes corresponds to $z \rightarrow 1$, which identifies the production threshold. Given that infra-red singularities are of logarithmic nature and that the divergence at $z = 1$ is always factorised, the soft singular behaviour can be exposed as follows

$$\sigma(z)[\mathcal{J}] = \delta(1-z)\tilde{\sigma}_V(\epsilon)[\mathcal{J}]|_{z=1} + \sum_n \frac{\tilde{\sigma}_R^{(n)}(z, \epsilon)[\mathcal{J}]}{(1-z)^{1+n\epsilon}}, \quad (8.17)$$

where $\tilde{\sigma}_V$ denotes the purely virtual correction, while $\tilde{\sigma}_R^{(n)}(z, \epsilon)$ denotes real corrections collectively (at NNLO this includes both real-virtual as well as double real corrections). Separation into soft and hard parts can now be achieved by adding

and subtracting the soft limit from the second term in the above, yielding

$$\begin{aligned} \sigma(z)[\mathcal{J}] &= \underbrace{\delta(1-z)\tilde{\sigma}_V(\epsilon)[\mathcal{J}]|_{z=1} + \sum_n \frac{\tilde{\sigma}_R^{(n)}(1, \epsilon)[\mathcal{J}]|_{z=1}}{(1-z)^{1+n\epsilon}}}_{\equiv \sigma_S} \\ &+ \underbrace{\sum_n \frac{\tilde{\sigma}_R^{(n)}(z, \epsilon)[\mathcal{J}] - \tilde{\sigma}_R^{(n)}(1, \epsilon)[\mathcal{J}]|_{z=1}}{(1-z)^{1+n\epsilon}}}_{\equiv \sigma_H}, \end{aligned} \quad (8.18)$$

such that σ_H is integrable in the range $z \in [\tau, 1]$. Of course this decomposition of the partonic cross section into its soft and hard components is not unique: one could use any other subtraction term with the correct limit, thereby including, for example, the luminosity function. Our choice, however, has the nice property that the soft part σ_S can be expanded purely in terms of δ - and plus-distributions via eq.(3.7),

$$\sigma_S[\mathcal{J}] = c_0 \delta(1-z) \mathcal{J}|_{z=1} + \sum_{n=0}^{\infty} c_n \mathcal{D}_n(1-z) \mathcal{J}|_{z=1}.$$

Thereby all threshold divergences between $\tilde{\sigma}_V$ and $\tilde{\sigma}_R^{(n)}$ are cancelled analytically, leaving only a finite threshold contribution. Furthermore this framework provides a natural way to incorporate threshold re-summation in fully differential calculations. Finally let us mention that we can extend the above to cross sections containing n massive particles in the final state. This can be achieved identically by writing

$$\sigma_n(\sqrt{s}, m_1, \dots, m_n) = \int \frac{du_{1..n}}{2\pi} \sigma_n(\sqrt{s}, m_1, \dots, m_n) 2\pi \delta(s - u_{1..n}) \quad (8.19)$$

and then identifying

$$z = \frac{u_{1..n}}{s}. \quad (8.20)$$

The soft behaviour of the real

Using the parameterisation of section 5.2, we can see that the soft singularity structure of this contribution is

$$\sigma_{bb \rightarrow Hg}^{(0)}[\mathcal{J}] = \frac{\tilde{\sigma}_{bb \rightarrow Hg}^{(0)}[\mathcal{J}]}{(1-z)^{1+2\epsilon}}. \quad (8.21)$$

The soft contribution is therefore

$$\sigma_{bb \rightarrow Hg}^{S(0)}[\mathcal{J}] = \frac{\lim_{z \rightarrow 1} \tilde{\sigma}_{bb \rightarrow Hg}^{(0)}[\mathcal{J}]}{(1-z)^{1+2\epsilon}}. \quad (8.22)$$

The soft behaviour of the double real

Using the parameterisation of section 5.2, we can see that the soft singularity structure of this contribution is

$$\sum_{k,l \in S_{\text{partons}}} \sigma_{bb \rightarrow Hkl}^{(0)}[\mathcal{J}] = \sum_{k,l \in S_{\text{partons}}} \frac{\tilde{\sigma}_{bb \rightarrow Hkl}^{(0)}[\mathcal{J}]}{(1-z)^{1+4\epsilon}}. \quad (8.23)$$

Similarly then

$$\sum_{k,l} \sigma_{bb \rightarrow Hkl}^{S(0)}[\mathcal{J}] = \sum_{k,l \in S_{\text{partons}}} \frac{\lim_{z \rightarrow 1} \tilde{\sigma}_{bb \rightarrow Hkl}^{(0)}[\mathcal{J}]}{(1-z)^{1+4\epsilon}}. \quad (8.24)$$

The soft behaviour of the real-virtual

The soft singularity structure of the real-virtual may be extracted as

$$\sigma_{bb \rightarrow Hg}^{(1)}[\mathcal{J}] = \sum_{m=2}^4 \frac{\tilde{\sigma}_{bb \rightarrow Hg}^{(1),m}[\mathcal{J}]}{(1-z)^{1+m\epsilon}}. \quad (8.25)$$

In the soft limit only the $m = 2, 4$ coefficients survive and the integration over λ can be carried out analytically, yielding

$$\sigma_{bb \rightarrow Hg}^{S(1)}[\mathcal{J}] = \frac{\lim_{z \rightarrow 1} \tilde{\sigma}_{bb \rightarrow Hg}^{(1),2}[\mathcal{J}]}{(1-z)^{1+2\epsilon}} + \frac{\lim_{z \rightarrow 1} \tilde{\sigma}_{bb \rightarrow Hg}^{(1),4}[\mathcal{J}]}{(1-z)^{1+4\epsilon}}. \quad (8.26)$$

The combined soft limit

The combined soft limit is then defined as

$$\begin{aligned} \sigma_{bb \rightarrow HX}^S[\mathcal{J}] &= y_b^2 \left[\sigma_{bb \rightarrow H}^{(0)}[\mathcal{J}] + \left(\frac{\alpha_s}{\pi} \right) \left(\sigma_{bb \rightarrow H}^{(1)}[\mathcal{J}] + \sigma_{bb \rightarrow Hg}^{S(0)}[\mathcal{J}] \right) \right. \\ &\quad \left. + \left(\frac{\alpha_s}{\pi} \right)^2 \left(\sigma_{bb \rightarrow H}^{(2)}[\mathcal{J}] + \sigma_{bb \rightarrow Hg}^{S(1)}[\mathcal{J}] + \sum_{k,l} \sigma_{bb \rightarrow Hkl}^{S(0)}[\mathcal{J}] \right) + \mathcal{O}(\alpha_s^3) \right] \end{aligned} \quad (8.27)$$

All the soft real, real-virtual and double real emission integrals were carried out analytically yielding the final result

$$\sigma_{bb \rightarrow HX}^S[\mathcal{J}] = \mathcal{B} \cdot \left(\delta(1-z) + \frac{\alpha_s}{\pi} \Delta_{S,NLO} + \left(\frac{\alpha_s}{\pi} \right)^2 \Delta_{S,NNLO} + \mathcal{O}(\alpha_s^3) \right) \mathcal{J}|_{z=1}, \quad (8.28)$$

where

$$\mathcal{B} = \frac{\pi y_b^2}{6m_H^2}. \quad (8.29)$$

The NLO correction $\Delta_{S,NLO}$ may be expressed as

$$\begin{aligned} \Delta_{S,NLO} = & \frac{1}{\epsilon} \left(-\frac{2}{3} \delta(1-z) - \frac{8}{3} \mathcal{D}_0(1-z) \right) + \left(\frac{8}{3} \zeta_2 - \frac{4}{3} \right) \delta(1-z) \\ & + \frac{8}{3} \mathcal{D}_0(1-z) l_H + \frac{16}{3} \mathcal{D}_1(1-z) + \mathcal{O}(\epsilon), \end{aligned} \quad (8.30)$$

while the NNLO correction $\Delta_{S,NNLO}$ can be expanded as follows

$$\Delta_{S,NNLO} = \sum_n \Delta_{S,NNLO}^{(n)} \epsilon^n + \mathcal{O}(\epsilon), \quad (8.31)$$

with the only non-vanishing contributions [124]

$$\begin{aligned}
\Delta_{S,NNLO}^{(0)} = & \left(\left(\frac{2}{27} - \frac{10}{27}\zeta_2 + \frac{2}{3}\zeta_3 \right) n_f - \frac{64}{9}\zeta_2 l_H^2 + \left(-\frac{17}{3} + \frac{8}{3}\zeta_2 + \frac{250}{9}\zeta_3 \right) l_H \right. \\
& + \frac{211}{18} + \frac{58}{9}\zeta_2 - \frac{26}{3}\zeta_3 - \frac{17}{6}\zeta_4 \Big) \delta(1-z) \\
& + \left(\left(\frac{56}{81} - \frac{20}{27}l_H + \frac{2}{9}l_H^2 - \frac{8}{9}\zeta_2 \right) n_f - l_H^2 + \left(\frac{70}{9} - \frac{164}{9}\zeta_2 \right) l_H \right. \\
& - \frac{212}{27} + \frac{20}{3}\zeta_2 + \frac{638}{9}\zeta_3 \Big) \mathcal{D}_0(1-z) \\
& + \left(\left(\frac{8}{9}l_H - \frac{40}{27} \right) n_f + \frac{68}{3} + \frac{128}{9}l_H^2 - 4l_H - 72\zeta_2 \right) \mathcal{D}_1(1-z) \\
& + \left(-4 + \frac{8}{9}n_f + \frac{128}{3}l_H \right) \mathcal{D}_2(1-z) + \frac{896}{27}\mathcal{D}_3(1-z), \tag{8.32}
\end{aligned}$$

$$\begin{aligned}
\Delta_{S,NNLO}^{(-1)} = & \left(\left(\frac{1}{36} + \frac{2}{9}\zeta_2 \right) n_f + \frac{64}{9}\zeta_2 l_H + \frac{43}{24} - \frac{23}{3}\zeta_2 - \frac{125}{9}\zeta_3 \right) \delta(1-z) \\
& + \left(\frac{10}{27}n_f - \frac{16}{3}l_H - \frac{35}{9} + \frac{82}{9}\zeta_2 \right) \mathcal{D}_0(1-z) \\
& - \left(\frac{32}{3} + \frac{128}{9}l_H \right) \mathcal{D}_1(1-z) - \frac{64}{3}\mathcal{D}_2(1-z) \tag{8.33}
\end{aligned}$$

and

$$\begin{aligned}
\Delta_{S,NNLO}^{(-2)} = & \left(\frac{19}{4} - \frac{1}{6}n_f - \frac{32}{9}\zeta_2 \right) \delta(1-z) + \left(9 - \frac{2}{9}n_f \right) \mathcal{D}_0(1-z) \\
& + \frac{64}{9}\mathcal{D}_1(1-z). \tag{8.34}
\end{aligned}$$

Here n_f is the number of light flavors, ζ_n are the usual Riemann zeta values and

$$l_H = \log \left(\frac{m_H^2}{\mu^2} \right). \tag{8.35}$$

8.4 Collinear Factorisation

Parton distribution functions are renormalized to absorb initial state collinear singularities via

$$\tilde{f}_i(z, \mu) = (\Gamma_{ij}(\mu) \otimes f_j)(z), \tag{8.36}$$

where μ is the factorisation scale and f_i are the bare parton densities. In the following discussion summation over indices will always be assumed unless explicitly stated. We will also need the convolution integral, which is defined as

$$(f \otimes g)(z) = \int_0^1 dx dy f(x) g(y) \delta(z - xy). \quad (8.37)$$

The kernel Γ_{ij} is defined in the $\overline{\text{MS}}$ scheme by

$$\Gamma_{ij}(z) = \delta_{ij} \delta(1-z) + \left(\frac{\alpha_s}{\pi}\right) \Gamma_{ij}^{(1)}(z) + \left(\frac{\alpha_s}{\pi}\right)^2 \Gamma_{ij}^{(2)}(z) + \mathcal{O}(\alpha_s^3), \quad (8.38)$$

where the coefficients of the expansion in the strong coupling involve the Altarelli-Parisi splitting functions. Specifically,

$$\Gamma_{ij}^{(1)}(z) = -\frac{P_{ij}^0(z)}{\epsilon}, \quad (8.39)$$

$$\Gamma_{ij}^{(2)}(z) = -\left\{ \frac{P_{ij}^1(z)}{2\epsilon} - \frac{1}{2\epsilon^2} [(P_{ik}^0 \otimes P_{kj}^0)(z) + \beta_0 P_{ij}^0(z)] \right\}, \quad (8.40)$$

with $\beta_0 = \frac{11}{4} - \frac{1}{6} N_F$. Let us define the inverse of the kernel Γ_{ij} as

$$\Delta_{ij}(z) = \sum_{n=0}^2 \Delta_{ij}^{(n)}(z) \left(\frac{\alpha_s}{\pi}\right)^n + \mathcal{O}(\alpha_s^3), \quad (8.41)$$

such that it satisfies the condition $(\Gamma_{ik} \otimes \Delta_{kj})(z) = \delta_{ij} \delta(1-z)$. Solving for the coefficients yields

$$\Delta_{ij}^{(0)}(z) = \delta_{ij} \delta(1-z), \quad (8.42)$$

$$\Delta_{ij}^{(1)}(z) = -\Gamma_{ij}^{(1)}(z) = \frac{P_{ij}^0(z)}{\epsilon}, \quad (8.43)$$

$$\begin{aligned} \Delta_{ij}^{(2)}(z) &= -\Gamma_{ij}^{(2)}(z) + (\Gamma_{ik}^{(1)} \otimes \Gamma_{kj}^{(1)})(z) \\ &= \frac{P_{ij}^1(z)}{2\epsilon} + \frac{1}{2\epsilon^2} [(P_{ik}^0 \otimes P_{kj}^0)(z) - \beta_0 P_{ij}^0(z)]. \end{aligned} \quad (8.44)$$

The strong coupling expansion of the bare PDFs then reads

$$f_i(z) = \sum_{n=0}^2 f_i^{(n)}(z) \left(\frac{\alpha_s}{\pi}\right)^n + \mathcal{O}(\alpha_s^3), \quad (8.45)$$

with

$$f_i^{(n)} = \Delta_{ij}^{(n)} \otimes \tilde{f}_j. \quad (8.46)$$

In evaluating the collinear counter terms we encounter convolutions of the type $(f \otimes \Delta)(x)$, where the function f is regular and $\Delta(x)$ can in general be written as

$$\Delta(x) = a\delta(1-x) + \sum_n b_n \mathcal{D}_n(1-x) + C(x). \quad (8.47)$$

Expressing the convolution as a single integral we obtain

$$(f \otimes \Delta)(x) = \int_x^1 \frac{dy}{y} f\left(\frac{x}{y}\right) \left\{ a\delta(1-x) + \sum_n b_n \mathcal{D}_n(1-x) + C(x) \right\}. \quad (8.48)$$

Care has to be taken with convolutions over \mathcal{D}_n . Since the integration does not start at zero a boundary term must be included

$$(\mathcal{D}_m \otimes f)(x) = \frac{\log(1-x)^{m+1}}{m+1} f(x) + \int_x^1 dy \log(1-y)^m \frac{\frac{1}{y} f\left(\frac{x}{y}\right) - f(x)}{1-y}. \quad (8.49)$$

Because of the downward sloping shape of all parton distribution functions, a quadratic remapping of the integration variable y was found to optimize the convergence behaviour, i.e. we parameterise the integral like

$$y = x + (1-x)z^2,$$

with z uniformly spaced between 0 and 1. In our code, this integration is carried out numerically. For every bare PDF used, we construct a one-dimensional grid in the Bjorken- x variable and interpolate from it during runtime. An alternative to constructing a grid is to perform the integration numerically along with the phase space ones, thereby increasing the dimensionality of the Monte Carlo integration by one (or by two in the case of double NLO kernels convoluted with the Born). We have implemented this as well and found that it yields the same results as the grid approach.

This procedure allows us to expand the (singular) bare PDFs via eq.(8.45) order by order in the dimensional regulator ϵ and substitute them directly in eq.(8.2). The singularities in the resulting convolutions, appearing as poles in the ϵ -expansion, cancel the initial state collinear singularities of the partonic cross section. This cancellation is achieved numerically in our calculation and can be observed bin by

bin in e.g. the rapidity distribution of the Higgs boson. One can achieve this cancellation in each initial state channel separately, at the cost of separating the convolution integrals depending on the initial state parton in the convolution, i.e. by not performing the implicit j -summation in eq.(8.46).

It is worth pointing out that the procedure described here is entirely generic, i.e. it provides the collinear counter terms for any NNLO process numerically. Moreover, we thereby circumvent the usual insertion of eq.(8.36) in the equivalent of eq.(8.2) for renormalized quantities and the resulting cumbersome and process specific analytic treatment of the convolutions.

8.5 Numerical Results

We have performed a number of tests to ensure that our results are consistent with each other and with results available in the literature:

- We have implemented the entire calculation in two different computer codes, one in **Fortran** and one in **C++**, and all results agree within their respective Monte Carlo errors, both inclusively and differentially.
- The coefficients of all poles in the ϵ -expansion of all cross sections cancel both inclusively and differentially for the entire process and also for all individual initial state channels.
- The inclusive cross section agrees with the one available in [90] and from **ihixs** [125] and so does the inclusive cross section per initial state channel. This is the first independent check of the inclusive cross section published in [90] and adopted in [125].
- The soft limit of both real-virtual and double real contributions were computed both numerically (as a limiting case of the generic matrix elements) and analytically. Moreover the integrated double real contributions were found to agree with an analytic computation provided by [124].
- The subtraction process for every double real integral was implemented in two different ways and were found in complete agreement.

We present results for the LHC with a center of mass energy of 8 TeV. We fix the mass of the Higgs boson at 125 GeV. We have used the MSTW2008 (the 68%CL set) PDFs for all results in this paper. The value of α_s at m_Z that we use is the

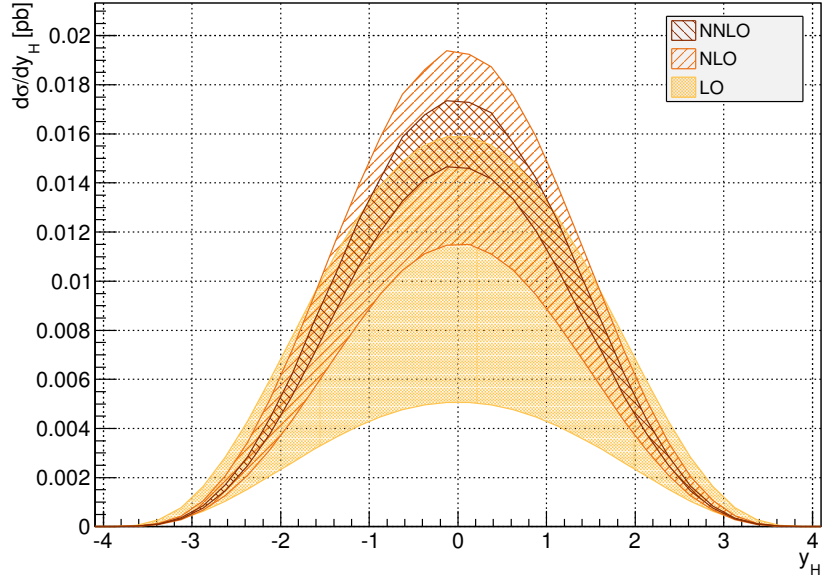


Figure 8.1: The Higgs rapidity distribution for $m_H = 125$ GeV at the 8 TeV LHC. The bands describe the uncertainty due to factorisation scale

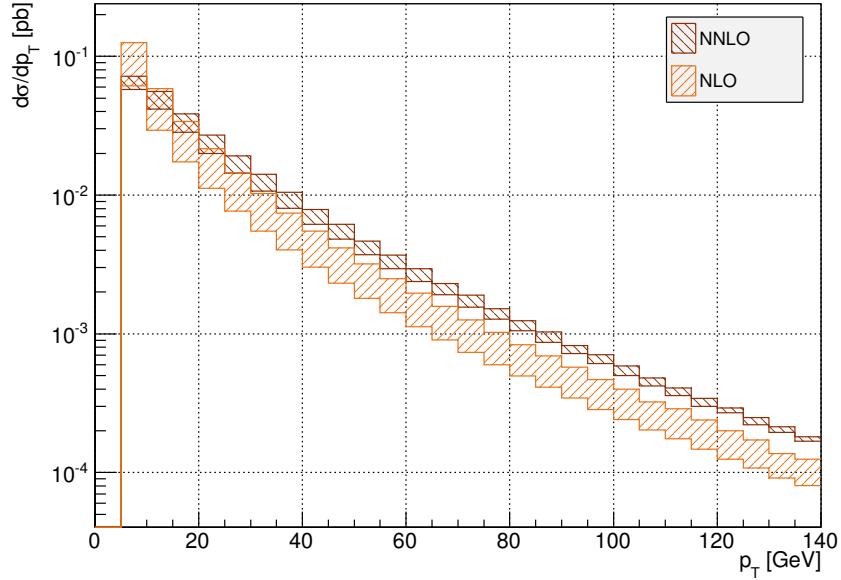


Figure 8.2: The Higgs transverse momentum distribution for $m_H = 125$ GeV at the 8 TeV LHC.

best-fit value of the PDF set at the corresponding order. We use $\mu_R = m_H$ as the central renormalisation scale. The value of α_s used is run from m_Z to μ_R through NNLO in QCD. The mass of the bottom quarks is set to zero in all matrix elements, consistently with the 5FS choice. The bottom Yukawa coupling, however, depends on the mass of the bottom. The Yukawa coupling at μ_R is obtained from the Yukawa coupling at $\mu^* = 10$ GeV, using $m_b(\mu^*) = 3.63$ GeV.

We do not vary μ_R in what follows, since the μ_R scale dependence of the total cross section has been found to be very mild. We have also checked that the μ_R -dependence of differential distributions is very small.

Previous studies have shown that the inclusive cross section is very sensitive to the choice of factorisation scale. Arguments related to the validity of the 5FS approximation with respect to the collinearity of final state b-quarks, as well as to the matching to the 4FS calculation or to the need for a smoother perturbative expansion, point to factorisation scales that are much lower than the Higgs boson mass. We adopt the choice $\mu_F = \frac{m_H}{4}$ as a central scale and vary it in the range $[\frac{m_H}{8}, \frac{m_H}{2}]$ to estimate the related uncertainty.

All Monte Carlo integrations was performed with the **Cuba** [126] implementation of the Vegas algorithm.

The rapidity distribution of the Higgs boson is shown at fig. 8.1. As expected, the perturbative expansion is converging smoothly for this choice of central μ_F and the NNLO uncertainty band is entirely engulfed by the NLO one.

The transverse momentum distribution for the Higgs boson is shown in fig. 8.2. This observable starts at NLO in QCD and the fixed order prediction fails, as usual, to describe the very low p_T spectrum due to the related large logarithms. At the large p_T range we see that the NNLO calculation leads to a harder spectrum than the NLO one and the NLO scale uncertainty fails to capture this feature. This implies that great care should be taken when relying on NLO predictions for observables that are highly exclusive in the transverse momentum of the Higgs boson.

The differential distribution in both the rapidity and the p_T of the Higgs is shown in fig. 8.3, both in a three-dimensional lego plot and in a density plot. We see that the bulk of the events are produced centrally (with $|y| < 2.5$) and at relatively low p_T (35 – 50 GeV).

In fig. 8.4 we show the cumulative distribution of the Higgs transverse momentum. This observable is equivalent to the cross section in the presence of a jet veto at NLO, but only related indirectly at NNLO. In fig. 8.5 we present the cross section in the presence of a jet veto. We see again that the perturbative description for high

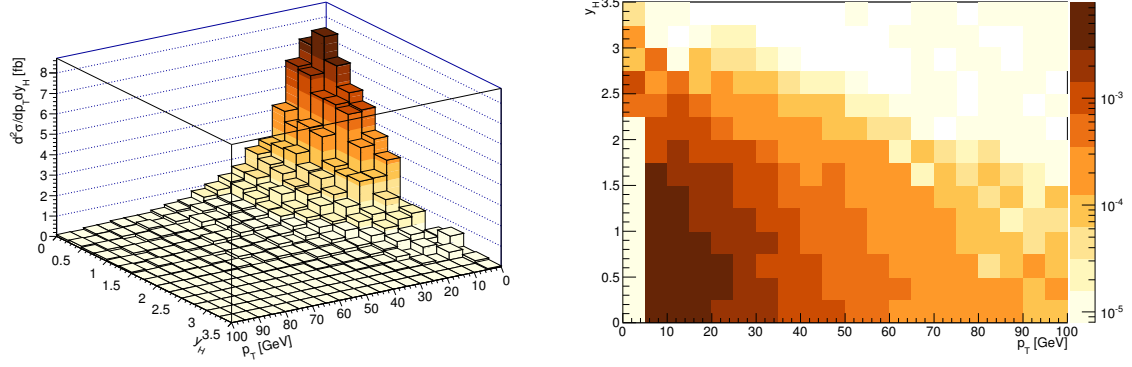


Figure 8.3: Differential distribution in rapidity and transverse momentum of the Higgs boson for $m_H = 125$ GeV at the 8 TeV LHC.

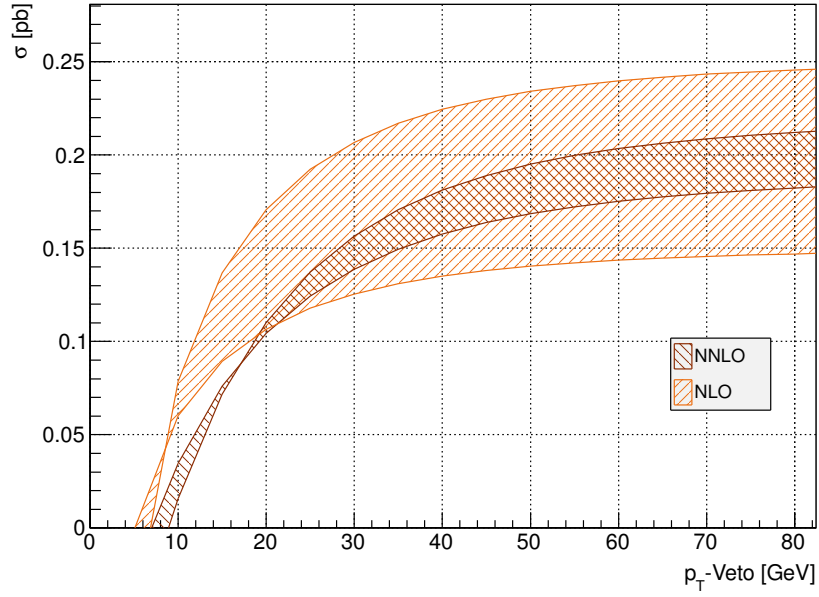


Figure 8.4: The cumulative distribution of the Higgs p_T for $m_H = 125$ GeV at the 8 TeV LHC.

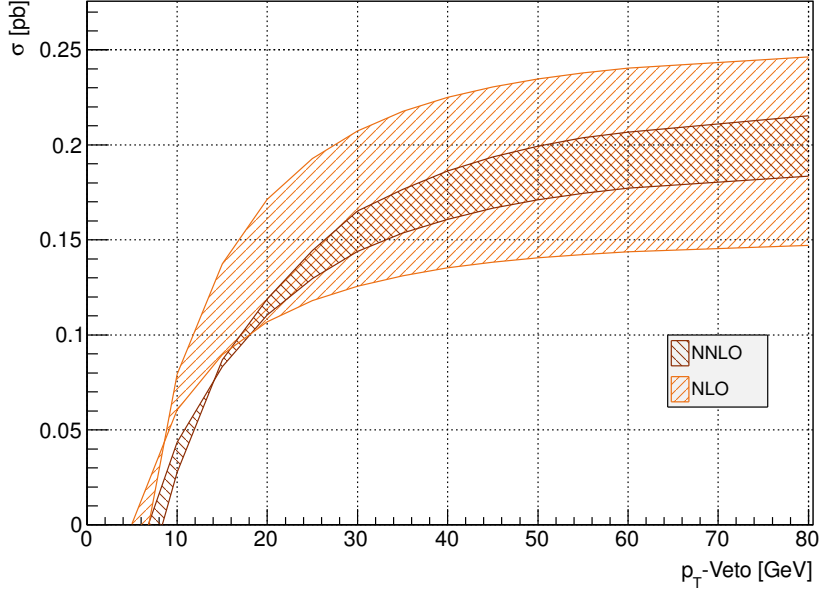


Figure 8.5: The cross section in the presence of a jet veto (the 0-jet rate) for $m_H = 125$ GeV at the 8 TeV LHC.

p_T cut-offs is satisfactory (despite the discrepancy in high p_T between NLO and NNLO, which is, in absolute terms, unimportant), while for cut-offs lower than 20 GeV the NLO description does not coincide with the NNLO one. The vanishing of the uncertainty around 15 GeV (which in the case of the jet veto is taking place at a slightly lower p_T -veto value) is a feature reminiscent of a similar situation in Higgs production via gluon fusion [127]. The fixed order prediction in this region is very stable under varying the factorisation scale, and any residual uncertainty in quantities like the acceptance in the presence of a veto is driven by the uncertainty in the total cross section. Various approaches to assign a larger uncertainty to similar observables involving re-summation exist, see for example [128].

An important observable in $b\bar{b} \rightarrow H$ is the cross section for zero, one and two jets. We use the anti- k_T algorithm [129] for jet clustering¹ with a cone in the $y - \phi$ plane of radius $R = 0.4$. We show in fig. 8.7 the jet rates as a function of the jet p_T^{max} used to define them. Here we do not distinguish between b-jets and light jets. We find the jet rates for $p_T^{max} = 20\text{GeV}$ to be in agreement with those published in [121].

¹At this order in perturbation theory, the anti- k_T , the k_T and the Cambridge-Aachen algorithms are completely equivalent.

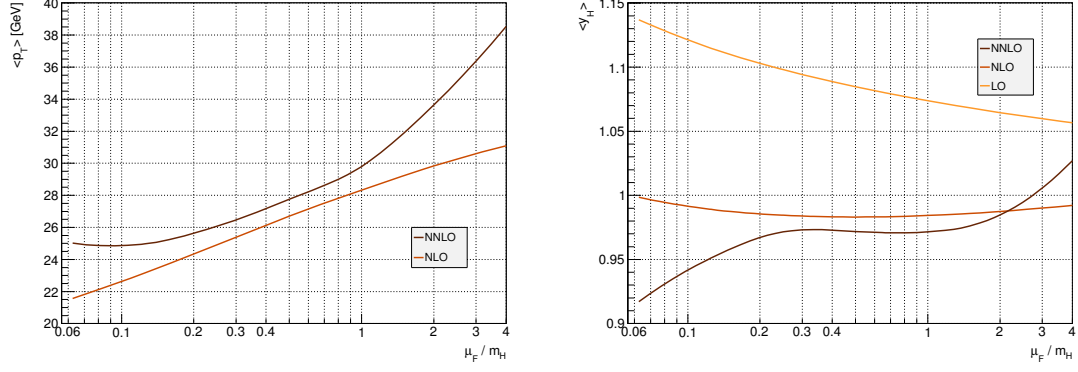


Figure 8.6: The average p_T (left) and rapidity (right) of the Higgs as a function of μ_F for $m_H = 125$ GeV at the 8 TeV LHC.

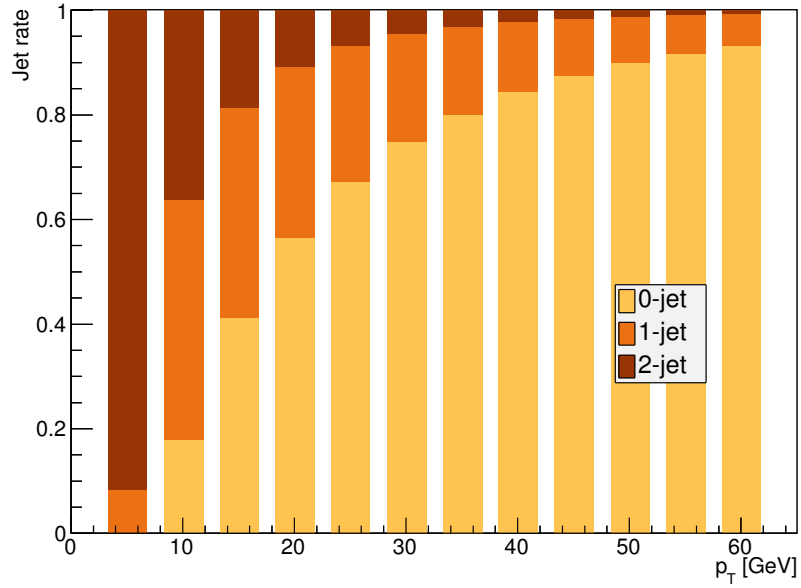


Figure 8.7: The 0-, 1- and 2-jet rate as a function of the p_T used in the jet definition for $m_H = 125$ GeV at the 8 TeV LHC.

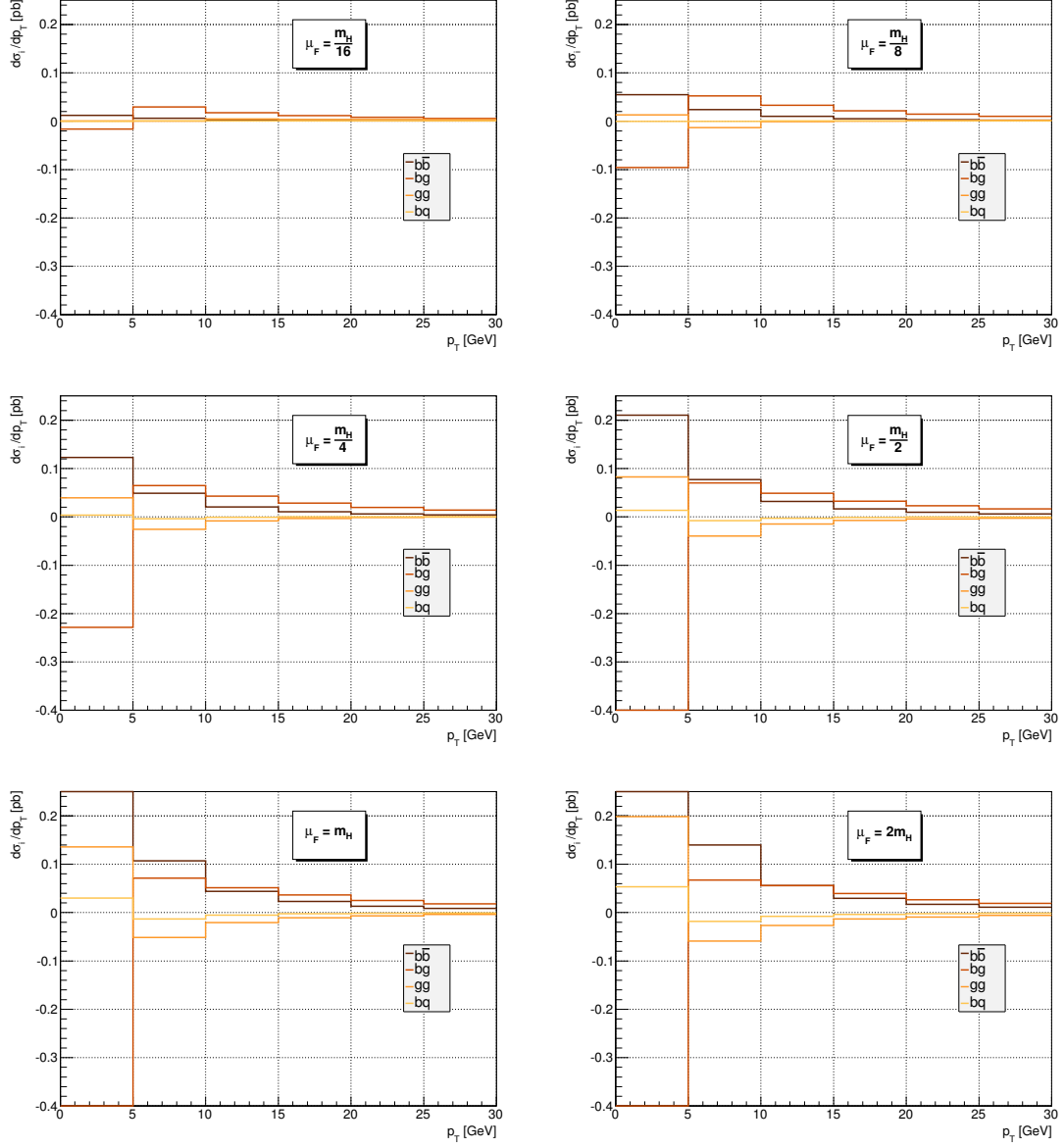


Figure 8.8: The distribution of the Higgs p_T per initial state channel for $m_H = 125$ GeV at the 8 TeV LHC

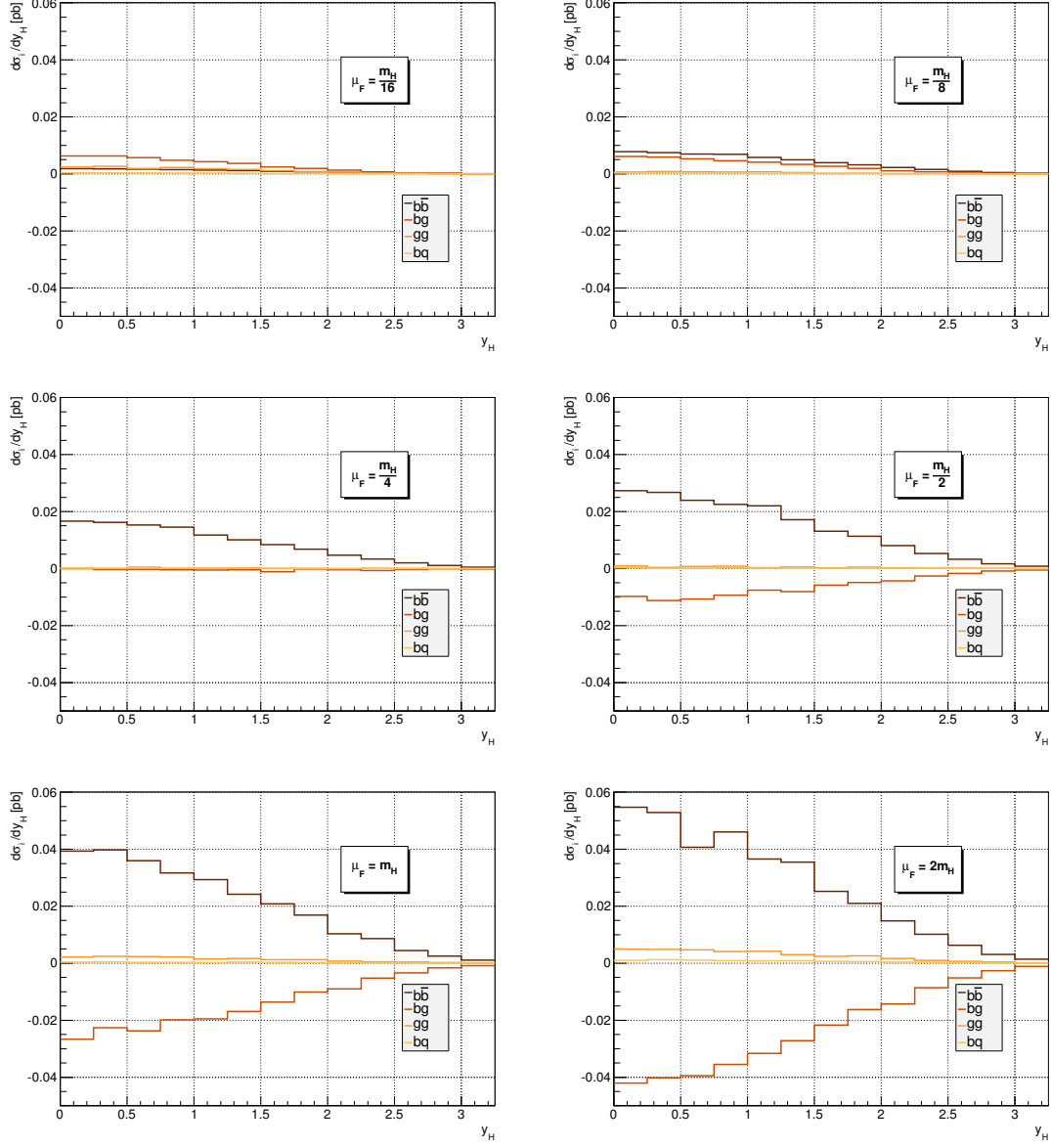


Figure 8.9: The distribution of the Higgs absolute rapidity, $|y|$ per initial state channel for $m_H = 125$ GeV at the 8 TeV LHC

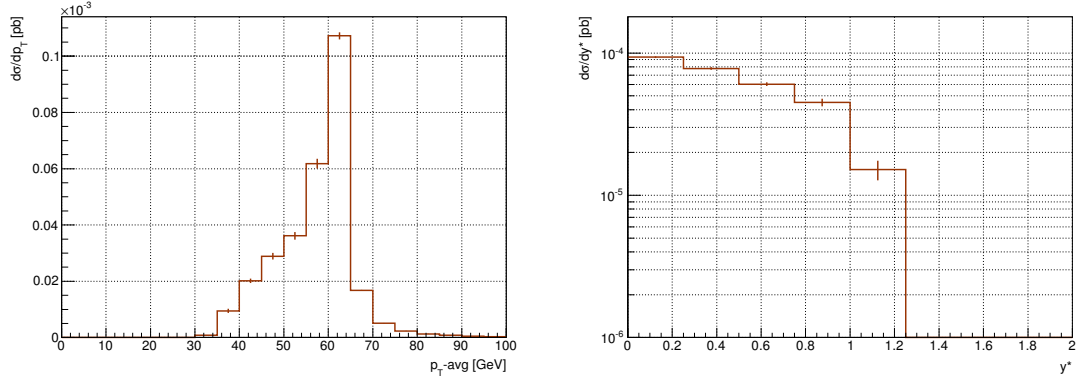


Figure 8.10: The average p_T of the two photons and the Y^* distribution for $b\bar{b} \rightarrow H + X \rightarrow \gamma\gamma + X$ for $m_H = 125$ GeV at the 8 TeV LHC, in the presence of cuts described in the text.

A wealth of information can be derived from examining the contribution of the different initial state channels to differential distributions. The six initial state channels that contribute to our NNLO calculation have singularities in various collinear regions that are cancelled against the collinear counter terms from mass factorisation. In order to make the cross section per channel finite one has to use collinear counter terms that include $\Gamma_{ij}^{(m)}$ kernels involving only the initial state partons of the channel considered. Since we calculate the collinear counter terms numerically this modification was relatively easy to achieve.

Initial state channel contributions to differential distributions have a strong dependence on the factorisation scale, as do initial state channel contributions to the inclusive cross section. In fig. 8.8 we see the contributions to the Higgs p_T distribution from each channel, for various factorisation scales ranging from $m_H/16$ to $2m_H$.

Within the 5FS, the factorisation scale regularizes the collinear singularities which in the 4FS are regularized by the bottom mass. At NNLO, three initial state channels, $b\bar{b}$, bg and gg share common collinear configurations whose leading logarithms cancel each other in different bins of the Higgs p_T distribution. In the zero p_T bin, in particular, squared logarithms from the double collinear limit of the gg channel cancel against the single collinear limit of the bg channel and the born contribution of the $b\bar{b}$ channel. Moreover at NNLO one also sees sub-leading (single) logarithms cancelling each other between the single collinear configurations of the gg channel and the regular contributions to the bg channel, a cancellation that appears in non-zero p_T bins as well. The magnitude of those logarithmic cancellations is regu-

lated by the value of the factorisation scale. The factorisation scale dependence is an artifact of the truncation of the perturbative series, so one would naively choose the scale in a way that minimizes the cross-channel logarithmic cancellations. However, choosing the scale too small reduces the regime where the logarithms are re-summed in the PDFs, destabilizing the perturbative expansion. Ideally one should choose the scale in the region where the collinear approximation implicit in the 5FS is still reasonable, which is at $m_H/4$ or lower.

These features are also seen in the rapidity distribution of the Higgs boson per initial state channel, shown in fig. 8.9 for various values of μ_F . There it is clearly seen that a scale like $\mu_F = m_H/4$ eliminates the cross-channel cancellations but a lower scale $\mu_F = m_H/16$ leads to a reduced, bg -dominated prediction.

We turn now to more exclusive observables. In large $\tan\beta$ models where the Higgs boson production gets significant contribution from the bottom quark annihilation process, one would like to examine differential distributions involving decay products of the Higgs boson, with cuts necessary in the experimental analyses. We focus here, for demonstration purposes, on the case where Higgs decays to two photons. In such an analysis the minimal cuts used by CMS and ATLAS include:

- A cut on the p_T of the leading photon: $p_{T;1} > 40\text{GeV}$.
- A cut on the p_T of the trailing photon: $p_{T;2} > 25\text{GeV}$.
- A cut on the rapidity of both photons: $|y_{1,2}| < 2.4$.
- An isolation cut on photons: no jet is allowed in a cone of radius 0.4 around any of the two photons if it is $p_T > 15\text{GeV}$.

We treat the Higgs boson in the zero width approximation in this article. We defer a more realistic treatment of the Higgs propagator to future work.

Within this setup we show in fig. 8.10 the distribution of the average transverse momentum of the two photons and the distribution of the absolute of the difference in pseudo-rapidity between the two photons, $Y^* = \frac{1}{2}|y_1 - y_2|$.

8.6 Conclusion

We have presented the fully differential NNLO calculation of $b\bar{b} \rightarrow H$, a process of prime phenomenological importance for the LHC in all models with enhanced bottom Yukawa couplings. This is the first independent cross-check of the inclusive

NNLO calculation performed in [90]. We have presented a variety of differential distributions for Higgs production that can only be obtained with a fully differential calculation and are useful for assessing the quality of the perturbative expansion and the level under which several features are under control at a fully differential level. We have also presented predictions for fully exclusive observables for the $b\bar{b} \rightarrow H \rightarrow \gamma\gamma$ process in the presence of tight cuts on the final state photons including isolation cuts, demonstrating that our calculation can fully simulate any experimental setup at the partonic level.

This is the second application of our approach to treat real emission singular amplitudes at NNLO [130]. It is the first application for the more complicated case of a hadron collider process. We find the approach particularly beneficial, both in terms of automatisation and in terms of performance of the resulting numerical code. We find that the improvement in performance compared to the sector decomposition approach is significant. We intend to release the computer code in the near future and we defer for then any detailed comments on performance issues.

A study of significantly wider scope, including the production via gluon fusion in models with enhanced bottom Yukawa couplings, as well as the decay of Higgs to bottom quarks or tau leptons would vastly benefit the experimental searches. We defer such a study for a future publication.

Chapter 9

The $H \rightarrow gggg$ amplitude and ϵ -helicities

The $gg \rightarrow H$ represents one of the most interesting processes for the LHC. As already mentioned, the fully differential computation of this process has already been accomplished in two independent calculations in [10] and in [46].

With the methods developed in chapter 5 it would be an ideal next application to recompute the $gg \rightarrow H$ double-real corrections. The primary problem with this method is that of finding a compact analytical representation for the double real squared amplitudes, which allows an easy identification of the different singularity structures. In contrast to the $H \rightarrow b\bar{b}gg$ and $H \rightarrow b\bar{b}b\bar{b}$ amplitudes, which are made up of 8 Feynman diagrams each, the $H \rightarrow gggg$, which contains 26 Feynman diagrams, is already considerable more complicated. Since we wish to compute the square of the amplitude analytically, the number of terms goes as $n(n-1)/2$ where n is the number of diagrams. While for 8 diagrams we expect 28 different terms, we already obtain 325 terms for 26 diagrams. This growth was of course what has limited the squaring amplitude procedure for more complicated final states and has nowadays made it more popular to square the amplitude numerically. That is, evaluate the amplitude as a complex number and then take the absolute value of it.

While this may sound counter-intuitive, it is not clear that the squared amplitude is necessarily much more complicated than the amplitude. At least for simple $2 \rightarrow 2$ processes this statement is true. For example the squared amplitude for the process $gg \rightarrow gg$ can be expressed simply as

$$|\mathcal{A}_{4g}^{(0)}|^2 = 16g^4(1-\epsilon)^2 \left(3 - \frac{su}{t^2} - \frac{ut}{s^2} - \frac{st}{u^2} \right). \quad (9.1)$$

But it turns out, that it is rather difficult to find such compact expressions of squared amplitudes when the number of external particles exceeds 4. Certainly this is the case with conventional Feynman diagrammatic methods in $d = 4 - 2\epsilon$ dimensions. This poses a serious challenge for our treatment of more complicated final states with the topological decomposition we described in chapter 5.

It has been shown in the last few decades that the complexity of gauge theory amplitudes can be tamed considerably. One observation is that one should work with so called *primitive amplitudes*, which are essentially believed to be the smallest gauge invariant building blocks from which the entire amplitude can be obtained. A method to obtain the primitive amplitudes was established via color ordering and working with explicit helicities of the external particles. A trick to extend the formalism to $4 - 2\epsilon$ dimensions was given in [131] for the case of external gluons only. We will use this method to compute the $H \rightarrow gggg$ helicity amplitudes in the following section.

9.1 The helicity approach with ϵ polarisations

Let us demonstrate these methods on the $H \rightarrow gggg$ amplitude, where due to the large discrete symmetry group S_4 these methods should be particularly fruitful.

We color decompose the amplitude as follows

$$\mathcal{A}_{H4g} = \sum_{\sigma \in S_4/Z_4} \text{Tr}(T^{a_{\sigma_1}} T^{a_{\sigma_2}} T^{a_{\sigma_3}} T^{a_{\sigma_4}}) A_{H4g}(\sigma(1), \sigma(2), \sigma(3), \sigma(4)). \quad (9.2)$$

It turns out that there is a particularly simple expression for the square of the amplitude. Using the photon decoupling identity,

$$A_{H4g}(1, 2, 3, 4) + A_{H4g}(2, 1, 3, 4) + A_{H4g}(2, 3, 1, 4) = 0, \quad (9.3)$$

one can show that

$$|\mathcal{A}_{H4g}|^2 = N^2(N^2 - 1) \sum_{\sigma \in S_4/Z_4} |A_{H4g}(\sigma(1), \sigma(2), \sigma(3), \sigma(4))|^2. \quad (9.4)$$

Furthermore, we may write the color ordered amplitude $A_{Hggg}(1, 2, 3, 4)$ as a sum over the helicities of the external gluons, i.e.

$$A_{H4g}(1, 2, 3, 4) = \sum_{\lambda_1, \lambda_2, \lambda_3, \lambda_4} A_{H4g}(1^{\lambda_1}, 2^{\lambda_2}, 3^{\lambda_3}, 4^{\lambda_4}). \quad (9.5)$$

For the positive and negative helicity states we will use the usual polarisation vectors in terms of massless chiral spinor products, i.e.

$$\varepsilon_\mu^\pm(p, n) = \pm \frac{\langle n^\mp | \gamma_\mu | p^\mp \rangle}{\langle n^\mp | p^\pm \rangle}, \quad (9.6)$$

where n is a massless reference spinor, which satisfies $n \cdot \varepsilon(p, n) = 0$. This satisfies the polarisation sum

$$P^{\mu\nu} = \sum_{\lambda=+,-} \varepsilon_\mu^\lambda(p, n) \varepsilon_\nu^\lambda(p, n) = -g_{\mu\nu} + \frac{p^\mu n^\nu + p^\nu n^\mu}{n \cdot p} \quad (9.7)$$

in 4 dimensions. To take into account the extra -2ϵ dimensional degrees of freedom a third helicity state $\lambda = \epsilon$ is added. The polarisation vector corresponding to this helicity state satisfies

$$\varepsilon^\epsilon(p, n) \cdot q = 0, \quad (9.8)$$

i.e. scalar products with all vectors vanish. This property can be traced back to the fact that such terms could never give rise to ϵ dependent pieces. Only terms where contractions of the metric appear with itself, can give rise to ϵ dependent terms in the square of the amplitude. This could, in the case of gluons only, only arise from terms where $P^{\mu\nu}$'s are contracted with each other.

The second identity which they must satisfy is:

$$\varepsilon^{\epsilon_1}(p_1, n_1) \cdot \varepsilon^{\epsilon_2}(p_2, n_2) = \delta_{i_1 i_2} \quad (9.9)$$

where the δ_{ij} is a Kronecker delta in -2ϵ dimensions. And therefore satisfies

$$\sum_i \delta_{ii} = -2\epsilon. \quad (9.10)$$

Using this formalism we are able to compute the helicity amplitudes also for the ϵ dimensional components. We compute these amplitudes using the standard Weyl-van Waerden spinor formalism, a good review of these methods is given in [132].

For the 4 dimensional pieces of the amplitude we require only:

$$A_{H4g}(1^+, 2^+, 3^+, 4^+) = -2 \frac{m_H^4}{\langle 23 \rangle \langle 14 \rangle \langle 12 \rangle \langle 34 \rangle}, \quad (9.11)$$

$$A_{H4g}(1^+, 2^+, 3^-, 4^-) = -2 \frac{(\langle 34 \rangle)^3}{\langle 23 \rangle \langle 14 \rangle \langle 12 \rangle} - 2 \frac{([12])^3}{[23][14][34]}, \quad (9.12)$$

and

$$\begin{aligned} A_{H4g}(1^+, 2^-, 3^-, 4^-) = & \\ & 2 \frac{\langle 24 \rangle ([13] \langle 23 \rangle + [14] \langle 24 \rangle)^2}{\langle 12 \rangle [34] [13] s_{14}} - 2 \frac{(\langle 24 \rangle)^2 (-[12] \langle 23 \rangle + \langle 34 \rangle [14])^2}{\langle 14 \rangle [14] \langle 12 \rangle [12] s_{124}} \\ & - 2 \frac{\langle 34 \rangle ([13] \langle 23 \rangle + [14] \langle 24 \rangle)^2}{\langle 14 \rangle [14] [34] s_{134}} + 2 \frac{\langle 24 \rangle (\langle 24 \rangle [12] + \langle 34 \rangle [13])^2}{\langle 14 \rangle [13] [23] s_{12}} \\ & - 2 \frac{\langle 23 \rangle (\langle 24 \rangle [12] + \langle 34 \rangle [13])^2}{\langle 12 \rangle [23] [12] s_{123}}. \end{aligned} \quad (9.13)$$

We have checked that these expressions indeed agree with the ones of [133]. All the others can be obtained using the dual ward identities, i.e.

$$A_{H4g}(1^+, 2^-, 3^+, 4^-) = A_{H4g}(1^+, 3^+, 4^-, 2^-) - A_{H4g}(3^+, 1^+, 4^-, 2^-), \quad (9.14)$$

the reflection identities or the cyclic properties of the color ordered amplitudes.

Amplitudes containing ϵ -polarisations are somehow more involved, we obtain

$$\begin{aligned}
A_{H4g}(1^{\epsilon_1}, 2^{\epsilon_2}, 3^+, 4^-) = & \\
& -2 \frac{\delta_{i_1 i_2} (\langle 24 \rangle [23] + \langle 14 \rangle [13]) (s_{14} [23] \langle 24 \rangle - s_{24} \langle 14 \rangle [13])}{\langle 34 \rangle [34] s_{12} s_{123}} \\
& -2 \frac{\delta_{i_1 i_2} \langle 24 \rangle [23] (-s_{34} \langle 14 \rangle [13] + s_{14} [23] \langle 24 \rangle - s_{24} \langle 14 \rangle [13])}{\langle 34 \rangle [34] s_{23} s_{123}} \\
& +2 \frac{\delta_{i_1 i_2} (\langle 24 \rangle [23] + \langle 14 \rangle [13]) (s_{13} \langle 24 \rangle [23] - s_{23} \langle 14 \rangle [13])}{\langle 34 \rangle [34] s_{12} s_{124}} \\
& +2 \frac{\delta_{i_1 i_2} \langle 14 \rangle [13] (s_{13} \langle 24 \rangle [23] + s_{34} \langle 24 \rangle [23] - s_{23} \langle 14 \rangle [13])}{\langle 34 \rangle [34] s_{14} s_{124}} \\
& -2 \frac{\delta_{i_1 i_2} (\langle 14 \rangle)^2 ([13])^2 (s_{23} + s_{24} + s_{12})}{\langle 34 \rangle [34] s_{14} s_{134}} - 2 \frac{\delta_{i_1 i_2} (\langle 24 \rangle)^2 ([23])^2 (s_{12} + s_{14} + s_{13})}{\langle 34 \rangle [34] s_{23} s_{234}} \\
& +2 \frac{\delta_{i_1 i_2} \langle 14 \rangle [13] (-\langle 14 \rangle [13] + \langle 24 \rangle [23])}{\langle 34 \rangle [34] s_{14}} - 2 \frac{\delta_{i_1 i_2} \langle 24 \rangle [23] (-\langle 14 \rangle [13] + \langle 24 \rangle [23])}{\langle 34 \rangle [34] s_{23}} \\
& +2 \frac{\delta_{i_1 i_2} \langle 24 \rangle \langle 14 \rangle [23] [13] (s_{34} + s_{13} + s_{24} + s_{12})}{\langle 34 \rangle [34] s_{23} s_{14}} \tag{9.15}
\end{aligned}$$

and

$$\begin{aligned}
A_{H4g}(1^{\epsilon_1}, 2^{\epsilon_2}, 3^+, 4^+) = & \\
& \frac{\delta_{i_1 i_2} \langle 12 \rangle [34] (\langle 14 \rangle [24] + [23] \langle 13 \rangle)}{\langle 13 \rangle \langle 14 \rangle s_{12}} - \frac{\delta_{i_1 i_2} [34] (\langle 13 \rangle [34] + \langle 12 \rangle [24])}{\langle 13 \rangle s_{123}} \\
& + \frac{\delta_{i_1 i_2} [34] (-[34] \langle 14 \rangle + \langle 12 \rangle [23])}{\langle 14 \rangle s_{124}} + 2 \frac{s_{14} \delta_{i_1 i_2} \langle 12 \rangle [23] (\langle 13 \rangle [34] + \langle 12 \rangle [24])}{\langle 13 \rangle \langle 14 \rangle s_{23} s_{123}} \\
& + \frac{\delta_{i_1 i_2} (s_{13} [34] \langle 14 \rangle - s_{23} [34] \langle 14 \rangle + 2s_{14} \langle 12 \rangle [23]) (\langle 13 \rangle [34] + \langle 12 \rangle [24])}{\langle 13 \rangle \langle 14 \rangle s_{12} s_{123}} \\
& - \frac{\delta_{i_1 i_2} (-[34] \langle 14 \rangle + \langle 12 \rangle [23]) ([34] s_{24} \langle 13 \rangle - [34] s_{14} \langle 13 \rangle + 2s_{13} \langle 12 \rangle [24])}{\langle 13 \rangle \langle 14 \rangle s_{124} s_{12}} \\
& + 2 \frac{\delta_{i_1 i_2} \langle 12 \rangle [23] (s_{12} + s_{14} + s_{13}) (\langle 13 \rangle [34] + \langle 12 \rangle [24])}{\langle 13 \rangle \langle 14 \rangle s_{23} s_{234}} \tag{9.16} \\
& + 2 \frac{\delta_{i_1 i_2} \langle 12 \rangle [34] (s_{12} + s_{14} + s_{13}) (\langle 14 \rangle [24] + [23] \langle 13 \rangle)}{\langle 13 \rangle \langle 14 \rangle s_{34} s_{234}} \\
& + 2 \frac{\delta_{i_1 i_2} \langle 12 \rangle [34] (s_{13} + s_{14}) (\langle 14 \rangle [24] + [23] \langle 13 \rangle)}{\langle 13 \rangle \langle 14 \rangle s_{34} s_{12}} \\
& + 2 \frac{\delta_{i_1 i_2} \langle 12 \rangle [23] (\langle 13 \rangle [34] + \langle 12 \rangle [24])}{\langle 13 \rangle \langle 14 \rangle s_{23}} + 2 \frac{\delta_{i_1 i_2} \langle 12 \rangle [34] (\langle 14 \rangle [24] + [23] \langle 13 \rangle)}{\langle 13 \rangle \langle 14 \rangle s_{34}}.
\end{aligned}$$

Using the dual Ward identity we can also obtain

$$A_{H4g}(1^{\epsilon_1}, 2^+, 3^{\epsilon_3}, 4^+) = A_{H4g}(1^{\epsilon_1}, 3^{\epsilon_3}, 4^+, 2^+) - A_{H4g}(1^{\epsilon_1}, 3^{\epsilon_3}, 4^+, 2^-) \quad (9.17)$$

and

$$A_{H4g}(1^{\epsilon_1}, 2^+, 3^{\epsilon_3}, 4^-) = A_{H4g}(1^{\epsilon_1}, 3^{\epsilon_3}, 4^+, 2^-) - A_{H4g}(1^{\epsilon_1}, 3^{\epsilon_3}, 4^+, 2^+). \quad (9.18)$$

Finally we find the all ϵ configuration:

$$\begin{aligned} A_{H4g}(1^{\epsilon_1}, 2^{\epsilon_2}, 3^{\epsilon_3}, 4^{\epsilon_4}) = & \\ & \frac{(s_{13} + s_{23} + s_{34})(-2\delta_{i_1 i_3} \delta_{i_2 i_4} + \delta_{i_1 i_2} \delta_{i_3 i_4} + \delta_{i_2 i_3} \delta_{i_1 i_4})}{s_{124}} \\ & + \frac{(s_{14} + s_{24} + s_{34})(-2\delta_{i_1 i_3} \delta_{i_2 i_4} + \delta_{i_1 i_2} \delta_{i_3 i_4} + \delta_{i_2 i_3} \delta_{i_1 i_4})}{s_{123}} \\ & + \frac{(-2\delta_{i_1 i_3} \delta_{i_2 i_4} + \delta_{i_1 i_2} \delta_{i_3 i_4} + \delta_{i_2 i_3} \delta_{i_1 i_4})(s_{12} + s_{14} + s_{13})}{s_{234}} \\ & + \frac{(-2\delta_{i_1 i_3} \delta_{i_2 i_4} + \delta_{i_1 i_2} \delta_{i_3 i_4} + \delta_{i_2 i_3} \delta_{i_1 i_4})(s_{23} + s_{24} + s_{12})}{s_{134}} \\ & + \frac{\delta_{i_2 i_3} \delta_{i_1 i_4} (s_{34} + s_{12} - s_{24} - s_{13})}{s_{14}} + \frac{\delta_{i_1 i_2} \delta_{i_3 i_4} (s_{23} + s_{14} - s_{24} - s_{13})}{s_{12}} \\ & + \frac{\delta_{i_2 i_3} \delta_{i_1 i_4} (s_{34} + s_{12} - s_{24} - s_{13})}{s_{23}} + \frac{\delta_{i_1 i_2} \delta_{i_3 i_4} (s_{23} + s_{14} - s_{24} - s_{13})}{s_{34}} \\ & - \frac{\delta_{i_2 i_3} \delta_{i_1 i_4} (-s_{34} + s_{13})(s_{23} + s_{24} + s_{12})}{s_{14} s_{134}} - \frac{\delta_{i_1 i_2} \delta_{i_3 i_4} (-s_{14} + s_{13})(s_{23} + s_{24} + s_{12})}{s_{34} s_{134}} \\ & + \frac{\delta_{i_1 i_2} \delta_{i_3 i_4} (s_{14} + s_{24} + s_{34})(-s_{13} + s_{23})}{s_{12} s_{123}} + \frac{\delta_{i_2 i_3} \delta_{i_1 i_4} (s_{14} + s_{24} + s_{34})(-s_{13} + s_{12})}{s_{23} s_{123}} \\ & + \frac{\delta_{i_2 i_3} \delta_{i_1 i_4} (s_{13} + s_{23} + s_{34})(-s_{24} + s_{12})}{s_{14} s_{124}} - \frac{\delta_{i_1 i_2} \delta_{i_3 i_4} (s_{24} - s_{14})(s_{13} + s_{23} + s_{34})}{s_{12} s_{124}} \\ & - \frac{\delta_{i_2 i_3} \delta_{i_1 i_4} (-s_{34} + s_{24})(s_{12} + s_{14} + s_{13})}{s_{23} s_{234}} + \frac{\delta_{i_1 i_2} \delta_{i_3 i_4} (s_{23} - s_{24})(s_{12} + s_{14} + s_{13})}{s_{34} s_{234}} \\ & + 2 \frac{\delta_{i_2 i_3} \delta_{i_1 i_4} (-s_{13} s_{24} + s_{12} s_{34})}{s_{14} s_{23}} + 2 \frac{\delta_{i_1 i_2} \delta_{i_3 i_4} (-s_{13} s_{24} + s_{14} s_{23})}{s_{12} s_{34}} \\ & - 4\delta_{i_1 i_3} \delta_{i_2 i_4} + 2\delta_{i_1 i_2} \delta_{i_3 i_4} + 2\delta_{i_2 i_3} \delta_{i_1 i_4}. \end{aligned} \quad (9.19)$$

9.2 Discussion

The relative compactness of these expressions and the fact that helicity amplitudes square independently, may lead one to believe that compact squared expressions

could be more easily obtained with these methods. This statement is partially true, however, upon squaring, some of these expressions contain terms which contain singularities of higher than logarithmic degree. This is a rather unwanted feature for the topology decomposition. While it is conceivable that one can re-write the above expressions, in such a way that the logarithmic nature of the singularities of each term becomes apparent, this does not appear to be a straightforward task.

The problem of un-physical singularities can be traced back to the use of eq.(9.6). It is clear that since we have introduced un-physical singularities into the amplitude they, unless we manage to explicitly cancel them, will remain there. We would prefer to be able to make a clear identification of the singularity structure of a diagram with its propagator structure. This can be realised when working in the Feynman gauge with external ghosts. However it is not clear how to combine the ghost formalism with the spinor-helicity formalism. We defer this discussion and possible resolutions to the future.

Chapter 10

Conclusions

Let us briefly summarize the achievements of chapter 3. We started by reviewing methods which allow to obtain Laurent expansions for singular, dimensionally regularised, integrals for arbitrary finite numerator functions. We showed how factorised singularities can be dealt with by expanding them in terms of delta and plus distributions. We then discussed the phenomenon of overlapping singularities, in particular we gave a condition to determine the degree of divergence of an arbitrary overlapping singularity. We demonstrated how the method of sector decomposition factorises overlapping singularities by splitting the integrand in such a way that the parameters, involved in the overlapping singularity, are rescaled with respect to each other, when mapped back onto the unit hyper cube in each sector. We showed how the phenomenon of rescaling could also be achieved with aid of non-linear mappings. We then applied the non-linear mapping to factorise some simple as well as some more complicated singularity structures, demonstrating how the method could be applied rather systematically. Further we remarked that there was not necessarily a unique way to apply the mapping but that there were a number of “philosophie” which one could follow. We also showed that non-linear mappings could be used to derive analytic continuation formulae for hypergeometric functions and showed that the non-linear mappings were intimately linked to Feynman parameters.

In chapter 4 we demonstrated how the non-linear technique could be applied to factorise singular loop integrals, in particular the massless one-loop box, the box with two adjacent external masses as well as the massless 2 loop non-planar triangle. In all cases we obtained completely factorised expressions, by relatively straightforward use of the techniques we developed in chapter 3. The method of non-linear

mappings, also in conjunction with the projective mapping as demonstrated for the massive box, therefore appears to be a useful tool for efficient numerical evaluations of singular loop integrals. Also for analytical evaluations it may turn out to be rather useful. This appears to be a very promising direction for future research.

In chapter 5 we discussed divergent single and double real emission phase space integrals for the hadronic production of massive systems. We showed that the singularities which appear in single real emission integrals can always be factorised by choosing an appropriate parametrisation in terms of the energy and angle variables of the massless final state particle. We then discussed the possible singularity structures which could appear in double real emissions. We gave an exhaustive list of the most singular topologies which could appear based on diagrammatic considerations. Considering interferences and squares of these topologies we derived a list of the most singular phase-space integrals to appear for these double real emissions. We derived two phase space parametrisations, one in terms of energy and angle variables and one based on a hierarchical decomposition. While neither of the two was able to factorise all singularities, either of them was more suited to different classes of the integrals. Using these parametrisations we numerically evaluated all of the most singular integrals of the list by applying non-linear mappings, when required, to factorise overlapping singularities. We showed that line-singularities can be avoided in most cases, via partial fractions, but can not be avoided within our proposed parametrisations, in situations where massive coloured states are found in the final state. Potential applications of this approach are plentiful and include for example the fully differential cross sections for the processes $pp \rightarrow WW, ZZ, WH, ZH, t\bar{t}, \gamma\gamma, \dots$ at NNLO.

In chapter 6 we discussed divergent single and double real emission phase space integrals for decay processes where a massive state decays into two massless states. For single real emissions all singularities can be factorised in a single parametrisation. For the double real emissions the situation is similar to the one found for the hadronic production of massive states. In contrast to the latter we only used a single parametrisation to factorise the most complicated singularity structures here. This demanded much more complicated applications of the non-linear mapping but served as a further powerful demonstration of the effectiveness of the approach. There are many potential applications of the methods which we presented here. These include the fully differential decay widths for the processes

$H \rightarrow q\bar{q}, W \rightarrow q, \bar{Q}, Z \rightarrow q\bar{q}, e^+e^- \rightarrow jj$ at NNLO.

In chapter 7 we applied the methods of chapter 6 in the fully differential calculation of the $H \rightarrow b\bar{b}$ decay width at NNLO, an important phenomenological result. For this we re-computed all the amplitudes needed with conventional diagrammatic methods. We find that the method of chapter 6 works well in this application and implement them in a numerical code. For the real-virtual corrections we found that the non-linear mappings can also be used to disentangle overlapping singularities between loop and phase space integrations. We also found that these non-linear mappings correspond to analytic continuation formulae of the hypergeometric functions which represent the box integrals found there. We checked that our numerical result for the inclusive decay width agrees with the known analytic result. Further we computed 2,3 and 4 jet-rates using the JADE jet algorithm as well as the Energy distribution of the leading jet in the 2-jet rate, a rather complicated observable, which can only be computed within a fully differential implementation. There remain very important future applications for this computation. Since the Higgs boson may be discovered in this channel when discovered in association with a W or a Z boson it is very interesting to have a Monte Carlo code where the production and decay are implemented at NNLO.

In chapter 8 we applied the methods of chapter 5 in the fully differential computation of the $b\bar{b} \rightarrow H$ cross-section. The amplitudes needed for this calculation were obtained from the ones computed in chapter 7. We put forward a novel approach for dealing with the purely soft contributions which allowed us to deal with these contributions purely analytically. This also resulted in a great speed-up factor of our numerical code. For the real-virtual contribution we found, as in chapter 7, that analytic continuation formulae could be used to disentangle overlapping singularities between phase-space and loop parameters. The analytic continuation formulae needed were different to the ones used in chapter 7 and somewhat more complicated. For the collinear counter terms required to cancel initial state singularities we used a purely numerical approach. This approach is completely process independent and may therefore be advantageous to analytic approaches. We implemented two different versions for the numerical evaluation of the convolution integrals required and found that both yielded very fast and stable results. With our numerical code we presented a large number of observables. We checked that our implementation is in agreement with other known results, like the inclusive cross-section as well jet rates and Higgs pt-veto plots. Furthermore, we computed

the rapidity distribution, the average Higgs p_t and the average Higgs rapidity with for a large variety of factorisation and renormalisation scales. We also interfaced our Monte Carlo program with a fully differential decay of the Higgs boson into photons and presented the average p_t and the average rapidity difference of the two photons. This wealth of differential results clearly demonstrates the potential of our approach and we are confident that it can be used with similar success for even more complicated final states.

In chapter 9 we presented helicity amplitudes for the process $H \rightarrow gggg$, including also epsilon dimensional polarisations for the gluons. These expressions were computed mainly to pioneer ways to square amplitudes analytically in ways suitable to identify the different singular topologies. Due to the appearance of unphysical singularities in some of these primitive amplitudes, we do not find them particularly useful for the topology method. We anticipate that using external ghosts should circumvent the problem. A possible idea could be to use Berends-Giele recursion relations with external ghosts. It could also be possible to use an approach similar to the OPP reduction method adapted for real-emissions. To find such a method is certainly an essential step for the topology method to become applicable for more complicated final states and represents an interesting direction for further research.

Appendix A

$H \rightarrow b\bar{b}$ double real amplitudes

The function $B(p_1, p_2, p_3, p_4)$ occurring in the $H \rightarrow b\bar{b}b\bar{b}$ squared amplitude can be expressed as

$$B(p_1, p_2, p_3, p_4) = B^{(0)}(p_1, p_2, p_3, p_4) + B^{(1)}(p_1, p_2, p_3, p_4)\epsilon + B^{(2)}(p_1, p_2, p_3, p_4)\epsilon^2 \quad (\text{A.1})$$

where

$$\begin{aligned} B^{(0)}(p_1, p_2, p_3, p_4) = & 2 s_{34}^{-1} - 2 s_{134}^{-1} - 4 s_{234}^{-1} + 2 s_{124}^{-1} + 4 \frac{s_{12}s_{23}}{s_{14}s_{124}s_{134}} \\ & - 2 \frac{s_{12}(s_{13}^2 + 2 s_{12}^2 + 2 s_{12}s_{13})}{s_{14}s_{34}s_{124}s_{234}} + 4 \frac{s_{12}s_{23}}{s_{34}s_{134}s_{234}} - 2 \frac{s_{12}(s_{23} + 2 s_{13} + s_{12})}{s_{14}s_{34}s_{124}} \\ & + \frac{4 s_{12} + 4 s_{23} + 8 s_{13}}{s_{14}s_{34}} + \frac{-6 s_{13} - 2 s_{14} - 4 s_{24}}{s_{34}s_{134}} + \frac{2 s_{23} - 2 s_{24} + 4 s_{12} - 2 s_{34} - 4 s_{13}}{s_{14}s_{134}} \\ & + \frac{-4 s_{23} - 10 s_{12} + 4 s_{24} - 6 s_{13}}{s_{14}s_{234}} + \frac{4 s_{12} + 4 s_{13} + 2 s_{23} + 2 s_{14}}{s_{34}s_{234}} \\ & + \frac{2 s_{14} + 4 s_{13} + 4 s_{12}}{s_{134}s_{234}} + \frac{2 s_{12} + 2 s_{24}}{s_{14}s_{124}} + \frac{-6 s_{13} - 6 s_{23} - 4 s_{12}}{s_{34}s_{124}} + \frac{2 s_{13} - 2 s_{14} + 4 s_{23}}{s_{124}s_{134}} \\ & + \frac{4 s_{14} + 4 s_{13} + 8 s_{12}}{s_{124}s_{234}} - 4 \frac{s_{13}(s_{12} + s_{24} + s_{23})}{s_{14}s_{134}^2} - 4 \frac{s_{13}(s_{12} + s_{24} + s_{23})}{s_{34}s_{134}^2} \\ & + \frac{-2 s_{23}^2 - 2 s_{12}s_{23} + 2 s_{13}^2 - 4 s_{13}s_{23} + 4 s_{12}^2 + 4 s_{24}^2 + 4 s_{12}s_{13} - 4 s_{24}s_{13} - 4 s_{12}s_{24}}{s_{14}s_{34}s_{234}} \\ & + \frac{-2 s_{12}^2 - 2 s_{24}^2 - 4 s_{23}^2 - 4 s_{12}s_{24} - 4 s_{24}s_{23} - 4 s_{12}s_{23}}{s_{14}s_{234}s_{134}} \\ & + \frac{-2 s_{23}^2 - 2 s_{12}^2 + 4 s_{23}s_{14} - 2 s_{14}^2}{s_{34}s_{124}s_{134}} + \frac{4 s_{12}^2 - 2 s_{24}s_{23} - 2 s_{24}^2}{s_{14}s_{124}s_{234}} \\ & + \frac{-4 s_{13}s_{14} - 8 s_{12}^2 - 2 s_{13}^2 - 2 s_{14}^2 - 8 s_{12}s_{13} - 6 s_{12}s_{14}}{s_{34}s_{124}s_{234}} \end{aligned} \quad (\text{A.2})$$

$$\begin{aligned}
B^{(1)}(p_1, p_2, p_3, p_4) = & -4 s_{14}^{-1} + 6 s_{34}^{-1} + 6 s_{134}^{-1} + 4 s_{234}^{-1} - 2 s_{124}^{-1} \\
& -4 \frac{s_{12}s_{23}}{s_{34}s_{134}s_{234}} - 4 \frac{s_{12}s_{23}}{s_{14}s_{124}s_{134}} - 2 \frac{s_{12}(-s_{23} - 2s_{13} + s_{12})}{s_{14}s_{34}s_{124}} + \frac{4s_{12} + 4s_{24} + 4s_{23}}{s_{134}^2} \\
& + \frac{-6s_{24} - 8s_{13}}{s_{14}s_{34}} + \frac{-6s_{12} - 2s_{23} + 6s_{34} + 8s_{13}}{s_{14}s_{134}} + \frac{6s_{13} + 6s_{24} - 2s_{14} + 2s_{23}}{s_{34}s_{134}} \\
& + \frac{6s_{13} + 4s_{24} + 10s_{12}}{s_{14}s_{234}} + \frac{-2s_{23} - 4s_{24} + 2s_{14} + 4s_{12}}{s_{34}s_{234}} + \frac{-4s_{13} - 2s_{14} - 4s_{12}}{s_{134}s_{234}} \\
& + \frac{-2s_{24} - 2s_{12}}{s_{14}s_{124}} + \frac{6s_{23} - 8s_{12} - 8s_{14} + 6s_{13}}{s_{34}s_{124}} + \frac{-2s_{13} - 4s_{23} + 2s_{14}}{s_{124}s_{134}} \\
& + \frac{-4s_{14} - 4s_{13} - 8s_{12}}{s_{124}s_{234}} + 4 \frac{s_{13}(s_{12} + s_{24} + s_{23})}{s_{14}s_{134}^2} + 4 \frac{s_{13}(s_{12} + s_{24} + s_{23})}{s_{34}s_{134}^2} \\
& + \frac{4s_{13}s_{23} + 2s_{12}s_{23} - 2s_{13}^2 - 2s_{23}^2}{s_{14}s_{34}s_{234}} + \frac{2s_{24}^2 + 2s_{24}s_{23} - 4s_{12}^2}{s_{14}s_{124}s_{234}} \\
& + \frac{2s_{12}^2 + 4s_{23}^2 + 8s_{24}s_{23} + 4s_{12}s_{23} + 6s_{24}^2 + 8s_{12}s_{24}}{s_{14}s_{234}s_{134}} + 2 \frac{s_{12}s_{13}^2}{s_{14}s_{34}s_{124}s_{234}} \\
& + \frac{-4s_{12}s_{23} + 6s_{14}^2 + 4s_{12}s_{14} + 2s_{23}^2 + 2s_{12}^2 - 8s_{23}s_{14}}{s_{34}s_{124}s_{134}} \\
& + \frac{-4s_{12}^2 - 6s_{12}s_{14} + 2s_{13}^2 - 2s_{14}^2}{s_{34}s_{124}s_{234}}
\end{aligned} \tag{A.3}$$

$$\begin{aligned}
B^{(2)}(p_1, p_2, p_3, p_4) = & \frac{4s_{13}s_{14} + 2s_{13}^2 + 4s_{12}s_{13} + 2s_{14}^2 + 2s_{12}s_{14}}{s_{34}s_{124}s_{234}} + \frac{-2s_{24} - 4s_{13}}{s_{14}s_{34}} \\
& + \frac{-2s_{24} + 2s_{12} - 2s_{23}}{s_{14}s_{234}} + \frac{4s_{14} - 4s_{23}}{s_{124}s_{134}} + \frac{-4s_{12} - 4s_{14} - 4s_{13}}{s_{134}s_{234}} + \frac{2s_{12} + 2s_{24}}{s_{14}s_{134}} \\
& + \frac{2s_{14} + 4s_{13} + 2s_{23}}{s_{34}s_{124}} + 2 \frac{s_{12}s_{13}}{s_{14}s_{34}s_{124}} + \frac{-2s_{24} + 2s_{12}}{s_{14}s_{124}} - 2 \frac{s_{13}(-s_{23} + s_{13})}{s_{14}s_{34}s_{234}} \\
& + \frac{-4s_{13} - 2s_{14} + 2s_{23}}{s_{34}s_{234}} + \frac{4s_{12}s_{13} + 2s_{24}s_{23} + 2s_{24}^2}{s_{14}s_{124}s_{234}} + \frac{-4s_{12} - 4s_{24} - 4s_{23}}{s_{134}^2} \\
& + \frac{2s_{24} + 2s_{23}}{s_{34}s_{134}} + 2s_{14}^{-1} + 2 \frac{s_{12}s_{13}^2}{s_{14}s_{34}s_{124}s_{234}} - 8s_{134}^{-1} + 2s_{234}^{-1} \\
& - 2s_{124}^{-1}
\end{aligned} \tag{A.4}$$

$$\begin{aligned}
A_{Hb\bar{b}gg}^{(0)} = & 20 s_{234}^{-1} + 20 s_{134}^{-1} + 32 s_{13}^{-1} + 24 s_{24}^{-1} + 24 s_{14}^{-1} + 32 s_{23}^{-1} \\
& + 4 \frac{3 s_{13} - 6 m_H^2 + 3 s_{14} + 6 s_{34}}{s_{24} s_{23}} + 8 \frac{3 s_{24} - 6 m_H^2 + 3 s_{14} + 3 s_{34}}{s_{13} s_{23}} \\
& + 4 \frac{6 m_H^2 - 3 s_{13} + 3 s_{34} + 3 s_{24}}{s_{234} s_{14}} + 4 \frac{-s_{24} - s_{14} + s_{34} + 4 m_H^2}{s_{234} s_{13}} \\
& - 4 \frac{-3 s_{14} - 6 m_H^2 + 3 s_{23} - 3 s_{34}}{s_{134} s_{24}} + 4 \frac{3 s_{23} + 6 s_{34} - 6 m_H^2 + 3 s_{24}}{s_{13} s_{14}} \\
& + 8 \frac{-5 s_{34} - 8 m_H^2 - 4 s_{24} - 4 s_{14}}{s_{134} s_{234}} + 8 \frac{m_H^2}{s_{134}^2} + 8 \frac{m_H^2}{s_{234}^2} \\
& - 4 \frac{8 m_H^2 - 5 s_{14} - 7 s_{34} - 5 s_{23}}{s_{24} s_{13}} + 4 \frac{-s_{24} - s_{14} + s_{34} + 4 m_H^2}{s_{134} s_{23}} \\
& - 4 \frac{-5 s_{24} + 8 m_H^2 - 5 s_{13} - 7 s_{34}}{s_{14} s_{23}} - 4 \frac{-s_{14} - 2 s_{34} + s_{13} - 3 m_H^2}{s_{234} s_{24}} \\
& + 8 \frac{3 s_{23} + 3 s_{13} + 3 s_{34} - 6 m_H^2}{s_{24} s_{14}} - 4 \frac{-3 m_H^2 - 2 s_{34} - s_{24} + s_{23}}{s_{134} s_{14}} \\
& + 4 \frac{(m_H^2 + s_{34})(-2 m_H^4 - s_{34}^2 - 2 m_H^2 s_{34})}{s_{234} s_{134} s_{13} s_{23}} \\
& + 4 \frac{(m_H^2 + s_{34})(-2 m_H^4 - s_{34}^2 - 2 m_H^2 s_{34})}{s_{234} s_{134} s_{14} s_{24}} \\
& + 4 \frac{(-s_{34} + m_H^2)(-2 m_H^4 - s_{34}^2 + 2 m_H^2 s_{34})}{s_{13} s_{14} s_{23} s_{24}} \\
& - 4 \frac{3 m_H^2 s_{13} - s_{34}^2 - s_{13}^2 - 4 m_H^4 - 3 m_H^2 s_{34} + s_{13} s_{34}}{s_{234} s_{24} s_{14}} \\
& - 4 \frac{-s_{34}^2 - 4 m_H^4 - s_{24}^2 + s_{24} s_{34} + 3 m_H^2 s_{24} - 3 m_H^2 s_{34}}{s_{134} s_{13} s_{23}} \\
& - 4 \frac{3 m_H^2 s_{14} - s_{14}^2 + s_{14} s_{34} - 3 m_H^2 s_{34} - 4 m_H^4 - s_{34}^2}{s_{234} s_{13} s_{23}} \\
& - 4 \frac{s_{23} s_{34} - 4 m_H^4 - 3 m_H^2 s_{34} - s_{34}^2 - s_{23}^2 + 3 m_H^2 s_{23}}{s_{134} s_{14} s_{24}} \\
& + 4 \frac{-s_{34}^2 - 4 m_H^4 - s_{24}^2 + s_{24} s_{34} + 3 m_H^2 s_{24} - 3 m_H^2 s_{34}}{s_{134} s_{13} s_{234}} \\
& + 4 \frac{-s_{24}^2 - 3 s_{24} s_{34} - 4 m_H^4 - 3 s_{34}^2 - 6 m_H^2 s_{34} - 3 m_H^2 s_{24}}{s_{234} s_{134} s_{14}} \\
& + 4 \frac{-3 s_{34}^2 - 3 s_{14} s_{34} - 4 m_H^4 - 3 m_H^2 s_{14} - s_{14}^2 - 6 m_H^2 s_{34}}{s_{134} s_{234} s_{24}} \\
& + 4 \frac{3 m_H^2 s_{14} - s_{14}^2 + s_{14} s_{34} - 3 m_H^2 s_{34} - 4 m_H^4 - s_{34}^2}{s_{234} s_{134} s_{23}}
\end{aligned}$$

$$\begin{aligned}
& +4 \frac{4 m_H^4 + s_{23}^2 + 3 s_{34}^2 - 3 m_H^2 s_{23} - 6 m_H^2 s_{34} + 3 s_{23} s_{34}}{s_{24} s_{13} s_{14}} \\
& +4 \frac{4 m_H^4 + 3 s_{34}^2 + s_{24}^2 - 6 m_H^2 s_{34} + 3 s_{24} s_{34} - 3 m_H^2 s_{24}}{s_{13} s_{14} s_{23}} \\
& +4 \frac{-3 m_H^2 s_{14} + 4 m_H^4 + s_{14}^2 + 3 s_{14} s_{34} + 3 s_{34}^2 - 6 m_H^2 s_{34}}{s_{24} s_{13} s_{23}} \\
& +4 \frac{-6 m_H^2 s_{34} + 4 m_H^4 + 3 s_{13} s_{34} + s_{13}^2 - 3 m_H^2 s_{13} + 3 s_{34}^2}{s_{24} s_{14} s_{23}} \quad (A.5)
\end{aligned}$$

$$\begin{aligned}
A_{H\bar{b}b\bar{g}g}^{(1)} = & -16 s_{234}^{-1} - 32 s_{13}^{-1} - 24 s_{14}^{-1} - 16 s_{134}^{-1} - 24 s_{24}^{-1} - 32 s_{23}^{-1} \\
& -16 \frac{m_H^2}{s_{234}^2} - 16 \frac{m_H^2}{s_{134}^2} - 4 \frac{s_{14} + 2 s_{34}}{s_{234} s_{24}} - 4 \frac{s_{24} + 2 s_{34}}{s_{134} s_{14}} \\
& +8 \frac{-3 s_{24} - 3 s_{34} + 2 m_H^2 - 3 s_{14}}{s_{13} s_{23}} + 4 \frac{-5 s_{34} - 2 s_{13} + m_H^2 - 2 s_{14}}{s_{24} s_{23}} \\
& +4 \frac{-3 m_H^2 - s_{34} + s_{14} + s_{24}}{s_{134} s_{23}} + 4 \frac{-3 s_{24} - 3 s_{34} - 3 m_H^2 + 4 s_{13}}{s_{234} s_{14}} \\
& -4 \frac{-3 m_H^2 + 8 s_{34} + 6 s_{23} + 6 s_{14}}{s_{24} s_{13}} - 4 \frac{3 m_H^2 + 3 s_{34} + 3 s_{14} - 4 s_{23}}{s_{134} s_{24}} \\
& +4 \frac{-3 m_H^2 - s_{34} + s_{14} + s_{24}}{s_{234} s_{13}} - 4 \frac{-3 m_H^2 + 8 s_{34} + 6 s_{13} + 6 s_{24}}{s_{14} s_{23}} \\
& +8 \frac{5 s_{34} + 4 m_H^2 + 4 s_{14} + 4 s_{24}}{s_{134} s_{234}} - 4 \frac{-m_H^2 + s_{14}}{s_{234} s_{23}} - 4 \frac{-m_H^2 + s_{24}}{s_{134} s_{13}} \\
& +8 \frac{2 m_H^2 - 3 s_{23} - 3 s_{13} - 3 s_{34}}{s_{24} s_{14}} + 4 \frac{-2 s_{24} - 5 s_{34} - 2 s_{23} + m_H^2}{s_{13} s_{14}} \\
& -4 \frac{s_{13}^2 - m_H^2 s_{13} - s_{13} s_{34} + m_H^2 s_{34} + s_{34}^2}{s_{234} s_{24} s_{14}} \\
& -4 \frac{s_{24}^2 - m_H^2 s_{24} - s_{24} s_{34} + s_{34}^2 + m_H^2 s_{34}}{s_{134} s_{13} s_{23}} \\
& -4 \frac{-s_{14} s_{34} + m_H^2 s_{34} + s_{34}^2 - m_H^2 s_{14} + s_{14}^2}{s_{234} s_{13} s_{23}} \\
& -4 \frac{m_H^2 s_{34} + s_{23}^2 - s_{23} s_{34} - m_H^2 s_{23} + s_{34}^2}{s_{134} s_{14} s_{24}} \\
& +4 \frac{-s_{14} s_{34} + m_H^2 s_{34} + s_{34}^2 - m_H^2 s_{14} + s_{14}^2}{s_{234} s_{134} s_{23}} \\
& +4 \frac{s_{24}^2 - m_H^2 s_{24} - s_{24} s_{34} + s_{34}^2 + m_H^2 s_{34}}{s_{134} s_{13} s_{234}} \\
& +4 \frac{s_{24}^2 + 3 s_{34}^2 + m_H^2 s_{24} + 3 s_{24} s_{34} + 2 m_H^2 s_{34}}{s_{234} s_{134} s_{14}}
\end{aligned}$$

$$\begin{aligned}
& +4 \frac{2m_H^2 s_{34} + m_H^2 s_{14} + s_{14}^2 + 3s_{34}^2 + 3s_{14}s_{34}}{s_{134}s_{234}s_{24}} \\
& +4 \frac{-s_{13}^2 + 2m_H^2 s_{34} + m_H^2 s_{13} - 3s_{13}s_{34} - 3s_{34}^2}{s_{24}s_{14}s_{23}} \\
& +4 \frac{-3s_{23}s_{34} + m_H^2 s_{23} - s_{23}^2 - 3s_{34}^2 + 2m_H^2 s_{34}}{s_{24}s_{13}s_{14}} \\
& +4 \frac{m_H^2 s_{24} + 2m_H^2 s_{34} - 3s_{24}s_{34} - s_{24}^2 - 3s_{34}^2}{s_{13}s_{14}s_{23}} \\
& +4 \frac{-3s_{34}^2 - s_{14}^2 + m_H^2 s_{14} + 2m_H^2 s_{34} - 3s_{14}s_{34}}{s_{24}s_{13}s_{23}} \\
& +4 \frac{(-s_{34} + m_H^2) s_{34}^2}{s_{13}s_{14}s_{23}s_{24}} + 4 \frac{(m_H^2 + s_{34}) s_{34}^2}{s_{234}s_{134}s_{13}s_{23}} + 4 \frac{(m_H^2 + s_{34}) s_{34}^2}{s_{234}s_{134}s_{14}s_{24}} \quad (\text{A.6})
\end{aligned}$$

$$\begin{aligned}
A_{Hb\bar{b}gg}^{(2)} = & -4s_{23}^{-1} - 4s_{13}^{-1} - 8s_{134}^{-1} - 8s_{234}^{-1} \\
& +8 \frac{m_H^2}{s_{134}^2} + 8 \frac{m_H^2}{s_{234}^2} + 8 \frac{2m_H^2 + 2s_{34}}{s_{134}s_{234}} - 4 \frac{s_{34} + m_H^2 - s_{23}}{s_{134}s_{14}} \\
& -4 \frac{s_{34} - s_{13} + m_H^2}{s_{234}s_{24}} + 4 \frac{-2s_{34} + s_{13} - s_{24}}{s_{234}s_{14}} - 4 \frac{3s_{34} + s_{14} + s_{23}}{s_{24}s_{13}} \\
& +4 \frac{s_{14} + s_{24} - s_{34}}{s_{134}s_{23}} - 4 \frac{s_{14} + 2s_{34} - s_{23}}{s_{134}s_{24}} + 4 \frac{s_{14} + s_{24} - s_{34}}{s_{234}s_{13}} \\
& -4 \frac{s_{24} + 3s_{34} + s_{13}}{s_{14}s_{23}} - 4 \frac{m_H^2 - s_{14}}{s_{234}s_{23}} - 4 \frac{m_H^2 - s_{24}}{s_{134}s_{13}} \\
& +4 \frac{-s_{13} + m_H^2 - 3s_{34} - s_{14}}{s_{24}s_{23}} + 4 \frac{-s_{24} - 3s_{34} + m_H^2 - s_{23}}{s_{13}s_{14}} \\
& -4 \frac{m_H^2 s_{34} - s_{13}s_{34} + s_{34}^2}{s_{234}s_{24}s_{14}} - 4 \frac{s_{34}^2 - s_{24}s_{34} + m_H^2 s_{34}}{s_{134}s_{13}s_{23}} \\
& -4 \frac{s_{34}^2 + m_H^2 s_{34} - s_{14}s_{34}}{s_{234}s_{13}s_{23}} - 4 \frac{-s_{23}s_{34} + m_H^2 s_{34} + s_{34}^2}{s_{134}s_{14}s_{24}} \\
& +4 \frac{s_{34}^2 - s_{24}s_{34} + m_H^2 s_{34}}{s_{134}s_{13}s_{234}} + 4 \frac{s_{24}s_{34} + m_H^2 s_{34} + 2s_{34}^2}{s_{234}s_{134}s_{14}} \\
& +4 \frac{s_{14}s_{34} + m_H^2 s_{34} + 2s_{34}^2}{s_{134}s_{234}s_{24}} + 4 \frac{s_{34}^2 + m_H^2 s_{34} - s_{14}s_{34}}{s_{234}s_{134}s_{23}} \\
& +4 \frac{-2s_{34}^2 - s_{23}s_{34} + m_H^2 s_{34}}{s_{24}s_{13}s_{14}} + 4 \frac{-s_{24}s_{34} + m_H^2 s_{34} - 2s_{34}^2}{s_{13}s_{14}s_{23}} \\
& +4 \frac{-2s_{34}^2 - s_{14}s_{34} + m_H^2 s_{34}}{s_{24}s_{13}s_{23}} + 4 \frac{-2s_{34}^2 - s_{13}s_{34} + m_H^2 s_{34}}{s_{24}s_{14}s_{23}} \\
& +4 \frac{(-s_{34} + m_H^2) s_{34}^2}{s_{13}s_{14}s_{23}s_{24}} + 4 \frac{(m_H^2 + s_{34}) s_{34}^2}{s_{234}s_{134}s_{13}s_{23}} + 4 \frac{(m_H^2 + s_{34}) s_{34}^2}{s_{234}s_{134}s_{14}s_{24}} \quad (\text{A.7})
\end{aligned}$$

$$\begin{aligned}
B_{H\bar{b}b\bar{g}g}^{(0)} = & 8 s_{14}^{-1} + 16 s_{23}^{-1} + 8 s_{24}^{-1} + 16 s_{13}^{-1} + 40 s_{134}^{-1} + 40 s_{234}^{-1} \\
& + 8 \frac{m_H^2 (-2 m_H^2 + s_{34} + s_{14})}{s_{234} s_{24} s_{13}} + 8 \frac{m_H^2 (-2 m_H^2 + s_{34} + s_{24})}{s_{134} s_{14} s_{23}} \\
& - 8 \frac{m_H^2 (2 m_H^2 - s_{13} + s_{24})}{s_{234} s_{14} s_{23}} - 8 \frac{m_H^2 (2 m_H^2 + s_{14} - s_{23})}{s_{134} s_{13} s_{24}} \\
& + 16 \frac{m_H^6}{s_{134} s_{13} s_{234} s_{24}} + 16 \frac{m_H^6}{s_{234} s_{134} s_{14} s_{23}} + 8 \frac{s_{14} + 2 m_H^2}{s_{234} s_{13}} + 8 \frac{m_H^2}{s_{134} s_{13}} \\
& - 8 \frac{-3 m_H^2 + s_{23} - s_{24} - s_{34}}{s_{134} s_{14}} + 8 \frac{2 s_{13} + s_{34} + 2 s_{24} - m_H^2}{s_{14} s_{23}} \\
& - 8 \frac{s_{13} - s_{34} - 3 m_H^2 - s_{14}}{s_{234} s_{24}} + 8 \frac{m_H^2}{s_{234} s_{23}} - 8 \frac{m_H^2 s_{24}}{s_{23} s_{234}^2} + 8 \frac{m_H^2 s_{34}}{s_{134}^2 s_{14}} \\
& + 8 \frac{m_H^2 s_{34}}{s_{234}^2 s_{24}} - 8 \frac{m_H^2 s_{14}}{s_{134}^2 s_{13}} + 8 \frac{-s_{24}^2 - 4 m_H^4 + 3 m_H^2 s_{24}}{s_{134} s_{13} s_{234}} \\
& + 8 \frac{-2 s_{24} s_{34} - 3 m_H^2 s_{34} - 4 m_H^4 - s_{24}^2 - s_{34}^2 - 3 m_H^2 s_{24}}{s_{234} s_{134} s_{14}} \\
& + 8 \frac{-3 m_H^2 s_{34} - s_{14}^2 - 2 s_{14} s_{34} - s_{34}^2 - 4 m_H^4 - 3 m_H^2 s_{14}}{s_{134} s_{234} s_{24}} \\
& + 8 \frac{3 m_H^2 s_{14} - 4 m_H^4 - s_{14}^2}{s_{234} s_{134} s_{23}} + 24 \frac{m_H^2}{s_{134}^2} + 24 \frac{m_H^2}{s_{234}^2} \\
& - 8 \frac{-s_{34} + s_{13} - 3 m_H^2 - 2 s_{24}}{s_{234} s_{14}} + 8 \frac{-m_H^2 + s_{34} + 2 s_{14} + 2 s_{23}}{s_{24} s_{13}} \\
& + 8 \frac{s_{24} + 2 m_H^2}{s_{134} s_{23}} - 8 \frac{-s_{34} - 2 s_{14} - 3 m_H^2 + s_{23}}{s_{134} s_{24}} \\
& + 16 \frac{-6 m_H^2 - 4 s_{24} - 4 s_{14} - 3 s_{34}}{s_{134} s_{234}}
\end{aligned} \tag{A.8}$$

$$\begin{aligned}
B_{H\bar{b}b\bar{g}g}^{(1)} = & -8 s_{14}^{-1} - 16 s_{23}^{-1} - 8 s_{24}^{-1} - 16 s_{13}^{-1} - 48 s_{134}^{-1} - 48 s_{234}^{-1} \\
& + 8 \frac{m_H^2 (-2 s_{34} - s_{14})}{s_{234} s_{24} s_{13}} + 8 \frac{m_H^2 (-2 s_{34} - s_{24})}{s_{134} s_{14} s_{23}} - 8 \frac{m_H^2 (s_{13} - 2 s_{24})}{s_{234} s_{14} s_{23}} \\
& - 8 \frac{m_H^2 (-2 s_{14} + s_{23})}{s_{134} s_{13} s_{24}} + 8 \frac{s_{13}}{s_{234} s_{23}} - 8 \frac{-m_H^2 + s_{34} - s_{23}}{s_{134} s_{14}} \\
& - 8 \frac{-s_{13} - m_H^2 + s_{34}}{s_{234} s_{24}} + 16 \frac{m_H^2 s_{24}}{s_{23} s_{234}^2} - 16 \frac{m_H^2 s_{34}}{s_{134}^2 s_{14}} \\
& - 16 \frac{m_H^2 s_{34}}{s_{234}^2 s_{24}} + 16 \frac{m_H^2 s_{14}}{s_{134}^2 s_{13}} - 32 \frac{m_H^2}{s_{134}^2} - 32 \frac{m_H^2}{s_{234}^2} \\
& + 8 \frac{s_{24}^2 - m_H^2 s_{24}}{s_{134} s_{13} s_{234}} + 8 \frac{2 s_{24} s_{34} + s_{34}^2 + s_{24}^2 + m_H^2 s_{24} + m_H^2 s_{34}}{s_{234} s_{134} s_{14}} \\
& + 8 \frac{s_{34}^2 + 2 s_{14} s_{34} + m_H^2 s_{14} + s_{14}^2 + m_H^2 s_{34}}{s_{134} s_{234} s_{24}} + 8 \frac{s_{14}^2 - m_H^2 s_{14}}{s_{234} s_{134} s_{23}} \\
& - 8 \frac{-s_{13} + m_H^2 + 2 s_{24} + s_{34}}{s_{234} s_{14}} + 8 \frac{-2 s_{14} + m_H^2 - s_{34} - 2 s_{23}}{s_{24} s_{13}} \\
& + 8 \frac{-2 s_{24} - 3 m_H^2}{s_{134} s_{23}} + 8 \frac{s_{23}}{s_{134} s_{13}} - 8 \frac{m_H^2 - s_{23} + s_{34} + 2 s_{14}}{s_{134} s_{24}} \\
& + 8 \frac{-3 m_H^2 - 2 s_{14}}{s_{234} s_{13}} + 8 \frac{-s_{34} - 2 s_{24} - 2 s_{13} + m_H^2}{s_{14} s_{23}} \\
& + 16 \frac{4 s_{14} + 4 s_{24} + 2 m_H^2 + 3 s_{34}}{s_{134} s_{234}}
\end{aligned} \tag{A.9}$$

$$\begin{aligned}
B_{H\bar{b}b\bar{g}g}^{(2)} = & -8 \frac{s_{34} + s_{24}}{s_{134} s_{14}} - 8 s_{23}^{-1} - 8 s_{13}^{-1} - 16 s_{134}^{-1} - 16 s_{234}^{-1} \\
& + 8 \frac{m_H^2 s_{34}}{s_{234} s_{24} s_{13}} + 8 \frac{m_H^2 s_{34}}{s_{134} s_{14} s_{23}} - 8 \frac{m_H^2 s_{24}}{s_{234} s_{14} s_{23}} - 8 \frac{m_H^2 s_{14}}{s_{134} s_{13} s_{24}} \\
& + 8 \frac{-s_{13} + m_H^2}{s_{234} s_{23}} - 8 \frac{s_{34} + s_{14}}{s_{234} s_{24}} - 8 \frac{m_H^2 s_{24}}{s_{23} s_{234}^2} \\
& + 8 \frac{m_H^2 s_{34}}{s_{134}^2 s_{14}} + 8 \frac{m_H^2 s_{34}}{s_{234}^2 s_{24}} - 8 \frac{m_H^2 s_{14}}{s_{134}^2 s_{13}}
\end{aligned}$$

$$\begin{aligned}
& +8 \frac{-s_{24}s_{34} + m_H^2 s_{34}}{s_{134}s_{13}s_{234}} + 8 \frac{s_{34}^2 + s_{24}s_{34} + m_H^2 s_{34}}{s_{234}s_{134}s_{14}} \\
& +8 \frac{s_{34}^2 + m_H^2 s_{34} + s_{14}s_{34}}{s_{134}s_{234}s_{24}} + 8 \frac{-s_{14}s_{34} + m_H^2 s_{34}}{s_{234}s_{134}s_{23}} \\
& +8 \frac{m_H^2}{s_{134}^2} + 8 \frac{m_H^2}{s_{234}^2} - 8 \frac{s_{34} + m_H^2 + s_{24} - s_{13}}{s_{234}s_{14}} \\
& +8 \frac{-s_{23} - s_{14} - s_{34} + m_H^2}{s_{24}s_{13}} + 8 \frac{s_{24} + s_{14}}{s_{134}s_{23}} + 8 \frac{-s_{23} + m_H^2}{s_{134}s_{13}} \\
& -8 \frac{m_H^2 + s_{34} - s_{23} + s_{14}}{s_{134}s_{24}} + 8 \frac{s_{24} + s_{14}}{s_{234}s_{13}} \\
& +8 \frac{m_H^2 - s_{34} - s_{13} - s_{24}}{s_{14}s_{23}} + 16 \frac{2m_H^2 + 2s_{34}}{s_{134}s_{234}} \tag{A.10}
\end{aligned}$$

$$\begin{aligned}
C_{Hb\bar{b}gg}^{(0)} = & 8 \frac{2s_{24} + 4m_H^2 + s_{14} - s_{13}}{s_{234}s_{34}} - 4 \frac{-s_{14} - 2s_{13} + 4m_H^2 - 4s_{23}}{s_{24}s_{34}} \\
& -4 \frac{-2s_{14} - 2s_{23} + 2m_H^2 - s_{24}}{s_{13}s_{34}} - 4 \frac{2m_H^2 - 2s_{13} - s_{14} - 2s_{24}}{s_{23}s_{34}} \\
& +16 \frac{-m_H^2 s_{24} - 4m_H^4 - 2s_{24}s_{14} - s_{14}^2 - s_{24}^2 - m_H^2 s_{14}}{s_{134}s_{34}s_{234}} \\
& -4 \frac{-s_{24}^2 + 2m_H^2 s_{24} - 2m_H^4 - s_{14}^2 + 2m_H^2 s_{14} - 2s_{24}s_{14}}{s_{234}s_{34}s_{13}} \\
& -4 \frac{2s_{24}s_{13} - 2m_H^4 - s_{24}^2 - s_{13}^2 + 2m_H^2 s_{13} - 2m_H^2 s_{24}}{s_{234}s_{34}s_{14}} \\
& -32 \frac{s_{24}s_{14}m_H^2}{s_{134}s_{34}^2 s_{234}} - 4 \frac{-s_{24} - 2s_{23} + 4m_H^2 - 4s_{13}}{s_{14}s_{34}} \\
& -4 \frac{2s_{14}s_{23} - s_{23}^2 + 2m_H^2 s_{23} - 2m_H^4 - s_{14}^2 - 2m_H^2 s_{14}}{s_{134}s_{34}s_{24}} \\
& -8 \frac{-s_{24} - 4m_H^2 - 2s_{14} + s_{23}}{s_{134}s_{34}} + 16 \frac{m_H^2 s_{24}}{s_{234}^2 s_{34}} \\
& -4 \frac{2m_H^2 s_{24} + 2m_H^2 s_{13} - 2m_H^4 - s_{24}^2 - 2s_{24}s_{13} - s_{13}^2}{s_{14}s_{23}s_{34}} \\
& +16 \frac{s_{24}^2 m_H^2}{s_{34}^2 s_{234}^2} + 16 \frac{m_H^2 s_{14}}{s_{134}^2 s_{34}} + 16 \frac{s_{14}^2 m_H^2}{s_{34}^2 s_{134}^2} \\
& -4 \frac{-2s_{14}s_{23} + 2m_H^2 s_{23} - 2m_H^4 - s_{23}^2 + 2m_H^2 s_{14} - s_{14}^2}{s_{24}s_{13}s_{34}} \\
& -4 \frac{-s_{24}^2 + 2m_H^2 s_{24} - 2m_H^4 - s_{14}^2 + 2m_H^2 s_{14} - 2s_{24}s_{14}}{s_{134}s_{34}s_{23}} \tag{A.11}
\end{aligned}$$

$$\begin{aligned}
C_{Hb\bar{b}gg}^{(1)} = & 8 \frac{-s_{14} - 2s_{24} + s_{13}}{s_{234}s_{34}} - 4 \frac{s_{24} + 2s_{23} + s_{14}}{s_{13}s_{34}} - 4 \frac{s_{14} + s_{24} + 2s_{13}}{s_{23}s_{34}} \\
& + 32 \frac{s_{24}s_{14}m_H^2}{s_{134}s_{34}^2s_{234}} - 4 \frac{2s_{23} + 4s_{13} + s_{24}}{s_{14}s_{34}} - 4 \frac{-3s_{14}s_{23} + s_{23}^2 + s_{14}^2}{s_{134}s_{34}s_{24}} \\
& - 8 \frac{2s_{14} + s_{24} - s_{23}}{s_{134}s_{34}} - 16 \frac{m_H^2s_{24}}{s_{234}^2s_{34}} - 4 \frac{3s_{24}s_{13} + s_{13}^2 + s_{24}^2}{s_{14}s_{23}s_{34}} \\
& - 16 \frac{s_{24}^2m_H^2}{s_{34}^2s_{234}^2} - 4 \frac{4s_{23} + s_{14} + 2s_{13}}{s_{24}s_{34}} - 16 \frac{m_H^2s_{14}}{s_{134}^2s_{34}} \\
& + 16 \frac{m_H^2s_{14} + 2s_{24}s_{14} + m_H^2s_{24} + s_{14}^2 + s_{24}^2}{s_{134}s_{34}s_{234}} - 16 \frac{s_{14}^2m_H^2}{s_{34}^2s_{134}^2} \\
& - 4 \frac{s_{24}^2 + s_{14}^2 + 3s_{24}s_{14}}{s_{234}s_{34}s_{13}} - 4 \frac{s_{24}^2 + s_{14}^2 + 3s_{24}s_{14}}{s_{134}s_{34}s_{23}} \\
& - 4 \frac{s_{14}^2 + 3s_{14}s_{23} + s_{23}^2}{s_{24}s_{13}s_{34}} - 4 \frac{s_{13}^2 + s_{24}^2 - 3s_{24}s_{13}}{s_{234}s_{34}s_{14}}
\end{aligned} \tag{A.12}$$

Appendix B

The pdf convolution

The integral measure

$$I = \int_0^1 dx_1 dx_2 \theta(x_1 x_2 - \tau), \quad (\text{B.1})$$

with

$$\tau = \frac{M^2}{s}, \quad (\text{B.2})$$

is essential for the evaluation of hadronic cross sections. For numerical evaluations one wishes to deal with integrals situated on the unit hypercube. The simplest implementation option is therefore to just integrate over the theta-function directly, we shall regard to this as the *brute force* parametrisation. However it may be more beneficial to find parametrisations which do not require the θ constraint. We shall present a number of such parametrisations in this appendix and will test their relative performances on a suitable test integral.

B.1 Parametrisation 1

The most straight forward parameterisation is probably

$$I = \int_{\tau}^1 dx_1 \int_{\frac{\tau}{x_1}}^1 dx_2. \quad (\text{B.3})$$

Mapping linearly on the hypercube yields

$$(x_1, x_2) = \left(\tau + y_1(1 - \tau), \frac{\tau + y_1 y_2(1 - \tau)}{\tau + y_1(1 - \tau)} \right)$$

where the $y_1, y_2 \in [0, 1]$ and the measure becomes

$$I = \int_0^1 dy_1 dy_2 \left(\frac{y_1(1-\tau)^2}{\tau + y_1(1-\tau)} \right). \quad (\text{B.4})$$

B.2 Parametrisation 2

If there are singularities at $z = 1$ then it may be necessary to use the variable $z = \frac{\tau}{x_1 x_2}$. Mapping $x_2 \mapsto \tau/(x_1 z)$, yields

$$I = \tau \int_{\tau}^1 \frac{dx_1}{x_1} \int_{\frac{\tau}{x_1}}^1 \frac{dz}{z^2}. \quad (\text{B.5})$$

Linearly mapping onto the unit-hypercube results in

$$(x_1, x_2) = \left(\tau + y_1(1-\tau), \frac{\tau}{\tau + y_1 y_2(1-\tau)} \right)$$

where $y_1, y_2 \in [0, 1]$ and the measure becomes

$$I = \int_0^1 dy_1 dy_2 \left(\frac{y_1 \tau (1-\tau)^2}{(\tau + y_1 y_2(1-\tau))^2} \right). \quad (\text{B.6})$$

B.3 Parametrisation 3

Another parametrisation is in terms of the “partonic” rapidity

$$y = \frac{1}{2} \log \left(\frac{x_1}{x_2} \right)$$

and the partonic center of mass energy $\hat{s} = s x_1 x_2$, where s is the total collision energy here. One can then map $(x_1, x_2) \mapsto \sqrt{\frac{\hat{s}}{s}}(e^y, e^{-y})$ which yields

$$I = \int_{M^2}^s \frac{d\hat{s}}{s} \int_{\log \sqrt{\frac{\hat{s}}{s}}}^{\log \sqrt{\frac{s}{\hat{s}}}} dy. \quad (\text{B.7})$$

The above mapping has the nice feature that one gains explicit control over \hat{s} . Since amplitudes tend to behave as $1/(1-z)$, we nevertheless prefer to use the variable

$$\rho = 1 - z, \quad \in [0, 1 - \tau].$$

Remapping ρ and y linearly on the unit hypercube results in the following mapping for the Bjorken x-variables

$$(x_1, x_2) = \left(\left(\frac{\tau}{1 - y_1(1 - \tau)} \right)^{1-y_2}, \left(\frac{\tau}{1 - y_1(1 - \tau)} \right)^{y_2} \right)$$

with the $y_1, y_2 \in [0, 1]$ and

$$\rho = 1 - z = y_1(1 - \tau).$$

The measure is then given by

$$I = \int_0^1 dy_1 dy_2 \frac{\tau(1 - \tau)}{(1 - y_1(1 - \tau))^2} \log \left(\frac{1 - y_1(1 - \tau)}{\tau} \right). \quad (\text{B.8})$$

B.4 Numerical performance

We shall test the numerical performance of the different parametrisations on the integral

$$I = \int_0^1 dx_1 dx_2 \theta(x_1 x_2 - \tau) \frac{f_g(x_1, \mu_F) f_g(x_2, \mu_F)}{2x_1 x_2}, \quad (\text{B.9})$$

where $f_g(x_1, \mu_F)$ shall denote the gluon parton density. In Tables B.4 and B.4 we compare our parametrisations to the brute force approach, denoted as parameterisation 4. For our test integral we conclude that for both parameter choices for τ parameterisation 3 outperforms the others. A further conclusion which one can make is that all parametrisations show better convergence than the brute force approach.

Table B.1: Using MSTW NLO central set and $\mu_f = 100$, $\tau = 0.1$, 10^6 points with Cuba Vegas

Param.	I	ΔI
1	$5.42830 \cdot 10^{-3}$	$0.00112 \cdot 10^{-3}$
2	$5.42841 \cdot 10^{-3}$	$0.00097 \cdot 10^{-3}$
3	$5.42837 \cdot 10^{-3}$	$0.00078 \cdot 10^{-3}$
4	$5.42536 \cdot 10^{-3}$	$0.00936 \cdot 10^{-3}$

Table B.2: Using MSTW NLO central set and $\mu_f = 100$, $\tau = 0.0001$, 10^6 points with Cuba Vegas

Param.	I	ΔI
1	$7.25694 \cdot 10^5$	$0.000546 \cdot 10^5$
2	$7.25675 \cdot 10^5$	$0.000143 \cdot 10^5$
3	$7.25678 \cdot 10^5$	$0.000088 \cdot 10^5$
4	$7.25689 \cdot 10^5$	$0.001659 \cdot 10^5$

Appendix C

The one-loop box with one external mass

We begin by applying the massless propagator combination trick [134], to get a suitable Feynman parameterization. Feynman parameterizing, or “combining”, the first and second propagator as well as the third and fourth we arrive at

$$\text{BoxF}(s_{23}, s_{34}) = \int_0^1 dx dy \int \frac{d^d k}{i\pi^{\frac{d}{2}}} \frac{1}{[(k + xp_2)^2]^2 [(k + p_{23} + yp_4)^2]^2}.$$

We then Feynman parameterize the final two propagators, Wick rotate and integrate the loop momentum and the final Feynman parameter to get

$$\text{BoxF}(s_{23}, s_{34}) = \frac{\Gamma(2 + \epsilon)\Gamma(-\epsilon)^2}{\Gamma(-2\epsilon)} \int_0^1 dx dy [\Delta(x, y)]^{-2-\epsilon}$$

where

$$\Delta(x, y) = s_{24}xy - s_{23}\bar{x} - (s_{24} + s_{34})y.$$

We then perform the integration over y and end up with

$$\text{BoxF}(s, t) = \frac{\Gamma(2 + \epsilon)\Gamma(-\epsilon)^2}{\Gamma(-2\epsilon)(1 + \epsilon)} \left[\int_0^1 dx \frac{(-sx)^{-1-\epsilon}}{-t - ux} - \int_0^1 dx \frac{(-x(M^2 - t) - t)^{-1-\epsilon}}{-t - ux} \right]$$

where we defined $M^2 = s + t + u$. The first integral is of Euler type and we can immediately identify a hypergeometric function,

$$I_1 = \int_0^1 dx \frac{(-sx)^{-1-\epsilon}}{-t - ux} = -\frac{(-s)^{-\epsilon}}{st\epsilon} {}_2F_1(1, -\epsilon, 1 - \epsilon, -\frac{u}{t})$$

where

$${}_2F_1(1, -\epsilon, 1 - \epsilon, z) = \frac{\Gamma(1 - \epsilon)}{\Gamma(-\epsilon)} \int_0^1 dx \frac{x^{-1-\epsilon}}{1 - zx}.$$

In the second we change variable $y = x(1 - \frac{t}{M^2}) + \frac{t}{M^2}$, to get

$$I_2 = \int_0^1 dx \frac{(-x(M^2 - t) - t)^{-1-\epsilon}}{-t - ux} = \frac{(-M^2)^{-\epsilon}}{st} \int_{\frac{t}{M^2}}^1 dy \frac{y^{-1-\epsilon}}{1 + y \left(\frac{uM^2}{st}\right)}$$

We then split the integral such that

$$I_2 = \frac{(-M^2)^{-\epsilon}}{st} \int_0^1 dy \frac{y^{-1-\epsilon}}{1 + y \left(\frac{uM^2}{st}\right)} - \frac{(-M^2)^{-\epsilon}}{st} \int_0^{\frac{t}{M^2}} dy \frac{y^{-1-\epsilon}}{1 + y \left(\frac{uM^2}{st}\right)}$$

and bring the limits back from 0 to 1 in the second using $y = x \frac{t}{M^2}$ to obtain

$$I_2 = -\frac{(-M^2)^{-\epsilon}}{st\epsilon} {}_2F_1(1, -\epsilon, 1 - \epsilon, -\frac{uM^2}{st}) + \frac{(-t)^{-\epsilon}}{st\epsilon} {}_2F_1(1, -\epsilon, 1 - \epsilon, -\frac{u}{s}).$$

Noting that

$$\frac{\Gamma(2 + \epsilon)\Gamma(-\epsilon)^2}{\Gamma(-2\epsilon)(1 + \epsilon)} = -\frac{2\Gamma(1 + \epsilon)\Gamma(1 - \epsilon)^2}{\epsilon\Gamma(1 - 2\epsilon)}$$

gives the final result.

Appendix D

Scale dependence and separation

To all orders in perturbation theory any physical observable has to be independent of the regularisation scale. For the partonic cross-section $\sigma(\mu) = \sigma(\log \mu^2, m(\mu), a(\mu))$, where we introduced $\alpha_s(\mu)/\pi = a(\mu)$, this implies

$$\frac{d\sigma(\mu)}{d \log \mu^2} = 0. \quad (\text{D.1})$$

The statement is completely equivalent to saying that $\sigma(\mu_0) = \sigma(\mu_1)$. Expanding the total derivative we obtain

$$\frac{d\sigma(\mu)}{d \log \mu^2} = \frac{\partial \sigma(\mu)}{\partial \log \mu^2} + \frac{\partial \sigma(\mu)}{\partial a} \frac{\partial a(\mu)}{\partial \log \mu^2} + \frac{\partial \sigma(\mu)}{\partial m} \frac{\partial m(\mu)}{\partial \log \mu^2} \quad (\text{D.2})$$

Substituting the evolution equations of eqs.(2.21) we thus get

$$\frac{\partial \sigma(\mu)}{\partial \log \mu^2} + a(\mu)\beta(\mu)\frac{\partial \sigma(\mu)}{\partial a} + m(\mu)\gamma(\mu)\frac{\partial \sigma(\mu)}{\partial m} = 0. \quad (\text{D.3})$$

The explicit $\log \mu^2$ dependence of $\sigma(\mu)$ is therefore such as to cancel the dependence on $\log \mu^2$ created by the running couplings. In turn this implies that if we know the explicit dependence of the couplings on $\log \mu^2$ we can recover also the explicit dependence of the partonic cross-section on $\log \mu^2$. A solution to the renormalisation group equation eq.(D.3) can be constructed by solving the evolution equations for

$m(\mu)$ and $a(\mu)$. We can obtain all order expressions by integrating eqs.(2.21)

$$\begin{aligned} m(\mu_1) &= m(\mu_0) + \int_{\mu_0}^{\mu_1} d\log(\mu^2) \gamma(\mu) m(\mu) \\ a(\mu_1) &= a(\mu_0) + \int_{\mu_0}^{\mu_1} d\log(\mu^2) \beta(\mu) a(\mu). \end{aligned} \quad (\text{D.4})$$

In fact all eq.(D.3) is telling us is that it is invariant under such shifts and its solution is simply

$$\begin{aligned} \sigma(\log \mu_1^2, m(\mu_1), a(\mu_1)) &= \sigma(\log \mu_0^2, m(\mu_0), a(\mu_0)) = \\ \sigma\left(\log \mu_1^2, m(\mu_0) + \int_{\mu_0}^{\mu_1} d\log(\mu^2) \gamma(\mu) m(\mu), a(\mu_0) + \int_{\mu_0}^{\mu_1} d\log(\mu^2) \beta(\mu) a(\mu)\right) \end{aligned} \quad (\text{D.5})$$

One can check that this indeed satisfies eq.(D.3). This equation is probably the essence of why the “renormalisation group” is called a group after all, the group transformations then just correspond to scale transformations which leave the physical quantity invariant.

These coupled integral equations can be solved to any order in a by recursively re-substituting the left hand side back into the right hand side. Performing this once we find

$$\begin{aligned} m(\mu_1) &= m(\mu_0) + \int_{\mu_0}^{\mu_1} d\log(\mu^2) \gamma(\mu) \left[m(\mu_0) + \int_{\mu_0}^{\mu} d\log(\mu_s^2) \gamma(\mu_s) m(\mu_s) \right] \\ a(\mu_1) &= a(\mu_0) + \int_{\mu_0}^{\mu_1} d\log(\mu^2) \beta(\mu) \left[a(\mu_0) + \int_{\mu_0}^{\mu} d\log(\mu_s^2) \beta(\mu_s) a(\mu_s) \right] \end{aligned} \quad (\text{D.6})$$

Substituting the perturbative expansions of the the evolution equations and repeating the procedure until all a s and m s to $\mathcal{O}(a^3)$ depend only the scale μ_0 , the integrals can be evaluated trivially and yield just logarithms to some power. We then obtain

$$\begin{aligned} m(\mu_1) &= m(\mu_0) \left\{ 1 + a(\mu_0) \gamma_0 \log\left(\frac{\mu_0^2}{\mu_1^2}\right) \right. \\ &\quad \left. + a(\mu_0)^2 \left[\gamma_1 \log\left(\frac{\mu_0^2}{\mu_1^2}\right) + \frac{1}{2}(\gamma_0 \beta_0 + \gamma_0^2) \log^2\left(\frac{\mu_0^2}{\mu_1^2}\right) \right] + \mathcal{O}(a(\mu_0)^3) \right\} \end{aligned} \quad (\text{D.7})$$

and

$$\begin{aligned}
a(\mu_1) = & a(\mu_0) + a(\mu_0)^2 \beta_0 \log \left(\frac{\mu_0^2}{\mu_1^2} \right) \\
& + a(\mu_0)^3 \left[\beta_1 \log \left(\frac{\mu_0^2}{\mu_1^2} \right) + \beta_0^2 \log^2 \left(\frac{\mu_0^2}{\mu_1^2} \right) \right] + \mathcal{O}(a(\mu_0)^4)
\end{aligned} \tag{D.8}$$

We remark that formally these are the NLO “unresummed” evolution equations of $m(\mu)$ and $a(\mu)$. Substituting these expressions into $\sigma(\mu)$ allows us to derive the renormalisation dependence on $\log \mu^2$ of the partonic cross section at NNLO. Effectively the NNLO scale dependence cancels the LO and NLO contributions of the running of the coupling constants, thereby reducing the sensitivity to the renormalisation scale. However since in any practical calculation one always uses re-summed evolution equations at one order higher than the one at which one does the computation, there are residual scale dependence effects which are not cancelled. Varying the scales therefore estimates the size of those higher order contributions and hence allows to estimate the convergence of the perturbative series.

In practical calculations the evolution equations allow us to do a calculation at any conveniently fixed scale, e.g. $\mu = m_H$, and restore the full scale dependence at a later stage in the calculation. For example the NLO $\log \mu^2$ can be retrieved by expanding

$$\sigma(\mu)|_{\mu=m_H} = \sigma \left(\log \mu^2, m(\mu) + m(\mu)a(\mu)\gamma_0 \log \frac{\mu^2}{m_H^2}, a(\mu) + a(\mu)^2 \beta_0 \log \frac{\mu^2}{m_H^2} \right) \tag{D.9}$$

consistently to $\mathcal{O}(a^{n+2})$, where we assume the LO to be of $\mathcal{O}(a^n)$.

So far we have only discussed the renormalisation scale dependence. Let us now analyse the factorisation scale dependence of the hadronic cross section. The hadronic cross section is given by

$$\sigma(\mu) = f_i(\mu) \otimes f_j(\mu) \otimes \hat{\sigma}_{ij}(\mu). \tag{D.10}$$

We can follow exactly the same strategy as before by solving the evolution equation for the parton distribution function

$$\frac{\partial f(\mu)}{\partial \log(\mu^2)} = a(\mu) P(\mu) \otimes f(\mu) \tag{D.11}$$

known as the DGLAP equation. Integrating

$$f(\mu_F) = f(\mu_0) + \int_{\mu_0}^{\mu_F} d\log(\mu^2) a(\mu) P(\mu) \otimes f(\mu) \quad (\text{D.12})$$

and resubstituting we obtain

$$f(\mu_F) = f(\mu_0) + \int_{\mu_0}^{\mu_F} d\log(\mu^2) a(\mu) P(\mu) \otimes \left[f(\mu_0) + \int_{\mu_0}^{\mu} d\log(\mu_s^2) a(\mu_s) P(\mu_s) \otimes f(\mu_s) \right]. \quad (\text{D.13})$$

Expanding the splitting function $P(\mu) = P^0 + a(\mu)P^1 + \dots$ and using the evolution of $a(\mu)$ we then derive

$$\begin{aligned} f_i(\mu_F) &= f_i(\mu_0) + a(\mu_0) \log\left(\frac{\mu_F^2}{\mu_0^2}\right) P_{ij}^0 \otimes f_j(\mu_0) \\ &\quad + a(\mu_0)^2 \left[\log\left(\frac{\mu_F^2}{\mu_0^2}\right) P_{ij}^1 \otimes f_j(\mu_0) \right. \\ &\quad \left. + \frac{1}{2} \log^2\left(\frac{\mu_F^2}{\mu_0^2}\right) (P_{ij}^0 \otimes P_{jk}^0 \otimes f_k(\mu_0) - \beta_0 P_{ij}^0 \otimes f_j(\mu_0)) \right] + \mathcal{O}(a(\mu_0)^3) \end{aligned} \quad (\text{D.14})$$

A simple method to separate the renormalisation and factorisation scales

The renormalisation and factorization scales, μ_R and μ_F , can be conveniently separated by first performing the calculation at $\mu = \mu_F$. Applying the relations (and letting $y_b = m/v$)

$$\begin{aligned} \frac{\alpha_s(\mu_F)}{\pi} &= \frac{\alpha_s(\mu_R)}{\pi} + \left(\frac{\alpha_s(\mu_R)}{\pi}\right)^2 \beta_0 \log\left(\frac{\mu_R^2}{\mu_F^2}\right) \\ &\quad + \left(\frac{\alpha_s(\mu_R)}{\pi}\right)^3 \left[\beta_1 \log\left(\frac{\mu_R^2}{\mu_F^2}\right) + \beta_0^2 \log^2\left(\frac{\mu_R^2}{\mu_F^2}\right) \right] + \mathcal{O}(\alpha_s^4), \\ y_b(\mu_F) &= y_b(\mu_R) \left\{ 1 + \frac{\alpha_s(\mu_R)}{\pi} \gamma_0 \log\left(\frac{\mu_R^2}{\mu_F^2}\right) \right. \\ &\quad \left. + \left(\frac{\alpha_s(\mu_R)}{\pi}\right)^2 \left[\gamma_1 \log\left(\frac{\mu_R^2}{\mu_F^2}\right) + \frac{1}{2}(\gamma_0 \beta_0 + \gamma_0^2) \log^2\left(\frac{\mu_R^2}{\mu_F^2}\right) \right] + \mathcal{O}(\alpha_s^3) \right\} \end{aligned} \quad (\text{D.15})$$

then allows to separate the scales a posteriori.

Bibliography

- [1] G. Altarelli and G. Parisi, *Asymptotic Freedom in Parton Language*, *Nucl.Phys.* **B126** (1977) 298.
- [2] G. Altarelli, R. K. Ellis, and G. Martinelli, *Leptonproduction and Drell-Yan Processes Beyond the Leading Approximation in Chromodynamics*, *Nucl.Phys.* **B143** (1978) 521.
- [3] B. Humpert and W. Van Neerven, *On The Nonleading Q Anti- q And Q G Contributions In Drell-yan Processes*, *Phys.Lett.* **B85** (1979) 293–296.
- [4] S. Gorishnii, A. Kataev, and S. Larin, *Next-To-Leading $O(\alpha_s^3)$ QCD Correction to $\Sigma_t (e^+ e^- \rightarrow \text{Hadrons})$: Analytical Calculation and Estimation of the Parameter $\Lambda(\overline{MS})$* , *Phys.Lett.* **B212** (1988) 238–244.
- [5] R. Hamberg, W. van Neerven, and T. Matsuura, *A Complete calculation of the order $\alpha - s^2$ correction to the Drell-Yan K factor*, *Nucl.Phys.* **B359** (1991) 343–405.
- [6] S. Dawson, *Radiative corrections to Higgs boson production*, *Nucl.Phys.* **B359** (1991) 283–300.
- [7] A. Djouadi, M. Spira, and P. Zerwas, *Production of Higgs bosons in proton colliders: QCD corrections*, *Phys.Lett.* **B264** (1991) 440–446.
- [8] R. V. Harlander and W. B. Kilgore, *Next-to-next-to-leading order Higgs production at hadron colliders*, *Phys.Rev.Lett.* **88** (2002) 201801, [[hep-ph/0201206](#)].
- [9] C. Anastasiou and K. Melnikov, *Higgs boson production at hadron colliders in NNLO QCD*, *Nucl.Phys.* **B646** (2002) 220–256, [[hep-ph/0207004](#)].

- [10] C. Anastasiou, K. Melnikov, and F. Petriello, *Higgs boson production at hadron colliders: Differential cross sections through next-to-next-to-leading order*, *Phys.Rev.Lett.* **93** (2004) 262002, [[hep-ph/0409088](#)].
- [11] T. Binoth and G. Heinrich, *An Automatized algorithm to compute infrared divergent multiloop integrals*, *Nucl.Phys.* **B585** (2000) 741–759, [[hep-ph/0004013](#)].
- [12] K. Hepp, *Proof of the Bogolyubov-Parasiuk theorem on renormalization*, *Commun.Math.Phys.* **2** (1966) 301–326.
- [13] M. Roth and A. Denner, *High-energy approximation of one loop Feynman integrals*, *Nucl.Phys.* **B479** (1996) 495–514, [[hep-ph/9605420](#)].
- [14] F. A. Berends and W. Giele, *Recursive Calculations for Processes with n Gluons*, *Nucl.Phys.* **B306** (1988) 759.
- [15] R. Britto, F. Cachazo, and B. Feng, *New recursion relations for tree amplitudes of gluons*, *Nucl.Phys.* **B715** (2005) 499–522, [[hep-th/0412308](#)].
- [16] W. Giele and E. N. Glover, *Higher order corrections to jet cross-sections in $e^+ e^-$ annihilation*, *Phys.Rev.* **D46** (1992) 1980–2010.
- [17] W. Giele, E. N. Glover, and D. A. Kosower, *Higher order corrections to jet cross-sections in hadron colliders*, *Nucl.Phys.* **B403** (1993) 633–670, [[hep-ph/9302225](#)].
- [18] S. Frixione, Z. Kunszt, and A. Signer, *Three jet cross-sections to next-to-leading order*, *Nucl.Phys.* **B467** (1996) 399–442, [[hep-ph/9512328](#)].
- [19] R. Frederix, S. Frixione, F. Maltoni, and T. Stelzer, *Automation of next-to-leading order computations in QCD: The FKS subtraction*, *JHEP* **0910** (2009) 003, [[arXiv:0908.4272](#)].
- [20] Z. Nagy and Z. Trocsanyi, *Calculation of QCD jet cross-sections at next-to-leading order*, *Nucl.Phys.* **B486** (1997) 189–226, [[hep-ph/9610498](#)].
- [21] S. Catani and M. Seymour, *A General algorithm for calculating jet cross-sections in NLO QCD*, *Nucl.Phys.* **B485** (1997) 291–419, [[hep-ph/9605323](#)].

- [22] S. Catani, S. Dittmaier, M. H. Seymour, and Z. Trocsanyi, *The Dipole formalism for next-to-leading order QCD calculations with massive partons*, *Nucl.Phys.* **B627** (2002) 189–265, [[hep-ph/0201036](#)].
- [23] G. 't Hooft and M. Veltman, *Scalar One Loop Integrals*, *Nucl.Phys.* **B153** (1979) 365–401.
- [24] G. Passarino and M. Veltman, *One Loop Corrections for $e^+ e^-$ Annihilation Into $\mu^+ \mu^-$ in the Weinberg Model*, *Nucl.Phys.* **B160** (1979) 151.
- [25] W. van Neerven and J. Vermaseren, *The Role Of The Five Point Function In Radiative Corrections To Two Photon Physics*, *Phys.Lett.* **B142** (1984) 80.
- [26] Z. Bern, L. J. Dixon, and D. A. Kosower, *Dimensionally regulated pentagon integrals*, *Nucl.Phys.* **B412** (1994) 751–816, [[hep-ph/9306240](#)].
- [27] Z. Bern, L. J. Dixon, D. C. Dunbar, and D. A. Kosower, *Fusing gauge theory tree amplitudes into loop amplitudes*, *Nucl.Phys.* **B435** (1995) 59–101, [[hep-ph/9409265](#)].
- [28] R. Britto, F. Cachazo, and B. Feng, *Generalized unitarity and one-loop amplitudes in $N=4$ super-Yang-Mills*, *Nucl.Phys.* **B725** (2005) 275–305, [[hep-th/0412103](#)].
- [29] C. Berger, Z. Bern, L. J. Dixon, F. Febres Cordero, D. Forde, et al., *Precise Predictions for $W + 4$ Jet Production at the Large Hadron Collider*, *Phys.Rev.Lett.* **106** (2011) 092001, [[arXiv:1009.2338](#)].
- [30] K. Melnikov and F. Petriello, *Electroweak gauge boson production at hadron colliders through $O(\alpha(s)^2)$* , *Phys.Rev.* **D74** (2006) 114017, [[hep-ph/0609070](#)].
- [31] A. Gehrmann-De Ridder, T. Gehrmann, E. Glover, and G. Heinrich, *NNLO corrections to event shapes in $e^+ e^-$ annihilation*, *JHEP* **0712** (2007) 094, [[arXiv:0711.4711](#)].
- [32] G. Dissertori, A. Gehrmann-De Ridder, T. Gehrmann, E. Glover, G. Heinrich, et al., *First determination of the strong coupling constant using NNLO predictions for hadronic event shapes in $e^+ e^-$ annihilations*, *JHEP* **0802** (2008) 040, [[arXiv:0712.0327](#)].

- [33] S. Catani, L. Cieri, D. de Florian, G. Ferrera, and M. Grazzini, *Diphoton production at hadron colliders: a fully-differential QCD calculation at NNLO*, *Phys.Rev.Lett.* **108** (2012) 072001, [[arXiv:1110.2375](#)].
- [34] G. Ferrera, M. Grazzini, and F. Tramontano, *Associated WH production at hadron colliders: a fully exclusive QCD calculation at NNLO*, *Phys.Rev.Lett.* **107** (2011) 152003, [[arXiv:1107.1164](#)].
- [35] C. Anastasiou, K. Melnikov, and F. Petriello, *A New method for real radiation at NNLO*, *Phys.Rev.* **D69** (2004) 076010, [[hep-ph/0311311](#)].
- [36] C. Anastasiou, K. Melnikov, and F. Petriello, *Fully differential Higgs boson production and the di-photon signal through next-to-next-to-leading order*, *Nucl.Phys.* **B724** (2005) 197–246, [[hep-ph/0501130](#)].
- [37] K. Melnikov and F. Petriello, *The W boson production cross section at the LHC through $O(\alpha_s^2)$* , *Phys.Rev.Lett.* **96** (2006) 231803, [[hep-ph/0603182](#)].
- [38] K. Melnikov, *$O(\alpha(s)^{**2})$ corrections to semileptonic decay $b \rightarrow cl$ anti- $\nu(l)$* , *Phys.Lett.* **B666** (2008) 336–339, [[arXiv:0803.0951](#)].
- [39] C. Anastasiou, K. Melnikov, and F. Petriello, *The Electron energy spectrum in muon decay through $O(\alpha^{**2})$* , *JHEP* **0709** (2007) 014, [[hep-ph/0505069](#)].
- [40] H. Asatrian, A. Hovhannisyan, V. Poghosyan, T. Ewerth, C. Greub, et al., *NNLL QCD contribution of the electromagnetic dipole operator to $\Gamma(\text{anti-}B \rightarrow X(s) \gamma)$* , *Nucl.Phys.* **B749** (2006) 325–337, [[hep-ph/0605009](#)].
- [41] A. Gehrmann-De Ridder and E. N. Glover, *A Complete $O(\alpha \alpha_s)$ calculation of the photon + 1 jet rate in $e^+ e^-$ annihilation*, *Nucl.Phys.* **B517** (1998) 269–323, [[hep-ph/9707224](#)].
- [42] A. Gehrmann-De Ridder, T. Gehrmann, and E. N. Glover, *Antenna subtraction at NNLO*, *JHEP* **0509** (2005) 056.
- [43] A. Daleo, A. Gehrmann-De Ridder, T. Gehrmann, and G. Luisoni, *Antenna subtraction at NNLO with hadronic initial states: initial-final configurations*, *JHEP* **1001** (2010) 118.

- [44] E. Nigel Glover and J. Pires, *Antenna subtraction for gluon scattering at NNLO*, *JHEP* **1006** (2010) 096.
- [45] R. Boughezal, A. Gehrmann-De Ridder, and M. Ritzmann, *Antenna subtraction at NNLO with hadronic initial states: double real radiation for initial-initial configurations with two quark flavours*, *JHEP* **1102** (2011) 098.
- [46] S. Catani and M. Grazzini, *An NNLO subtraction formalism in hadron collisions and its application to Higgs boson production at the LHC*, *Phys.Rev.Lett.* **98** (2007) 222002, [[hep-ph/0703012](#)].
- [47] G. Somogyi, Z. Trocsanyi, and V. Del Duca, *Matching of singly- and doubly-unresolved limits of tree-level QCD squared matrix elements*, *JHEP* **0506** (2005) 024, [[hep-ph/0502226](#)].
- [48] G. Somogyi and Z. Trocsanyi, *A New subtraction scheme for computing QCD jet cross sections at next-to-leading order accuracy*, .
- [49] G. Somogyi and Z. Trocsanyi, *A Subtraction scheme for computing QCD jet cross sections at NNLO: Regularization of real-virtual emission*, *JHEP* **0701** (2007) 052, [[hep-ph/0609043](#)].
- [50] G. Somogyi, Z. Trocsanyi, and V. Del Duca, *A Subtraction scheme for computing QCD jet cross sections at NNLO: Regularization of doubly-real emissions*, *JHEP* **0701** (2007) 070.
- [51] P. Bolzoni, G. Somogyi, and Z. Trocsanyi, *A subtraction scheme for computing QCD jet cross sections at NNLO: integrating the iterated singly-unresolved subtraction terms*, *JHEP* **1101** (2011) 059.
- [52] W. B. Kilgore, *Subtraction terms for hadronic production processes at next-to-next-to-leading order*, *Phys.Rev.* **D70** (2004) 031501, [[hep-ph/0403128](#)].
- [53] S. Frixione and M. Grazzini, *Subtraction at NNLO*, *JHEP* **0506** (2005) 010, [[hep-ph/0411399](#)].
- [54] S. Weinzierl, *Subtraction terms at NNLO*, *JHEP* **0303** (2003) 062, [[hep-ph/0302180](#)].

- [55] T. Gehrmann and E. Remiddi, *Differential equations for two loop four point functions*, *Nucl.Phys.* **B580** (2000) 485–518, [[hep-ph/9912329](#)].
- [56] A. Kotikov, *Differential equations method: New technique for massive Feynman diagrams calculation*, *Phys.Lett.* **B254** (1991) 158–164.
- [57] V. A. Smirnov, *Analytical result for dimensionally regularized massless on shell double box*, *Phys.Lett.* **B460** (1999) 397–404, [[hep-ph/9905323](#)].
- [58] J. Tausk, *Nonplanar massless two loop Feynman diagrams with four on-shell legs*, *Phys.Lett.* **B469** (1999) 225–234, [[hep-ph/9909506](#)].
- [59] C. Anastasiou and A. Daleo, *Numerical evaluation of loop integrals*, *JHEP* **0610** (2006) 031, [[hep-ph/0511176](#)].
- [60] M. Czakon, *Automatized analytic continuation of Mellin-Barnes integrals*, *Comput.Phys.Commun.* **175** (2006) 559–571, [[hep-ph/0511200](#)].
- [61] M. E. Peskin and D. V. Schroeder, *An Introduction to quantum field theory*. 1995.
- [62] M. Srednicki, *Quantum Field Theory*. 2007.
- [63] S. Weinberg, *The Quantum theory of fields. Vol. 1: Foundations*. 1995.
- [64] S. Weinberg, *The Quantum theory of fields. Vol. 2: Modern applications*. 1996.
- [65] R. K. Ellis, W. J. Stirling, and B. Webber, *QCD and collider physics*, vol. 8. 1996.
- [66] G. Dissertori, I. Knowles, and M. Schmelling, *High energy experiments and theory*. 2003.
- [67] W. Greiner, S. Schramm, and E. Stein, *Quantum chromodynamics*. 2002.
- [68] F. Halzen and A. D. Martin, *Quarks And Leptons: An Introductory Course In Modern Particle Physics*. 1984.
- [69] J. C. Collins, *Renormalization. An Introduction To Renormalization, The Renormalization Group, And The Operator Product Expansion*. 1984.

- [70] G. Kramer and B. Lampe, *Integrals For Two Loop Calculations In Massless Qcd*, *J.Math.Phys.* **28** (1987) 945.
- [71] M. Czakon, *A novel subtraction scheme for double-real radiation at NNLO*, *Phys.Lett.* **B693** (2010) 259–268.
- [72] M. Czakon, *Double-real radiation in hadronic top quark pair production as a proof of a certain concept*, *Nucl.Phys.* **B849** (2011) 250–295.
- [73] R. Boughezal, K. Melnikov, and F. Petriello, *A subtraction scheme for NNLO computations*, *Phys.Rev.* **D85** (2012) 034025.
- [74] F. Petriello, “Private communication.”.
- [75] A. Gehrmann-De Ridder, T. Gehrmann, and G. Heinrich, *Four particle phase space integrals in massless QCD*, *Nucl.Phys.* **B682** (2004) 265–288, [[hep-ph/0311276](#)].
- [76] S. Biswas and K. Melnikov, *Second order QCD corrections to inclusive semileptonic $b \rightarrow gt$; $X(c) l \text{ anti-}\nu(l)$ decays with massless and massive lepton*, *JHEP* **1002** (2010) 089, [[arXiv:0911.4142](#)].
- [77] P. Baikov, K. Chetyrkin, and J. H. Kuhn, *Scalar correlator at $O(\alpha(s)^{**4})$, Higgs decay into b-quarks and bounds on the light quark masses*, *Phys.Rev.Lett.* **96** (2006) 012003, [[hep-ph/0511063](#)].
- [78] S. Gorishnii, A. Kataev, and S. Larin, *The Width of Higgs Boson Decay Into Hadrons: Three Loop Corrections Of Strong Interactions*, *Sov.J.Nucl.Phys.* **40** (1984) 329–334.
- [79] S. Gorishnii, A. Kataev, S. Larin, and L. Surguladze, *Corrected Three Loop QCD Correction To The Correlator Of The Quark Scalar Currents And Gamma (tot) ($H^0 \rightarrow \text{Hadrons}$)*, *Mod.Phys.Lett.* **A5** (1990) 2703–2712.
- [80] S. Gorishnii, A. Kataev, S. Larin, and L. Surguladze, *Scheme dependence of the next to next-to-leading QCD corrections to Gamma(tot) ($H^0 \rightarrow \text{hadrons}$) and the spurious QCD infrared fixed point*, *Phys.Rev.* **D43** (1991) 1633–1640.
- [81] C. Becchi, S. Narison, E. de Rafael, and F. Yndurain, *Light Quark Masses in Quantum Chromodynamics and Chiral Symmetry Breaking*, *Z.Phys.* **C8** (1981) 335.

- [82] N. Sakai, *Perturbative QCD Corrections to the Hadronic Decay Width of the Higgs Boson*, *Phys.Rev.* **D22** (1980) 2220.
- [83] T. Inami and T. Kubota, *Renormalization Group Estimate Of The Hadronic Decay Width Of The Higgs Boson*, *Nucl.Phys.* **B179** (1981) 171.
- [84] K. Chetyrkin, *Correlator of the quark scalar currents and $\Gamma_{\text{tot}}(H \rightarrow \text{hadrons})$ at $O(\alpha_s^3)$ in pQCD*, *Phys.Lett.* **B390** (1997) 309–317, [[hep-ph/9608318](#)].
- [85] K. Chetyrkin and M. Steinhauser, *Complete QCD corrections of order $O(\alpha_s^3)$ to the hadronic Higgs decay*, *Phys.Lett.* **B408** (1997) 320–324, [[hep-ph/9706462](#)].
- [86] J. M. Butterworth, A. R. Davison, M. Rubin, and G. P. Salam, *Jet substructure as a new Higgs search channel at the LHC*, *Phys.Rev.Lett.* **100** (2008) 242001, [[arXiv:0802.2470](#)].
- [87] T. Plehn, G. P. Salam, and M. Spannowsky, *Fat Jets for a Light Higgs*, *Phys.Rev.Lett.* **104** (2010) 111801, [[arXiv:0910.5472](#)].
- [88] A. Collaboration, *Atlas sensitivity to the standard model higgs in the HW and HZ channels at high transverse momenta*, *ATL-PHYS-PUB-2009-088* (2009).
- [89] D. E. Soper and M. Spannowsky, *Combining subjet algorithms to enhance ZH detection at the LHC*, *JHEP* **1008** (2010) 029, [[arXiv:1005.0417](#)].
- [90] R. V. Harlander and W. B. Kilgore, *Higgs boson production in bottom quark fusion at next-to-next-to leading order*, *Phys.Rev.* **D68** (2003) 013001, [[hep-ph/0304035](#)].
- [91] P. Nogueira, *Automatic Feynman graph generation*, *J.Comput.Phys.* **105** (1993) 279–289.
- [92] J. Vermaseren, *New features of FORM*, [math-ph/0010025](#).
- [93] “[<http://www.maplesoft.com>].”
- [94] K. Chetyrkin and F. Tkachov, *Integration by Parts: The Algorithm to Calculate beta Functions in 4 Loops*, *Nucl.Phys.* **B192** (1981) 159–204.

- [95] F. Tkachov, *A Theorem on Analytical Calculability of Four Loop Renormalization Group Functions*, *Phys.Lett.* **B100** (1981) 65–68.
- [96] S. Laporta, *High precision calculation of multiloop Feynman integrals by difference equations*, *Int.J.Mod.Phys.* **A15** (2000) 5087–5159, [[hep-ph/0102033](#)].
- [97] C. Anastasiou and A. Lazopoulos, *Automatic integral reduction for higher order perturbative calculations*, *JHEP* **0407** (2004) 046, [[hep-ph/0404258](#)].
- [98] **JADE Collaboration** Collaboration, W. Bartel et al., *Experimental Studies on Multi-Jet Production in $e^+ e^-$ Annihilation at PETRA Energies*, *Z.Phys.* **C33** (1986) 23.
- [99] K. Babu and S. Nandi, *Natural fermion mass hierarchy and new signals for the Higgs boson*, *Phys.Rev.* **D62** (2000) 033002, [[hep-ph/9907213](#)].
- [100] G. F. Giudice and O. Lebedev, *Higgs-dependent Yukawa couplings*, *Phys.Lett.* **B665** (2008) 79–85, [[arXiv:0804.1753](#)].
- [101] **CMS Collaboration** Collaboration, S. Chatrchyan et al., *Search for neutral Higgs bosons decaying to tau pairs in pp collisions at $\sqrt{s}=7$ TeV*, [arXiv:1202.4083](#).
- [102] G. A. et al. [ATLAS Collaboration], *Search for neutral mssm higgs bosons decaying to tau+tau-pairs in proton-proton collisions at $\sqrt{s} = 7$ tev with the atlas detector*, *ATLAS-CONF-2011-13* [<http://cdsweb.cern.ch/record/1383835>].
- [103] C. Kao, S. Sachithanandam, J. Sayre, and Y. Wang, *Discovering the Higgs Bosons of Minimal Supersymmetry with Bottom Quarks*, *Phys.Lett.* **B682** (2009) 291–296, [[arXiv:0908.1156](#)].
- [104] H. Baer, C. Kao, and J. Sayre, *Prospects for Higgs Searches with the Tri-bottom Channel in Unified SUSY Models*, *Phys.Rev.* **D85** (2012) 035021.
- [105] D. Atwood, S. Bar-Shalom, G. Eilam, and A. Soni, *Three heavy jet events at hadron colliders as a sensitive probe of the Higgs sector*, *Phys.Rev.* **D69** (2004) 033006, [[hep-ph/0309016](#)].

- [106] F. Maltoni, Z. Sullivan, and S. Willenbrock, *Higgs-boson production via bottom-quark fusion*, *Phys.Rev.* **D67** (2003) 093005.
- [107] E. Boos and T. Plehn, *Higgs boson production induced by bottom quarks*, *Phys.Rev.* **D69** (2004) 094005, [[hep-ph/0304034](#)].
- [108] T. Plehn, *Charged Higgs boson production in bottom gluon fusion*, *Phys.Rev.* **D67** (2003) 014018, [[hep-ph/0206121](#)].
- [109] R. Harlander, M. Kramer, and M. Schumacher, *Bottom-quark associated Higgs-boson production: reconciling the four- and five-flavour scheme approach*, [arXiv:1112.3478](#).
- [110] F. Maltoni, G. Ridolfi, and M. Ubiali, *b-initiated processes at the LHC: a reappraisal*, [arXiv:1203.6393](#).
- [111] S. Dittmaier, . Kramer, Michael, and M. Spira, *Higgs radiation off bottom quarks at the Tevatron and the CERN LHC*, *Phys.Rev.* **D70** (2004) 074010, [[hep-ph/0309204](#)].
- [112] S. Dawson, C. Jackson, L. Reina, and D. Wackeroth, *Higgs production in association with bottom quarks at hadron colliders*, *Mod.Phys.Lett.* **A21** (2006) 89–110.
- [113] S. Dawson, C. Jackson, L. Reina, and D. Wackeroth, *Higgs boson production with bottom quarks at hadron colliders*, *Int.J.Mod.Phys.* **A20** (2005) 3353–3355, [[hep-ph/0409345](#)].
- [114] S. Dawson, C. Jackson, L. Reina, and D. Wackeroth, *Exclusive Higgs boson production with bottom quarks at hadron colliders*, *Phys.Rev.* **D69** (2004) 074027.
- [115] S. Dawson, C. Jackson, L. Reina, and D. Wackeroth, *Higgs boson production with one bottom quark jet at hadron colliders*, *Phys.Rev.Lett.* **94** (2005) 031802.
- [116] S. Dawson and P. Jaiswal, *Weak Corrections to Associated Higgs-Bottom Quark Production*, *Phys.Rev.* **D81** (2010) 073008, [[arXiv:1002.2672](#)].
- [117] S. Dittmaier, . Kramer, Michael, A. Muck, and T. Schluter, *MSSM Higgs-boson production in bottom-quark fusion: Electroweak radiative corrections*, *JHEP* **0703** (2007) 114, [[hep-ph/0611353](#)].

- [118] N. Kidonakis, *Collinear and soft gluon corrections to Higgs production at NNNLO*, *Phys.Rev.* **D77** (2008) 053008, [[arXiv:0711.0142](#)].
- [119] B. Field, *Higgs boson resummation via bottom-quark fusion*, [hep-ph/0407254](#).
- [120] A. Belyaev, P. M. Nadolsky, and C.-P. Yuan, *Transverse momentum resummation for Higgs boson produced via b anti- b fusion at hadron colliders*, *JHEP* **0604** (2006) 004, [[hep-ph/0509100](#)].
- [121] R. Harlander and M. Wiesemann, *Jet-veto in bottom-quark induced Higgs production at next-to-next-to-leading order*, *JHEP* **1204** (2012) 066.
- [122] R. V. Harlander, K. J. Ozeren, and M. Wiesemann, *Higgs plus jet production in bottom quark annihilation at next-to-leading order*, *Phys.Lett.* **B693** (2010) 269–273, [[arXiv:1007.5411](#)].
- [123] T. Huber and D. Maitre, *HypExp 2, Expanding Hypergeometric Functions about Half-Integer Parameters*, *Comput.Phys.Commun.* **178** (2008) 755–776, [[arXiv:0708.2443](#)].
- [124] C. Anastasiou, “Private communication.”.
- [125] C. Anastasiou, S. Buehler, F. Herzog, and A. Lazopoulos, *Total cross-section for Higgs boson hadroproduction with anomalous Standard Model interactions*, *JHEP* **1112** (2011) 058.
- [126] T. Hahn, *CUBA: A Library for multidimensional numerical integration*, *Comput.Phys.Commun.* **168** (2005) 78–95, [[hep-ph/0404043](#)].
- [127] C. Anastasiou, G. Dissertori, F. Stockli, and B. R. Webber, *QCD radiation effects on the $H \rightarrow WW \rightarrow l \nu l \nu$ signal at the LHC*, *JHEP* **0803** (2008) 017, [[arXiv:0801.2682](#)].
- [128] A. Banfi, G. P. Salam, and G. Zanderighi, *NLL+NNLO predictions for jet-veto efficiencies in Higgs-boson and Drell-Yan production*, .
- [129] M. Cacciari, G. P. Salam, and G. Soyez, *The Anti- $k(t)$ jet clustering algorithm*, *JHEP* **0804** (2008) 063, [[arXiv:0802.1189](#)].
- [130] C. Anastasiou, F. Herzog, and A. Lazopoulos, *On the factorization of overlapping singularities at NNLO*, *JHEP* **1103** (2011) 038.

- [131] D. A. Kosower, *The Spinor helicity method in dimensional regularization*, *Phys.Lett.* **B254** (1991) 439–443.
- [132] L. J. Dixon, *Calculating scattering amplitudes efficiently*, [hep-ph/9601359](#).
- [133] L. J. Dixon, E. N. Glover, and V. V. Khoze, *MHV rules for Higgs plus multi-gluon amplitudes*, *JHEP* **0412** (2004) 015, [[hep-th/0411092](#)].
- [134] C. Anastasiou and A. Banfi, *Loop lessons from Wilson loops in $N=4$ supersymmetric Yang-Mills theory*, *JHEP* **1102** (2011) 064, [[arXiv:1101.4118](#)].